2005

Complex reaction dynamics in bromate-based chemical oscillators.

Yu Chen
University of Windsor

Complex Reaction Dynamics in Bromate-based Chemical Oscillators

By

Yu Chen

A Thesis
Submitted to the Faculty of Graduate Studies and Research
through the Department of Chemistry and Biochemistry
in Partial Fulfillment of the Requirements for
the Degree of Master of Science at the
University of Windsor

Windsor, Ontario, Canada
2005

Your file Votre référence
ISBN: 0-494-09733-7
Our file Notre référence
ISBN: 0-494-09733-7

Abstract

In this study new oscillations system have been constructed by introducing 1,4-cyclohexanedion (CHD) into the ferroin-or cerium-catalyzed classic BZ reaction as a second organic substrate further. Since 1,4-CHD alone is capable of forming a chemical oscillator with bromate in an acidic environment, the presence of 1,4-CHD actually implements new autocatalytic nonlinear feedbacks. As a result the mixed BZ reaction actually consists of two bromate oscillators that are coupled together through such reagents as bromine dioxide, metal catalysts (ferroin/ferriin or Ce^{3+}/Ce^{4+}) etc. This is unique difference from existing studies of the BZ reactions using mixed organic substrates.

Various complex oscillatory behaviors such as sequential oscillations and burst phenomena have been observed in this coupled oscillator. It is found that the development of complex oscillations depends on the ratio of [1,4-CHD]/[metal catalyst] and [1,4-CHD]/[MA] rather than their absolute concentrations, indicating that competitions between the1,4-CHD and metal catalyst for the bromine dioxide radicals and the competition between 1,4-CHD and malonic acid play the essential role in the observed complex oscillations.

To shed light on the properties of the complex oscillatory evolution, illumination was employed as a mean of perturbation to characterize the coupled oscillator. Our experimental results illustrate that the first oscillatory window (before complex) is governed by the BZ reaction while the 1,4-CHD-bromate oscillator plays a prominent role during the complex evolution and in the second oscillatory window. Our conclusion is further supported by numerical simulations in which complex oscillations observed in the experiments were qualitatively reproduced by a modified FKN mechanism.

Numerical simulations are also carried out in this thesis in order to understand the coexistence of two bifurcation regimes in the closed ferroin-BZ reaction, a phenomenon uncovered recently in our lab. Our calculation further illustrated that the existing ferroin-BZ model can be reduced to a small one without losing the ability of accounting the essential features of the BZ reaction

Acknowledgements

I would like to thank my supervisor Dr. Jichang Wang for his guidance and help on my studies and research during my graduate term at the University of Windsor. His scientific intelligence and attitude had a big influence on my academic training. His encouragement and support are greatly appreciated and will be remembered forever.

I would also like to thank Dr. Aroca Ricardo and Dr. Jianwen Yang for being my committee members.

I am also very grateful to our group members, Mr. Jinpei Zhao, Ms. Bei zhao, Ms. Erin Fortier, and Mr. Krishan Yadav for their help and advice, and to faculty and staff in the department of Chemistry and Biochemistry for their support and kind help.

Finally, my special thank goes to my parents for their encouragement and support.

Table of Contents

List of Tables

List of Figures

Chapter1. Introduction:

Nonlinear chemical dynamics has attracted more attention and has grown significantly in breadth and depth over the past three decades.[1-5] Its application encompasses the areas of mathematics, physics, biology, and engineering.

The prototypical phenomenon of nonlinear chemical dynamics is chemical oscillations, which are temporally periodic variation of concentrations of one or more species in a reaction system. The Belousov-Zhabotinsky (BZ) reaction has become a prototype model for the study of nonlinear chemical dynamics. The BZ reaction was discovered accidentally by a Russian chemist B.P. Belousov in the 1950s. Originally he mixed bromate, citric acid, and ceric ions, expecting to observe a monotonic change from yellow Ce^{4+} to colorless Ce^{3+}. But he was astonished to find that the yellow color reappeared at about one minute intervals.[6] In addition to the color change, oscillations can also be observed in the redox potential which is determined by the ratio of the oxidized and reduced cerium ions as well as in the concentration of bromide ion and several organic intermediates

1.1 The Cerium-catalyzed Belousov-Zhabotinsky Reaction

The Cerium-catalyzed BZ reaction is the most thoroughly studied oscillation system. In the early 1970s, Field, Koros and Noyes combined kinetic and thermodynamic approaches to propose a detailed mechanism (FKN mechanism) for the BZ reaction.[7] The skeleton FKN mechanism is listed in table1.1.

Table 1.1 Skeleton FKN Mechanism

	Process A
1	$Br^- + HOBr + H^+ \leftrightarrow Br_2 + H_2O$
2	$HBrO_2 + Br^- + H^+ \leftrightarrow 2HOBr$
3	$Br^- + BrO_3^- + 2H^+ \leftrightarrow HOBr + HBrO_2$
	Process B
4	$2HBrO_2 \leftrightarrow BrO_3^- + HOBr + H^+$
5	$BrO_3^- + HBrO2 + H^+ \leftrightarrow 2BrO_2^{\cdot} + H_2O$
6	$BrO_2^{\cdot} + Ce(III) + H^+ \leftrightarrow Ce(IV) + HBrO_2$
	Process C
7	$MA + Br_2 \rightarrow BrMA + Br^- + H^+$
8	$2Ce(IV) + MA + BrMA \rightarrow f\,Br^- + 2Ce(III) +$ other products

The heart of the FKN mechanism is the autocatalytic single-electron oxidation carried out by $BrO_2^{\cdot}$ in the process B. Process B can be inhibited by any species that compete for $HBrO_2$. Br^- concentration determines whether Process A or B is in control at a particular time. Process B is suppressed when the concentration of Br^- in sufficiently high as reaction 2 (in table 1.1) removes $HBrO_2$ before it can enter the chain-branching sequence. The net effect of Process A is to remove Br^- from the system. Autocatalytic oxidation of Ce^{3+} by process B begins when Process A has driven Br^- concentration to a sufficiently low value that the Br^- can no longer compete successfully for $HBrO_2$. Process B is accompanied by rapid production of Ce(IV) which becomes a reactant in process C to regenerate Br^-. When the concentration of Br^- reaches a high level, Process B is suppressed again. Beyond supplying Br^- to suppress Process B, Process C also resets

Process B by reducing Ce(IV) to Ce(III). Relaxation of oscillations occurs via switches between the oxidized and reduced states of the metal catalyst.[7]

The feature of bromide ion control in the BZ reaction elucidated by the FKN mechanism has been well accepted: Ce^{4+} is reduced by malonic acid, the resulting Ce^{3+} is oxidized by bromate during the autocatalytic reaction starting with the oxidization of Ce^{3+} by $BrO_2\cdot$ radical. Noszticzius and coworkers carried out an experimental test on the control intermediate Br^- in the BZ reaction.[8] From a theoretical point of view, both elementary bromine and bromide ions may act as control intermediates. The inhibitory effect of bromine is from its hydrolysis to produce bromide ion, which is the real inhibitory agent. Since the hydrolysis can be suppressed by adding hypobromous acid in the system, in this way if there is a direct reaction between bromine and bromous acid, a lengthening induction time should be observed in the presence of elementary bromine and hypobromous acid. But they did not observe an obviously lengthened induction time which indicated only bromide ions can react directly with bromous acid and the elementary Br_2 reacts indirectly via hydrolysis. Peter Ruoff also studied the BZ reaction to determine the control agent in the system[9]. In that study they reported the investigation on phase shift when the Br^- concentration of the BZ reaction is perturbed by solutions of KBr, $AgNO_3$ and HOBr. The phase shift observed in their experiments behaves exactly the same as that predicted by a mechanism which demonstrates the control of bromide ion in the BZ system.

Although it is well-accepted that the bromide ion is an important control intermediate, Noszticzius' silver ion perturbation experiment suggests that bromide ion is not always the control intermediate. After the addition of silver ions into the BZ reaction, they

observed that oscillations of the redox potential continued while the potential of a bromide-ion-specific electrode changed monotonically or underwent very small amplitude oscillations.[10] Forsterling and coworkers suggested that malonyl radical could also play the role of control intermediates in the BZ oscillation system.[11] They observed that during the experiments the Pt electrode potential was always above 111mV, a value recorded before the addition of bromate in the reaction mixture. From this result they concluded that the response of the electrode was not due to the bromide since the addition of bromide to the reaction mixture would lead to a decrease of potential below the value of 111mV. They suggested that the malonyl radical could be the control intermediate based on the following observations: they found that the autocatalytic reaction was switched off at the maximum of malonyl radical concentration (Br^- should be at the concentration maximum when the autocatalytic reaction is quenched in bromide ion control system) and the oscillations do not appear at the presence of the oxygen, which is considered as the scavenger of malonyl radicals. Venkataraman and Sorensen used electron spin resonance to study the oscillation of malonyl radical in the BZ reaction.[12] They introduced oxygen into the reaction mixture to determine the role of the free radical in the oscillation system, and observed that when the oscillations of free radicals were quenched by the oxygen, the bromide ion and cerium (IV) continue to oscillate, which cast doubt on the suggestion that the free-radical pathway is the most important route for the control of the oscillations.

1.2 The Ferroin-catalyzed Belousov-Zhabotinsky Reaction

The catalyst cerium in the BZ reaction can be replaced by ferroin complex [$Fe(phen)_3^{2+}$], which is originally added to the BZ reaction in order to better visualize the periodic changes. People later realized that ferroin was able to catalyze the BZ reaction independently and the addition of ferroin could change the BZ oscillation mechanism.[13]

The oscillation behavior in the ferroin-catalyzed system differs significantly from those observed in the cerium catalyzed one. For this reason systematic investigation of this system is highly desirable. One may think that the ferroin-catalyzed BZ reaction possesses the similar mechanism as that of the cerium system. Therefore, the ferroin-catalyzed mechanism could be constructed on the basis of the cerium-BZ mechanism by changing rate constants of a few elementary steps. However, Keki and co-workers failed to characterize the ferroin system within the framework of the FKN theory developed for the cerium-catalyzed BZ reaction.[13] Because during the induction time, a considerable amount of ferroin is oxidized to ferriin, which is contrary to that only a very small amount of cerium (III) is converted to cerium (IV). This could be explained on the basis of the standard reduction potential of $BrO_3^-/BrO_2\cdot$ couple in sulfuric acid, which is about 1.15V, slightly higher than the standard reduction potential of ferriin/ferroin couple, but much lower than that of Ce(IV)/Ce(III) redox pair. So after considering the direct interaction between ferroin (ferriin) and different bromine species, Keki constructed a model for the ferrin-BZ system.

Table 1.2 BZ-ferroin Oscillation Mechanism

	A Reactions between bromine- containing compounds
1	$Br^- + BrO_3^- + 2H^+ \rightarrow HOBr + HBrO_2$
2	$HOBr + HBrO_2 \rightarrow Br^- + BrO_3^- + 2H^+$
3	$HBrO_2 + Br^- + H^+ \rightarrow 2HOBr$
4	$2HOBr \rightarrow HBrO_2 + Br^- + H^+$
5	$HOBr + Br^- + H^+ \rightarrow Br_2 + H_2O$
6	$Br_2 + H_2O \rightarrow HOBr + Br^- + H^+$
7	$2HBrO_2 \rightarrow BrO_3^- + HOBr + H^+$
8	$BrO_3^- + HOBr + H^+ \rightarrow 2HBrO_2$
9	$BrO_3^- + HBrO2 + H^+ \rightarrow 2BrO_2\cdot + H_2O$
10	$2BrO_2\cdot + H_2O \rightarrow BrO_3^- + HBrO_2 + H^+$
	B Reactions with the participation of malonic acid
11	$MA + Br_2 \rightarrow BrMA + Br^- + H^+$
12	$MA + HOBr \rightarrow BrMA + H_2O$
13	$BrMA + HOBr \rightarrow$ product
14	$2BrMA\cdot + H_2O \rightarrow BrMA + BrTTA$
15	$BrMA\cdot + BrO_2\cdot + H_2O \rightarrow HBrO_2 + BrTTA$
16	$BrMA\cdot + MA\cdot + H_2O \rightarrow MA + BrTTA$
17	$MA\cdot + BrO_2\cdot \rightarrow$ product
18	$MA\cdot + BrO_3^- + H^+ \rightarrow BrO_2\cdot +$ product
19	$BrTTA \rightarrow Br^-$ + product
20	$BrMA\cdot + BrO_3^- + H^+ \rightarrow BrO_2\cdot + BrTTA$
	C Reaction with the participation of the catalysts
21	$Fe^{2+} + BrO_2\cdot + H^+ \rightarrow Fe^{3+} + HBrO_2$
22	$2\,Fe^{2+} + BrO_3^- + 3H^+ \rightarrow 2\,Fe^{3+} + HBrO_2 + H_2O$
23	$2\,Fe^{2+} + HBrO_2 + 2H^+ \rightarrow 2\,Fe^{3+} + HOBr + H_2O$
24	$2\,Fe^{2+} + HOBr + H^+ \rightarrow 2\,Fe^{3+} + Br^- + H_2O$
25	$2\,Fe^{2+} + Br_2 + H^+ \rightarrow 2\,Fe^{3+} + 2Br^-$
26	$2\,Fe^{3+} + 2\,Br^- \rightarrow 2\,Fe^{2+} + Br_2 + H^+$
27	$Fe^{3+} + MA \rightarrow Fe^{2+} + MA\cdot + H^+$
28	$Fe^{3+} + BrMA \rightarrow Fe^{2+} + BrMA\cdot + H^+$
29	$Fe^{2+} + BrMA\cdot + H^+ \rightarrow Fe^{3+} + BrMA$

Strizhak and coworkers investigated the periodic, mixed-mode, and chaotic oscillations in the ferroin-catalyzed BZ reaction in a continuous flow stirred tank reactor (CSTR) at various flow rates.[14] To simulate the experimental observation, they proposed a kinetic scheme which consists of 29 reactions and 12 variables, which is listed in table 1.2. This scheme can be subdivided into three groups of reactions: group A is common to all the bromate oscillators, which include reactions between bromine-containing compounds, such as bromate ions and their reduction products. Group B reactions

describe the oxidation of MA. Group C reactions describe reactions of ferroin (Fe^{2+}), ferriin (Fe^{3+}) and other components of the oscillation reaction.

1.3 The 1,4-CHD-bromate Oscillation System

Uncatalyzed bromate oscillators were first discoved in 1977-78 by Koros.[15] He found that phenol and aniline derivatives can react with bromate acid even in the absence of metal catalyst to give rise to oscillations. He screened about 50 compounds and the results indicated that it was possible to establish chemical oscillations in a system with bromate in proper conditions, such as the concentration and the ratio of the reactants, the acidity of the reaction mixture, and the temperature.

Although the catalyzed BZ reaction is the most well studied oscillation system, carbon dioxide produced in this oscillator hampered its application in the study of chemical waves. Since the oxidation of 1,4-cyclohexanedione by acidic bromate has been found to generate chemical oscillations without producing gas bubbles, it has become a frequently used tool for studying reaction-diffusion structure. However, the bromate-CHD oscillation system is much less understood than the BZ reaction system, which is the major drawback in the application of the system for studying spatiotemporal nonlinear behavior. Szalai and Koros studied the 1,4-CHD-bromate-acid oscillatory system by spectrophotometry and suggested that 1,4-CHD undergoes aromatization and one of the main resulting products 1,4-dihydroxybenzene(shown in figure 1.1) is further oxidized and brominated to 1,4-benzoquinone and bromoorganics.[16] Based on their earlier analytical and kinetic investigations, they constructed a detailed mechanistic model, which could simulate the experimental results very well. They found that

played an essential role in the mechanism. During the overall reaction between bromate and 1,4-CHD, H_2Q is an intermediate product from 1,4-CHD via BrCHD. When 1,4-H_2Q accumulates to a certain level, a direct reaction between bromate and H_2Q takes place. Then H_2Q is oxidized autocatalytically to 1,4-benzoquinone (Q) by $BrO_2\cdot$. The time scale difference between the slow production and the fast autocatalytic consumption of H_2Q leads to the oscillatory kinetics.

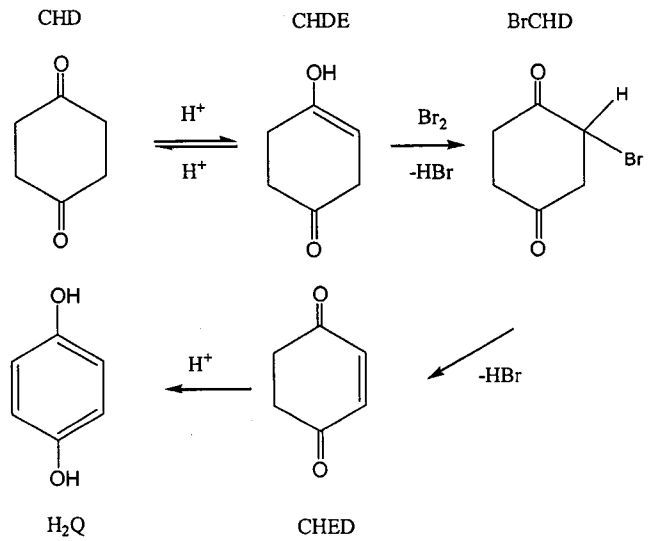

Figure 1.1

Ferroin, as an indicator for the purpose of visualization, could be added in the uncatalyzed bromate-1,4-CHD system. However, the presence of the metal catalyst may change the kinetics of the bromate –CHD system. For example: the amplitude increases and the period decreases proportionally with the increase of ferroin concentration; adding ferroin can also initiate new oscillations after the oscillations have terminated in the uncatalyzed system. Szalai and coworkers developed a model (table1.3) for describing the dynamic behavior of the bromate-1,4-CHD-ferroin oscillator by adding steps involving the reactions of ferroin.[17,18] This modified chemical mechanism includes 22 reactions and 15 species. In this mechanistic model the Br^- consumption processes

(R1-R3) are identical to that of the ferroin-free mechanism. There are two pathways for the autocatalytic production of $HBrO_2$: $BrO_2\cdot$ is reduced to $HBrO_2$ concurrently by 1,4-H_2Q (R7) and by ferroin (R8). This extended mechanism therefore contains two competitive autocatalytic steps: in the first H_2Q serves as the reductant, in the second ferroin is the reductant. The ferriin produced in the autocatalytic cycle can be reduced back to ferroin in several ways: it reacts with 1,4-CHD to produce Q via H_2Q; it can also react with BrCHD to form Q and intermediate Br^-, or it directly oxidizes H_2Q to Q. The metal catalyst effectively participates in both the positive and negative feedbacks, and opens a new autocatalytic pathway.

Table 1.3 Bromate-CHD Oscillation Mechanism

	A Reactions between bromine- containing compounds
1	$Br^- + HOBr + H^+ \leftrightarrow Br_2 + H_2O$
2	$Br^- + HBrO_2 + H^+ \leftrightarrow 2HOBr$
3	$Br^- + BrO_3^- + 2H^+ \leftrightarrow HOBr + HBrO_2$
4	$HBrO_2 + H^+ \leftrightarrow H_2BrO_2^+$
5	$HBrO_2 + H_2BrO_2^+ \rightarrow BrO_3^- + HOBr + H^+$
6	$HBrO2 + BrO_3^- + H^+ \rightarrow 2BrO_2\cdot + H_2O$
7	$H_2Q + 2BrO_2\cdot \rightarrow 2HBrO_2 + Q$
8	$Fe^{2+} + BrO_2\cdot + H^+ \leftrightarrow Fe^{3+} + HBrO_2$
9	$CHD + H^+ \leftrightarrow CHDE + H^+$
10	$CHDE + Br_2 \rightarrow BrCHD + Br^- + H^+$
11	$BrCHD + H^+ \rightarrow CHED + Br^- + 2H^+$
12	$CHED + H^+ \rightarrow H_2Q + H^+$
13	$CHD + BrO_3^- + H^+ \rightarrow H_2Q + HBrO_2 + H_2O$
14	$CHD + HBrO_2 \rightarrow H_2Q + HOBr + H_2O$
15	$H_2Q + BrO_3^- + H^+ \rightarrow Q + HBrO_2 + H_2O$
16	$H_2Q + HOBr \rightarrow Q + Br^- + H^+ + H_2O$
17	$H_2Q + Br_2 \rightarrow Q + 2Br^- + 2H^+$
18	$2Fe^{3+} + CHD \rightarrow 2Fe^{2+} + H_2Q + 2H^+$
19	$2Fe^{3+} + BrCHD \rightarrow Q + Br^- + 3H^+ + 2Fe^{2+}$
20	$2Fe^{3+} + H_2Q \rightarrow 2Fe^{2+} + Q + 2H^+$
21	$Fe^{2+} + BrO_2\cdot + H^+ \rightarrow Fe^{3+} + HBrO_2 + H_2O$

1.4 Complex Oscillations

Complex oscillations are very sensitive to the variation of reaction conditions, therefore they are very useful in characterizing the reaction mechanism. Various complex oscillations have been observed in the cerium catalyzed BZ system. For example, Hudson and coworkers studied the cerium-catalyzed BZ reaction in an isothermal continuously flow stirred tank reactor (CSTR),[19] and they observed simple single peak oscillations at low flow rate and several types of periodic multipeak oscillations at high flow rate. In a closed system, only transient behavior exists and the concept of period doubling and chaos cannot be applied. Wang and co-workers reported transient period doubling, torus oscillations and chaos in a closed BZ oscillatory system[20]. Their observation suggested that the genuine chemical chaos exists in the BZ system.

Transient complex oscillations which are described as the irregular mixture of large and small amplitude oscillations have also been observed in the ferroin-catalyzed BZ reaction. Strizhak and coworkers reported the transient period doubling[21], period adding[22] and regular transient behavior[23] in a closed ferroin-catalyzed BZ oscillation system. Rachwalska observed a new type of mixed-mode periodic oscillations in the BZ reaction in a CSTR. [24] These mixed-mode oscillations are described as LS_n where L donates oscillations with a large amplitude and S means oscillations with substantially smaller amplitudes as compared with L, and n= 0, 1,2,3.....

1.5 Oxygen Influences on the BZ Oscillatory Behaviors

The effect of oxygen has been studied to gain insight into the understanding of the BZ mechanism. The influence of oxygen on the BZ reaction has been investigated by several research groups. For example, oxygen influences on complex oscillations in a closed BZ reaction have been reported by Wang and coworkers,[25] in which the oxygen influence has been controlled via two ways: the first one is to control the concentration of the oxygen with mass flow controller at fixed stirring rate; the other way is to keep the oxygen concentration constant and control the influx of oxygen through the stirring rate. They suggested that the influence of stirring rate under aerobic condition is mainly an oxygen effect as the rate of oxygen transport in the reaction mixture depends on the stirring rate. Effects of oxygen on the cerium-catalyzed BZ reaction at low catalyst concentrations have also been investigated by Petrascu and coworkers.[26] Two phases of oscillations under aerobic condition were observed. The first phase oscillations could be shortened by flowing nitrogen in the reaction mixture to remove the oxygen and the biphasic behavior can be completely quenched by introducing nitrogen 40 minutes earlier than the addition of catalyst. Oliver and co-workers reported oxygen inhibition effect on the BZ reaction at low acid and high organic substrate conditions.[27] They treated oxygen as a dynamic variable and successfully developed a model which was capable of describing the oxygen quenching effect.

Significant progress has been achieved in understanding the effect of oxygen on the ferroin catalyzed BZ reaction. Increase of the oxygen concentration can increase oscillation period, lengthen the induction time and cause earlier death of oscillations.[25-28] Strizhak and coworkers studied the oxygen effects on the time-dependent bifurcations of

transient oscillations in the BZ reaction in a closed system. They proposed a kinetic scheme to describe the effects observed in the experiments which gave a good agreement between the experimental data and the simulations.[28] They suggested that oxygen effect was associate with the oxidation of organic compounds and their intermediates. At first, oxygen reacts with malonyl radicals (MA·) to produce peroxymalonyl radicals (MAOO·), then the next step is associated with chain reactions of MAOO· transformation.

$$BrMA\cdot + O_2 \longrightarrow BrMAOO\cdot$$

$$BrMAOO\cdot + BrMA \longrightarrow BrMA\cdot + BrMAOOH$$

$$Fe(phen)_3^{3+} + BrMAOOH \longrightarrow Fe(phen)_3^{2+} + BrMAOO\cdot$$

1.6 Stirring Effects on Oscillatory Behaviors

In the study of chemical oscillations, concentrations of reactants are taken as spatially uniform and the theoretical interpretation of the nonlinear phenomena are based on the homogeneous model. But one encounters the problem of instability due to the stirring rate in a batch reactor or in a CSTR. This suggests that the heterogeneities may play an unexpected role in nonlinear dynamics. Menzinger and coworkers investigated the heterogeneities and stirring effects in the cerium-catalyzed BZ reaction.[29] They suggested that in a stirred batch reactor large concentration fluctuations indeed exist and appear ubiquitously in the BZ reaction. They found that under anaerobic condition, stirring rate can modify the oscillation parameters such as amplitude and period. Stirring effects on the BZ reaction are also investigated experimentally in a batch reactor by Li and coworkers.[30] They found that the oscillating behavior was sensitive to the rate of stirring even under an atmosphere of nitrogen or argon. This result is further supported by Sevcik

who observed that in a closed batch BZ system the oscillation parameters depend on the rate of stirring rate even in an oxygen-free atmosphere.[31]

In 1985, Menzinger and coworkers studied the heterogeneity stirring effects, by micro- and macroelectrodes in the anaerobic BZ reaction. Their experimental observations proved that: in a stirred batch reactor large concentration fluctuations ubiquitously exist in the ferroin-catalyzed BZ reaction; the concentration fluctuations are spatially distributed rather than homogeneous.[32] Five years later, Menzinger and coworkers investigated the concentration fluctuation and stirring effect on BZ reaction in an open batch reactor.[33] They observed that the fluctuation was dramatically diminished if the gas space above the liquid was eliminated. They suggested that the concentration fluctuation in the aerobic condition primarily arise from the exchange between the liquid and gas phase. The residual fluctuation may arise from the concentration gradients due to the Br_2 adsorption at the wall of the reactor.

Stirring effects on the uncatalyzed 1,4-CHD system was first reported by Farage and Janjic in 1982. They observed that the amplitude of oscillations was amplified by the increase of stirring rate at low stirring rate. In contrast at higher stirring rate after chemical oscillations disappeared decreasing the stirring rate could revive spontaneous oscillations.[34,35] Recently, Bei and Wang in our group reported consecutive bifurcation phenomenon induced by changing stirring rate in the 1,4-CHD –bromate system.[36] They found out that stirring rate can induce transitions not only between oscillatory and nonoscillatory states but also between simple and period-doubled oscillations.

1.7 Temperature Effects on Oscillatory Behaviors:

Temperature is one of the external factors that have pronounced effect on oscillation parameters such as the induction period, the frequency of oscillation, and the duration and the total number of oscillations. Nagy and coworkers studied the effect of temperature in the cerium-catalyzed bromate-driven oscillator.[37] They defined the variation of period with temperature as $Q= (period_1/period_2)^{10/(T_2-T_1)}$ and related it to the activation energy Ea by $Ea = R (T_1T_2/10) \ln Q$. They found that changes in the initial concentration of the organic substrate, bromate ion, or sulfuric acid can induce different changes in the activation energy for various BZ systems. Masia and coworkers studied the temperature effect in a closed unstirred BZ system, and they pointed out that the temperature is a bifurcation parameter of the BZ reaction.[38]

1.8 Photosensitivity Chemical Oscillators

Investigation of photosensitive oscillation systems is a subject of considerable interest because it provides a unique approach to the understanding of interactions between intrinsic dynamics and external forcing The photochemistry of BZ reactions, especially in the Ruthenium (tris(2,2-bipyridine)ruthenium(II) complex) catalyzed oscillation system was studied by many research groups. They suggested that the photochemical production of bromous acid $HBrO_2$ and bromide ion Br^- played a very important role in the system. Kuhnert and coworkers explained the photoproduction of bromide ion by the interaction between the photoexcited $Ru(bpy)_3^{2+}*$ and bromate [39]

$$6Ru(bpy)_3^{2+}* + BrO_3^- + 6H^+ \longrightarrow 6Ru(bpy)_3^{3+} + Br^- + 3H_2O$$

Later, Hanazaki and co-workers found that while light has a accelerating effect on autocatalytic oxidation of $Ru(bpy)_3^{2+}$ by bromate ion and $HBrO_2$ also played an important role in the bromide ion production [40-43]:

$$Ru(bpy)_3^{2+}* + 3Ru(bpy)_3^{2+} + HBrO_2 + 3H^+ \longrightarrow 4Ru(bpy)_3^{3+} + Br^- + 2H_2O$$

Agladze and coworkers suggested that two general route for the production of photogenerated bromide ions,[44] the first one is:

$$Ru(bpy)_3^{2+}* + Ru(bpy)_3^{2+} + BrO_3^- + 3H^+ \longrightarrow 2Ru(bpy)_3^{3+} + HBrO_2 + H_2O$$

and the second one is:

$$4Ru(bpy)_3^{3+} + BrMA + 2\,H_2O \longrightarrow 4Ru(bpy)_3^{2+} + HCOOH + 2CO_2 + Br^- + 5H^+$$

Sorensen and coworkers also studied the light effect on the Ruthenium-catalyzed BZ reaction.[45] Their experimental results demonstrated that chemical oscillations in the Ru-catalyzed BZ reaction can be quenched by light. Their quenching results suggest that $HBrO_2$ and Br^- were produced when the reaction is exposed to light. Four years later, Peter Ruoff also investigated the light-perturbed Ru-catalyzed BZ reaction, which further supported Sorensen's conclusion by providing evidence for photochemically produced species bromous acid and bromide ions. Since explanations of the photochemistry in the Ru-catalyzed BZ differ to some extent, Peter Ruoff and coworkers studied the light-induced phase resetting in more detatil in order to provide the evidence of photochemically produced bromous acid and bromide ions.[46] Their experimental observations suggested that there were two major responses in the light-perturbed Ru-catalyzed BZ reaction. One is the photoproduction of bromous acid at the beginning of the reaction when little BrMA is present, while the other response is the photoproduction

of bromide ions in the presence of a large amount of bromomalonic acid (BrMA) and derivatives.

Huh and coworkers studied the light perturbation in the 1,4-CHD-bromate-ferroin reaction to understand the photosensitivity and hydroquinone effects.[47] They reported the observation of photo-controlled bifurcation phenomenon, in which illumination with visible light can induce or inhibit chemical oscillations. When they used 1,4-H_2Q to gradually replace 1,4-CHD, they found that the induction time decrease with respect to the increase of H_2Q concentration, which further supports the postulation that hydroquinone plays a key role in the 1,4-CHD-bromate-ferroin system.[18] To determine if ferroin plays an important role in the photosensitivity of the above system, Wang and coworkers further studied the uncatalyzed 1,4-CHD-bromate reaction in a batch reactor and in a CSTR.[48] Their new experimental results indicates that a moderate intensity favors oscillations while strong illumination quenches spontaneous oscillations. The experiments in a CSTR suggest that the light influence in the 1,4-CHD system depends not only on the intensity of illumination but also on the phase at which the illumination is switched on. Since the ferroin-catalyzed 1,4-CHD system exhibits similar effect of light, they suggested that ferroin does not play an essential role in the photosensitivity of the ferroin-1,4-CHD-bromate reaction. They also suggested that 1,4-benzoquinone (Q) a stable final product in this system, could be excited by light to produce 1,4-H_2Q, which is in accordance with a report by Gorner.[49]

1.9 The BZ-1,4-CHD Coupled Oscillatory System:

Complex oscillations in the BZ reaction with mixed organic substrates have been reported before. For example, in 1979 Epstein and coworkers reported complex oscillations in the BZ system using three organic substrates: malonic acid (MA), acetylacetone (AA), and ethyl acetoacetate (EA).[50] Each substrate when used alone in the BZ system can only give rise to simple oscillations. In that study, sequential oscillations were observed in the AA-MA (AA and MA mixed as organic substrates) and AA-EA (AA and EA mixed as organic substrates) BZ system catalyzed by Mn^{2+}. Rastogi and coworkers investigated bromate oscillators with ascorbic acid and cyclohexanone as the mixed organic substates.[51] Two types of oscillations separated by a time pause were observed in this system. They pointed out that the first type of oscillations is generated by the ascorbic acid/ cyclohexanone substrates in the BZ system. The second type of oscillations appearing after the time pause is caused by the oxalic acid which is converted from the ascorbic acid during the pause time. Oscillations in the BZ system with oxalic acid (OA) + xylose (XY) as mixed organic substrates have also been investigated by Rastogi and coworkers.[52] They observed single frequency oscillations at low organic concentration and dual frequency oscillations at high concentration. Notably, no oscillations occur when either of OA or XY is used as the organic substrate. Rastogi also investigated bifurcation phenomena in a BZ system with glucose + acetone/cyclohexane, and fructose + acetone/cyclohexanone as mixed substrates in which complex periodic and periodic oscillations were observed.[53] In this thesis, a new coupled oscillator is constructed by introducing 1,4-CHD into the classic BZ reaction. Due to the capability of 1,4-CHD forming an oscillatory system alone, we actually introduced an autocatalytic

feedback in the new coupled system. As a result, there are indeed two oscillatory systems in new system. Due to competitions of the autocatalytic feedbacks, various complex dynamical behaviors such as mixed-mode and sequential oscillations, and burst phenomena are observed.

Chapter2. Theory

2.1 A Cubic Autocatalysis Model

In this chapter, the onset of nonlinear chemical dynamic behaviors is analyzed with a cubic autocatalysis model to gain some insight into how chemical oscillations can arise in general and how it is possible to create chemical reactions that are able of showing oscillatory behavior.[54-56] The example involves the irreversible conversion of a reactant P to a final product C through two intermediate species A and B.[54] There are two chemical pathways by which intermediate A is converted to B.

The first one is an uncatalysed step: $A \longrightarrow B$ rate = $k_u a$

The second is an autocatalytic reaction step: $A+2B \longrightarrow 3B$ rate = $k_1 ab^2$

The second reaction step provides a feedback to the model, since the product B of this step accelerates the reaction rate. The full kinetic scheme is:

$$P \xrightarrow{k_0 p} A \underset{k_u a}{\overset{k_1 ab^2}{\rightleftarrows}} B \xrightarrow{k_2 b} C$$

Or

$$P \longrightarrow A \quad \text{rate} = k_0 p$$

$$A \longrightarrow B \quad \text{rate} = k_u a$$

$$A+2B \longrightarrow 3B \quad \text{rate} = k_1 ab^2$$

$$B \longrightarrow C \quad \text{rate} = k_2 b$$

2.1.1 Kinetic Rate Equations

From the above scheme, the kinetic equations for the change of the concentration of P, A, and B can be described as

$$dp/dt = -k_0 p \qquad (2.1)$$

$$da/dt = k_0p - k_1ab^2 - k_ua \qquad (2.2)$$

$$db/dt = k_1ab^2 + k_ua - k_2b \qquad (2.3)$$

2.1.2 Pseudo-stationary State:

At a stationary-state, the rate of concentrations change of A and B is zero. So

$$k_0p - k_1a_{ss}b_{ss}^2 - k_ua_{ss} = 0 \qquad (2.4)$$

$$k_1a_{ss}b_{ss}^2 + k_ua_{ss} - k_2b_{ss} = 0 \qquad (2.5)$$

Adding these two equations eliminates all terms containing a_{ss} and leads to the simple result

$$b_{ss} = k_0p/k_2 \qquad (2.6)$$

Substituting this into (2.5) we get for a_{ss}

$$a_{ss} = k_2^2k_0p/(k_1k_0^2p^2 + k_2^2k_u) \qquad (2.7)$$

Thus the stationary concentration of B is directly proportional to that of the reactant P.

(1) Dependence of a_{ss} and b_{ss} on P

It is necessary to establish the way in which a_{ss} and b_{ss} vary with P. Then the pseudo-stationary-state is regarded as a simple function of P. The stationary-state loci are shown in figure.2.1. At high concentration of reactant, the stationary-state concentration of B is higher than that of A, at low P, a_{ss} is greater than b_{ss}. The two loci cross when:

$$a_{ss} = b_{ss} = [(k_2 - k_u)/k_1]^{1/2} \qquad (2.8)$$

At the cross point:

$$p = (k_2/k_0)[(k_2-k_u)/k_1]^{1/2} \qquad (2.9)$$

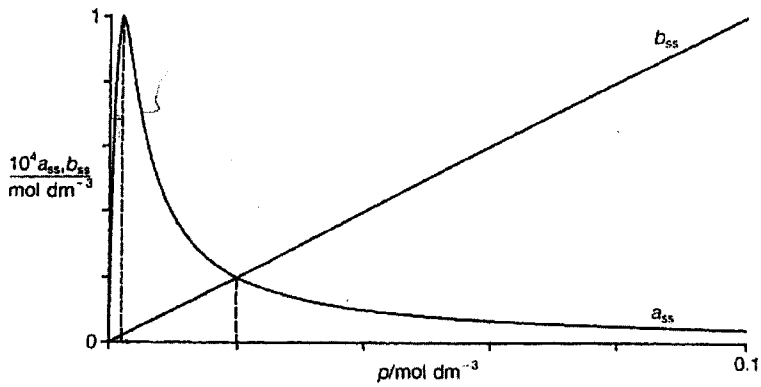

Figure 2.1 (taken from reference 54)

The maximum of stationary-state concentration of A is

$$(a_{ss})_{max} = \frac{1}{2}\, k_2/(k_1/k_u)^{1/2} \qquad (2.10)$$

and this is attained when

$$p = (k_2^2 k_u/k_1 k_0^2)^{1/2} \qquad (2.11)$$

The locations of crossing and maximum points in the figure give an upper and lower bound, on the range of conditions over which the oscillations are expected to be observed.

(2) Time dependence of pseudo-stationary states

It could also be estimated how they change during an experiment. From equation 2.1, we can get

$$p(t) = p_0 \exp(-k_0 t) \qquad (2.12)$$

By substituting eqn (2.6) and (2.7) for P from (2.12), we get

$$a(t) = k_2^2 k_0 p_0 \exp(-k_0 t) / [k_1 k_0^2 p_0^2 \exp(-2k_0 t) + k_2^2 k_u] \qquad (2.13)$$

$$b(t) = k_0/k_2\, p_0 \exp(-k_0 t) \qquad (2.14)$$

The pseudo-steady-state results are shown in figure 2.2, in which b(t) falls exponentially throughout the reaction while a(t) reaches the maximum before decaying.

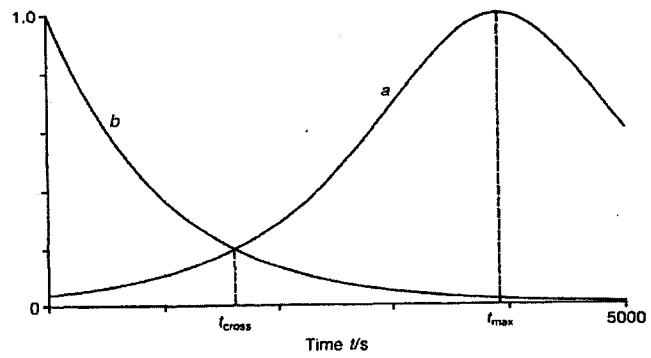

Figure 2.2 (taken from reference 54)

2.2 Dimensionless Analysis

It is convenient to make a full analysis of the above scheme by using dimensionless concentrations. In this section, we use α to present the dimensionless concentration of A and β for the dimensionless concentration of B. Once the transformation has been achieved we can make a comprehensive analysis of the behavior of this cubic chemical oscillator.

2.2.1 Dimensionless Equations:

Recall that the reaction rate equations for the model shown in section 2.1 are:

$$dp/dt = -k_0 p \qquad (2.15)$$

$$da/dt = k_0 p - k_1 a b^2 - k_u a \qquad (2.16)$$

$$db/dt = k_1 a b^2 + k_u a - k_2 b \qquad (2.17)$$

(1) Dimensionless concentration:

The dimensionless concentration can be obtained by dividing the physical concentration by some characteristic concentrantion scale. In section 2.1, the stationary-state concentration of A and B cross at a particular point, where in the limit k_u=0,

$a_{ss}=b_{ss}=(k_2/k_1)^{1/2}$. If the concentrations of species are divided by this scale, we can get the dimensionless form:[54]

Reactant P: $\pi= (k_1/k_2)^{1/2}p$ (2.18)

Intermediate A $\alpha= (k_1/k_2)^{1/2}a$ (2.19)

Intermediate B $\beta= (k_1/k_2)^{1/2}b$ (2.20)

(2) Dimensionless time:

The frequency of oscillations at the cross point is k_2. The inverse of this value $1/k_2$ can be used as standard time scale.[54] So the dimensionless time τ is

$$\tau = k_2 t \quad (2.21)$$

(3) Dimensionless rate constant ratios:

We can get dimensionless rate constant by dividing the rate constant by k_2.[54] So the dimensionless rate constant is defined as:

$$\epsilon = k_0/k_2 \quad \text{and } \kappa_u = k_u/k_2 \quad (2.22)$$

(4) Dimensionless forms of rate equations:

for P: $d\pi/d\tau = - \epsilon \pi$ (2.23)

for A $d\alpha/d\tau = \epsilon\pi - \alpha\beta^2 - \kappa_u \alpha$ (2.24)

for B $d\beta/d\tau = \alpha\beta^2 + \kappa_u \alpha - \beta$ (2.25)

and the initial conditions become

$$\pi = \pi_0 \quad \alpha=\beta= 0 \quad \text{at } \tau =0 \quad (2.26)$$

from eqn 2.23 we can get

$$\pi= \pi_0 e^{-\epsilon\tau}, \quad (2.27)$$

substituting equation 2.27 into the rate equation for A, we have

$$d\alpha/d\tau = \epsilon \pi_0 e^{-\epsilon\tau} - \alpha\beta^2 - \kappa_u \alpha \quad (2.28)$$

if we define $\mu_0 = \epsilon\ \pi_0$ (2.29)

and introducing μ_0 into eqn(2.28), we have

$$d\alpha/d\tau = \mu_0 e^{-\epsilon\tau} - \alpha\beta^2 - \kappa_u \alpha$$

$$= \mu - \alpha\beta^2 - \kappa_u \alpha \quad (2.30)$$

where $\mu = \mu_0 e^{-\epsilon\tau}$ (2.31)

So the dimensionless rate equations for intermediate concentrations are now: [54]

$$d\alpha/d\tau = \mu - \alpha\beta^2 - \kappa_u \alpha \quad (2.32)$$

$$d\beta/d\tau = \alpha\beta^2 + \kappa_u \alpha - \beta \quad (2.33)$$

(5) Stationary-state solutions

The stationary states are found by setting $d\alpha/d\tau = 0$, $d\beta/d\tau = 0$, so that

$$\mu - \alpha_{ss}\beta_{ss}^2 - \kappa_u \alpha_{ss} = 0 \quad (2.34)$$

$$\alpha_{ss}\beta_{ss}^2 + \kappa_u \alpha_{ss} - \beta_{ss} = 0 \quad (2.35)$$

We get

$$\alpha_{ss} = \mu / (\mu^2 + \kappa_u) \quad (2.36)$$

$$\beta_{ss} = \mu \quad (2.37)$$

there is a linear relationship between β_{ss} and μ, as shown in figure 2.3, and the α_{ss} shows a maximum

$$(\alpha_{ss})_{max} = \tfrac{1}{2} \kappa_u^{-1/2} \text{ at } \mu = \kappa_u^{1/2} \quad (2.38)$$

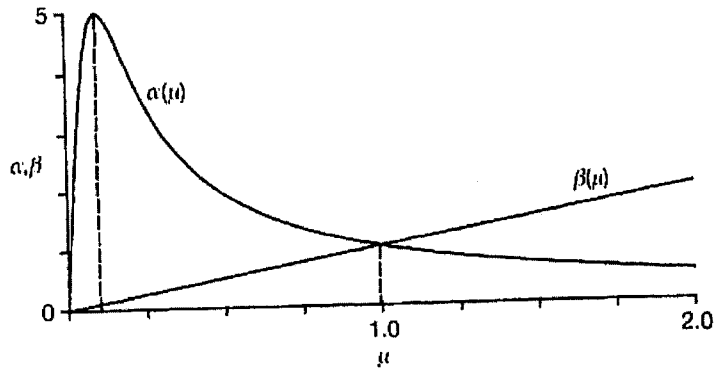

Figure 2.3 (taken from reference 54)

The α_{ss} and β_{ss} cross when

$$\alpha_{ss} = \beta_{ss} = (1 - \kappa_u)^{1/2} \quad \text{when} \quad \mu = (1 - \kappa_u)^{1/2} \tag{2.39}$$

2.2.2 Local Stability Analysis

The local stability of a given stationary state can be determined by the result when it is subjected to an infinitesimally small perturbation. If the perturbation grows, this stationary state is unstable. On the contrary, if the perturbation decays, this stationary state is local stable.

2.2.3 Time Dependence of Small Perturbations:

Equation (2.32) and (2.33) can be written in the shorthand form

$$d\alpha/d\tau = f(\alpha,\beta) \tag{2.40}$$

$$d\beta/d\tau = g(\alpha,\beta) \tag{2.41}$$

so

$$f(\alpha,\beta) = \mu - \alpha\beta^2 - \kappa_u \alpha \tag{2.42}$$

$$g(\alpha,\beta) = \alpha\beta^2 + \kappa_u \alpha - \beta \tag{2.43}$$

The stationary states are defined as the solution of

$$f(\alpha_{ss},\beta_{ss}) = 0 \qquad g(\alpha_{ss},\beta_{ss}) = 0 \qquad (2.44)$$

If the system is given a small perturbation, the concentration of A and B become

$$\alpha = \alpha_{ss} + \Delta\alpha \qquad \beta = \beta_{ss} + \Delta\beta \qquad (2.45)$$

If $\Delta\alpha << 1$ and $\Delta\beta << 1$, the rate of change of perturbations can be obtained by substituting these forms into eqns (2.40) and (2.41) and expanding as Taylor series:[54]

$$d\Delta\alpha/d\tau = d\alpha/d\tau = f(\alpha_{ss},\beta_{ss}) + (\partial f/\partial\alpha)_{ss}\,\Delta\alpha + (\partial f/\partial\beta)_{ss}\,\Delta\beta + \ldots\ldots (2.46)$$

$$d\Delta\beta/d\tau = d\beta/d\tau = g(\alpha_{ss},\beta_{ss}) + (\partial g/\partial\alpha)_{ss}\,\Delta\alpha + (\partial g/\partial\beta)_{ss}\,\Delta\beta + \ldots\ldots (2.47)$$

because the perturbation is infinitesimally small, the higher-order powers can be neglected.

Due to eqn. (2.44) $f(\alpha_{ss},\beta_{ss}) = 0$ and $g(\alpha_{ss},\beta_{ss}) = 0$, the first term on the right-hand side can be eliminated. Thus, the perturbation is governed by a pair of linear equations

$$d\Delta\alpha/d\tau = (\partial f/\partial\alpha)_{ss}\,\Delta\alpha + (\partial f/\partial\beta)_{ss}\,\Delta\beta \qquad (2.48)$$

$$d\Delta\beta/d\tau = (\partial g/\partial\alpha)_{ss}\,\Delta\alpha + (\partial g/\partial\beta)_{ss}\,\Delta\beta \qquad (2.49)$$

the solution of the above differential equations is:[54]

$$\Delta\alpha(\tau) = c_1 e^{\lambda_1\tau} + c_2 e^{\lambda_2\tau} \qquad (2.50)$$

$$\Delta\beta(\tau) = c_3 e^{\lambda_1\tau} + c_4 e^{\lambda_2\tau} \qquad (2.51)$$

The coefficients c_1-c_4 are constants which depend on the size and sign of the initial perturbation. The sign (positive or negative) and the character (real or complex) of λ_1 and λ_2 determine how the perturbations decay or grow. These exponent can be determined as the eigenvalues of the Jacobian matrix of eqns (2.48) and (2.49): [54]

$$J = \begin{pmatrix} \partial f/\partial\alpha & \partial f/\partial\beta \\ \partial g/\partial\alpha & \partial g/\partial\beta \end{pmatrix}_{ss} \qquad (2.52)$$

the subscript "ss" means the elements are evaluated at a stationary state. The eigenvalues of λ_1 and λ_2 are given by the roots of the equation

$$\lambda^2 - \mathrm{tr}(J)\,\lambda + \det(J) = 0 \qquad (2.53)$$

from the Jacobian matrix,we can get

$$\mathrm{tr}(J) = \partial f/\partial\alpha + \partial g/\partial\beta \qquad (2.54)$$

$$\det(J) = (\partial f/\partial\alpha)_{ss}\,(\partial g/\partial\beta)_{ss} - (\partial f/\partial\beta)_{ss}(\partial g/\partial\alpha)_{ss} \qquad (2.55)$$

so the roots of the eqns (2.50) and (2.51) are:

$$\lambda_{1,2} = \tfrac{1}{2}\,\{\,\mathrm{tr}(J) \pm [\mathrm{tr}(J)^2 - 4\det(J)]^{1/2}\} \qquad (2.56)$$

The sign and character of λ_1 and λ_2 depend on the signs and magnitudes of tr(J) and det(J) Figure 2.4 shows the different phase plane patterns.

(a) $\mathrm{tr}(J)<0$, $\det(J)>0$, and $\mathrm{tr}(J)^2 - 4\det(J)>0$

Under this condition, λ_1 and λ_2 are both real and have negative values. The perturbation will decay to zero and the system will return to a stationary state. This stationary state is called *stable node.* [54]

(b) $\mathrm{tr}(J)<0$, $\det(J)>0$, and $\mathrm{tr}(J)^2 - 4\det(J)<0$

In this case, the eigenvalues of λ_1 and λ_2 are complex numbers

$$\lambda_{1,2} = \mathrm{Re}(\lambda) \pm i\mathrm{Im}(\lambda) \qquad (2.57)$$

$$\mathrm{Re}(\lambda) = \tfrac{1}{2}\,\mathrm{tr}(J) \qquad \mathrm{Im}(\lambda) = \tfrac{1}{2}\,[4\det(J) - \mathrm{tr}(J)^2]^{1/2} \qquad (2.58)$$

The real part will have the same sign and both are negative, so the perturbation undergoes a cosine function decay. This stationary is known as *stable focus.*[54]

(c) $\mathrm{tr}(J)>0$, $\det(J)>0$, and $\mathrm{tr}(J)^2 - 4\det(J)<0$

λ_1 and λ_2 are complex eigenvalues, but now they have positive real parts. The perturbation will grow in time, so this is called *unstable focus.*

(d) $tr(J)>0$, $det(J)>0$, and $tr(J)^2 - 4\,det(J)>0$

λ_1 and λ_2 are real and both positive. The perturbation will increase monotonically in time. The system will move directly away from the *unstable nodal* state.

(e) $det(J)<0$

the root of eqn (2.53) are real and have opposite sign. The negative eigenvalue decreases exponentially, while the positive root will increase in time. Therefore, only in the very special case will the perturbation decay back to the stationary state. For a general perturbation, the system will move away from the stationary state. This is known as *saddle point* behavior.[54]

(f) $tr(J)=0$, $det(J)>0$ (hopf bifurcation)

under these conditions, the eigenvalues become imaginary numbers

$$\lambda_{1,2} = \pm i\,det(J)^{1/2} = \pm i\omega_0 \qquad (2.59)$$

The perturbations would be equivalent to an undamped cosine function of frequency ω_0, leading to indefinitely sustained oscillations.

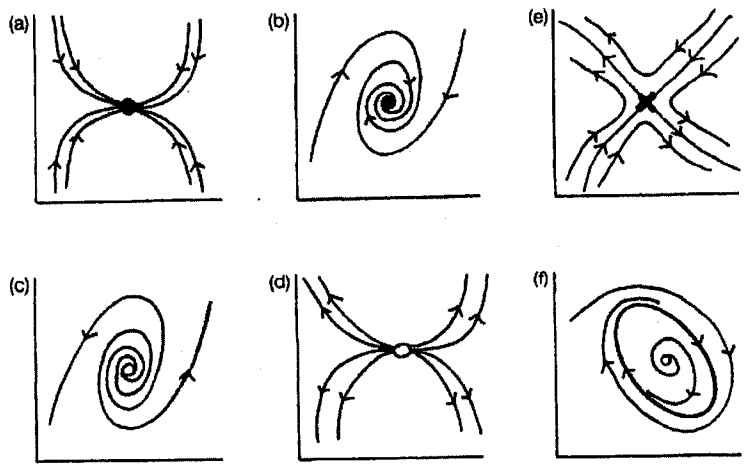

Figure 2.4 (taken from reference 54)

2.3 Analysis of the reaction behavior in a CSTR

2.3.1 Cubic autocatalysis:

Chemical oscillations can also be studied in a CSTR in which the reactor is fed by a stream of liquid with a volume flow rate of q dm^3s^{-1}in which the concentration of A is a_0. If the volume of the reactor is V dm^3, the average time spent by a molecule in the reactor is V/q s. This is called the mean residence time, $t_{res.}$ The inverse of t_{res} has units of s^{-1}.

For a simple cubic autocatalytic reaction:

$$A + 2B \longrightarrow 3B \quad \text{rate} = k_1ab^2$$

$$da/dt = (a_0\text{-}a)/t_{res} - k_1ab^2 \qquad (2.60)$$

$$db/dt = (b_0\text{-}b)/t_{res} + k_1ab^2 \qquad (2.61)$$

Due to stoichiometry of the reaction, the concentration of A and B are linked to the inflow concentration:

$$a + b = a_0 + b_0, \text{ so that } b = (a_0 + b_0) - a \qquad (2.62)$$

substituting this into (2.60), we got

$$da/dt = (a_0\text{-}a)/t_{res} - k_1a(a_0 + b_0 - a)^2 \qquad (2.63)$$

2.3.2 Dimensionless groups:

To obtain dimensionless forms for this model, we need a reference concentration and a reference timescale. The inflow concentration of the reactant a_0 could be a good concentration scale.

$$\alpha = a/a_0 \quad \beta = b/a_0 \text{ and } \beta_0 = b_0/a_0 \qquad (2.64)$$

There is a limit for α and β,

$$0 \le \alpha \le 1, \qquad 0 \le \beta \le 1 + \beta_0 \qquad (2.65)$$

Residence time t_{res} could be a timescale. However, if the experiment involves the variation of t_{res}, this is not that convenient. Instead, the rate constant k_1 can be used as a timescale if treated properly.

Since k_1 is a third-order reaction rate constant, with units of $(\text{concentration})^{-2}(\text{time})^{-1}$, it is multiplied by a_0^2, and taken an inverse can give a timescale.

$$t_{ch} = 1/ k_1 a_0^2 \qquad (2.66)$$

so the dimensionless time τ and residence time τ_{res} are:

$$\tau = k_1 a_0^2 t = t/t_{ch} \qquad (2.67)$$

$$\tau_{res} = k_1 a_0^2 t_{res} = t_{res}/t_{ch} \qquad (2.68)$$

so the dimensionless equation can be written as

$$d\alpha/d\tau = (1-\alpha) / \tau_{res} - \alpha (1+ \beta_0 - \alpha)^2 \qquad (2.69)$$

$$\text{L} \qquad\qquad \text{R}$$

In this equation, $1-\alpha$ is the extent of conversion. Figure 2.5 shows L (inflow rate) and R (reaction rate) as the functions of the extent of conversion. The reaction line R is not dependent on the residence time τ_{res}, and the flow line is zero at the complete conversion point $1-\alpha = 0$. Figure 2.5(b) shows the flow line at different residence times: it is steep for short residence time and flat for long τ_{res}. However, the flow line does not depend on the inflow concentration of autocatalyst β_0.

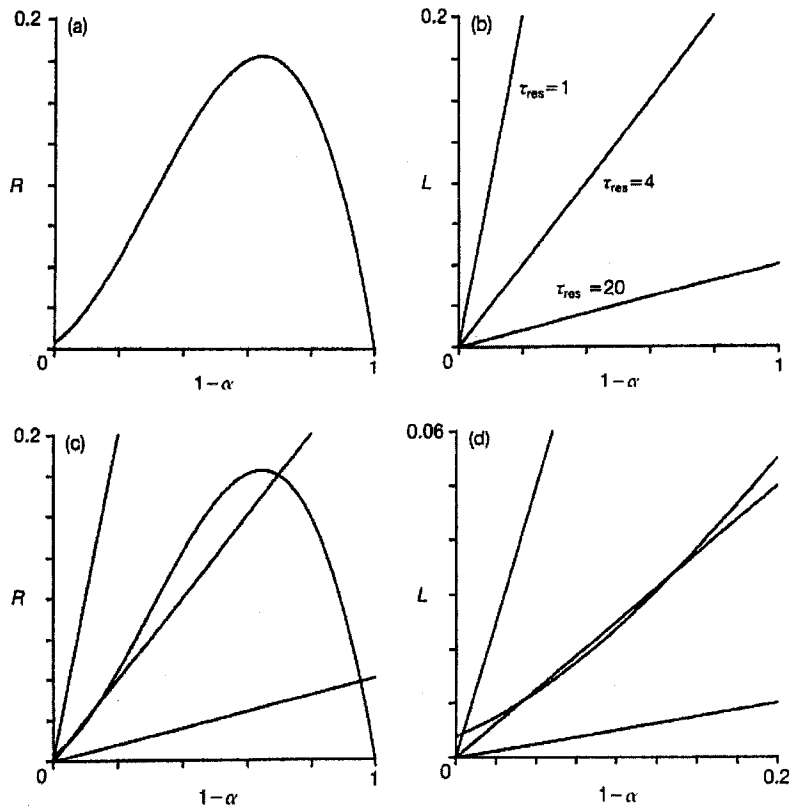

Figure 2.5 (taken from reference 54)

Stationary states are at the intersections of L and R line where $d\alpha/d\tau = 0$ shown in figure 2.5(c) and (d). For short residence time, L is steep and there is only one intersection close to the origin. If the τ_{res} is increased there are two intersections at high reaction extent. Further increasing τ_{res}, the two intersections merge leaving only one stationary state.[54]

Chapter3. Numerical Simulations of complex Oscillations in the Ferroin-catalyzed BZ Reaction

Due to the striking color changes between the oxidized and reduced states of the metal catalyst ($Fe(phen)_3^{3+}/Fe(phen)_3^{2+}$) in the BZ reaction, it has provided a convenient way to investigate pattern formation in a spatially extended medium.[57-68] In the early 1970's, FKN mechanism has been proposed to account for the behavior observed primarily in the cerium-catalyzed BZ reaction.[7] Ferroin, originally used as a redox indicator to enhance the color changes in the Cerium-BZ reaction, was later shown to be capable of acting on its own as a catalyst. One may think that the ferroin catalyzed BZ oscillation mechanism could be established by replacing Ce by ferroin and then modifying these rate constants of the FKN theory. However, Gaspar and co-workers failed to simulate chemical oscillations observed in the ferroin catalyzed BZ system by the mechanism based on the FKN theory.[13,14] They suggested that reactions between ferriin and bromide and between ferroin and bromine, HOBr, etc. should also be considered in the ferroin-catalyzed BZ model. To gain further insight into the ferroin-catalyzed BZ reaction mechanism, the dynamic behavior of the ferroin-BZ reaction in a batch reactor under anaerobic conditions was systematically investigated in our group which uncovered that the ferroin-catalyzed BZ system was capable of exhibiting two isolated bifurcation window even under closed reaction conditions. Detailed numerical simulations of these new complex phenomena in the ferroin-BZ reaction are conducted in this chapter.

3. 1 Examples of New Experimental Results

Figure 3.1 presents the time series obtained under the following initial compositions: $[H_2SO_4]$ = 0.38M, [MA] = 0.30M, [Ferroin] = 5.0×10^{-4}M, and $[BrO_3^-]$ = 0.10M. There is a short induction period before spontaneous oscillations emerge. Within the first 500 seconds every large peak is followed by a small peak, resembling period-doubled oscillations. As the amplitude of small peaks increases in time, the BZ reaction smoothly evolves into simple period-1 oscillations. Significantly, period-doubled oscillations appeared again at about t = 3200 seconds, followed by other modes of complex oscillations. In contrast to the short life time of the first group of complex oscillations, the second bifurcation sequence lasted for more than 4 hours.

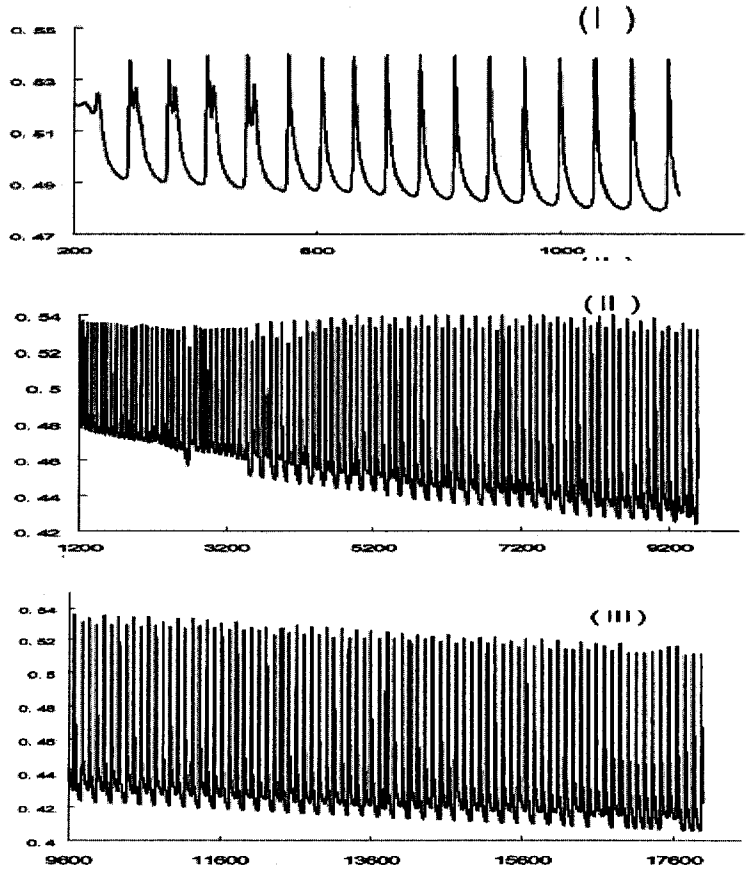

Figure 3.1

Figure 3.1 illustrates that the closed ferroin-BZ reaction evolves through two bifurcation regimes, where the first bifurcation regime appears as soon as spontaneous oscillations begin. Such phenomena has not been reported in the BZ system, despite the BZ system has been extensively investigated for more than three decades.

3.2 Computational Results:

Keki and co-workers suggested that reactions between ferriin and bromide and between ferroin and $HBrO_2$, HOBr, Br_2, etc. shall also be considered when simulating the ferroin-catalyzed BZ system.[13] Working out from the same viewpoint, Strizhak and co-workers proposed a model by incorporating those reactions suggested by Keki et al. to describe complex oscillations in the ferroin-catalyzed BZ reaction observed in a CSTR.[14] Their model, listed in Table 3.1, consists of 12 reagent species (variables) and 29 steps. Since the model successfully reproduced the bifurcation sequence observed in the CSTR, it was employed here as a prototype model to simulate the ferroin-BZ reaction in a batch reactor. When the model was directly applied to simulate the closed ferroin-catalyzed BZ reaction, no complex oscillations could be seen under the same conditions as employed in our experiments. Indeed, no complex phenomena could be achieved in the modeling even when initial concentrations of all reactants were adjusted over a broad range. To obtain transient complex oscillations, three rate constants, namely, k_{15}, k_{21}, and k_{29}, have been adjusted here. k_{15} was increased to be 100 times higher while k_{21} and k_{29} became, respectively, 7 and 40 times smaller than those values used by Strizhak and co-workers.[36]

An example of transient complex oscillations calculated from the model is presented in Figure 3.2, in which the initial concentration of bromate is (a) 0.11 M, (b) 0.09 M, (c)

0.07 M, and (d) 0.06 M. Initial values of other reactants in the above calculations matched those used in experiments, $[H_2SO_4]$ = 0.38M, [MA] = 0.30M, $[BrO_3^-]$ = 0.10M, [ferroin] = 5×10^{-4} M. Similar to the experimental observation, when the initial concentration of bromate was too low, such as 0.06 M in the time series Figure shown 3.2d, no complex oscillations occurred. On the other hand, as the bromate concentration was increased, complex oscillations became more complicated. Notably, in Figures 3.2 a and b the small peak of the period-doubled oscillations become invisible at $t \approx 2000$s even under logarithmic scale, implying that period-doubled oscillations tend to cease here. Beyond that point, the small peak revived and became more and more prominent in time. From a dynamic point of view, such a scenario implicates that a reverse period-doubling bifurcation takes place at $t \approx 1800$ s to lead the system back to simple oscillations, which is then followed by another forward period-doubling bifurcation leading the system to complex oscillations.

In Figure 3.2c, the first group of period-doubled oscillations, which appeared before $t = 1800$ s, disappeared spontaneously, while period-doubled oscillations which resembled the second part of period-doubled oscillations shown in Figure 3.2a, b were still there. This suggests that period-doubled oscillations appearing before $t \approx 1800$ s may correspond to the first bifurcation regime observed in experiments, whereas complex oscillations appearing after $t \approx 1800$ s correspond to the second bifurcation regime.

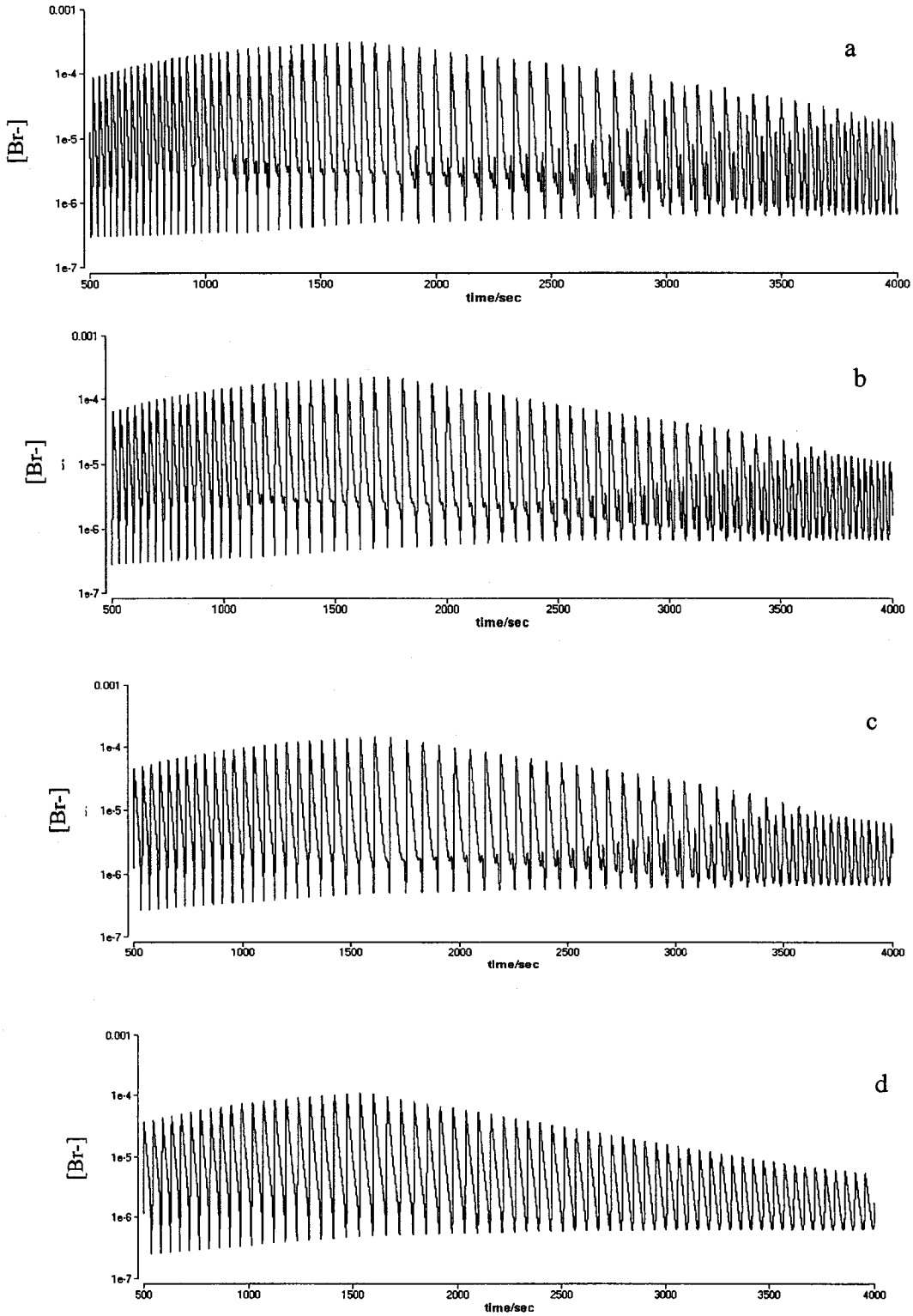

Figure 3.2

Our numerical simulations further illustrated that the complex dynamic behavior of the ferroin-catalyzed BZ reaction was particularly sensitive to variations of the following rate constants: k_1, k_{15}, k_{19}, k_{21}, k_{22}, and k_{29}. For example, both increasing and decreasing the value of k_1 from that used in this study reduced the complexity of BZ oscillations. The results are shown in figure 3.3: (a) k_1= 0.6, (b) k_1=2.0, and (c) k_1= 3.0

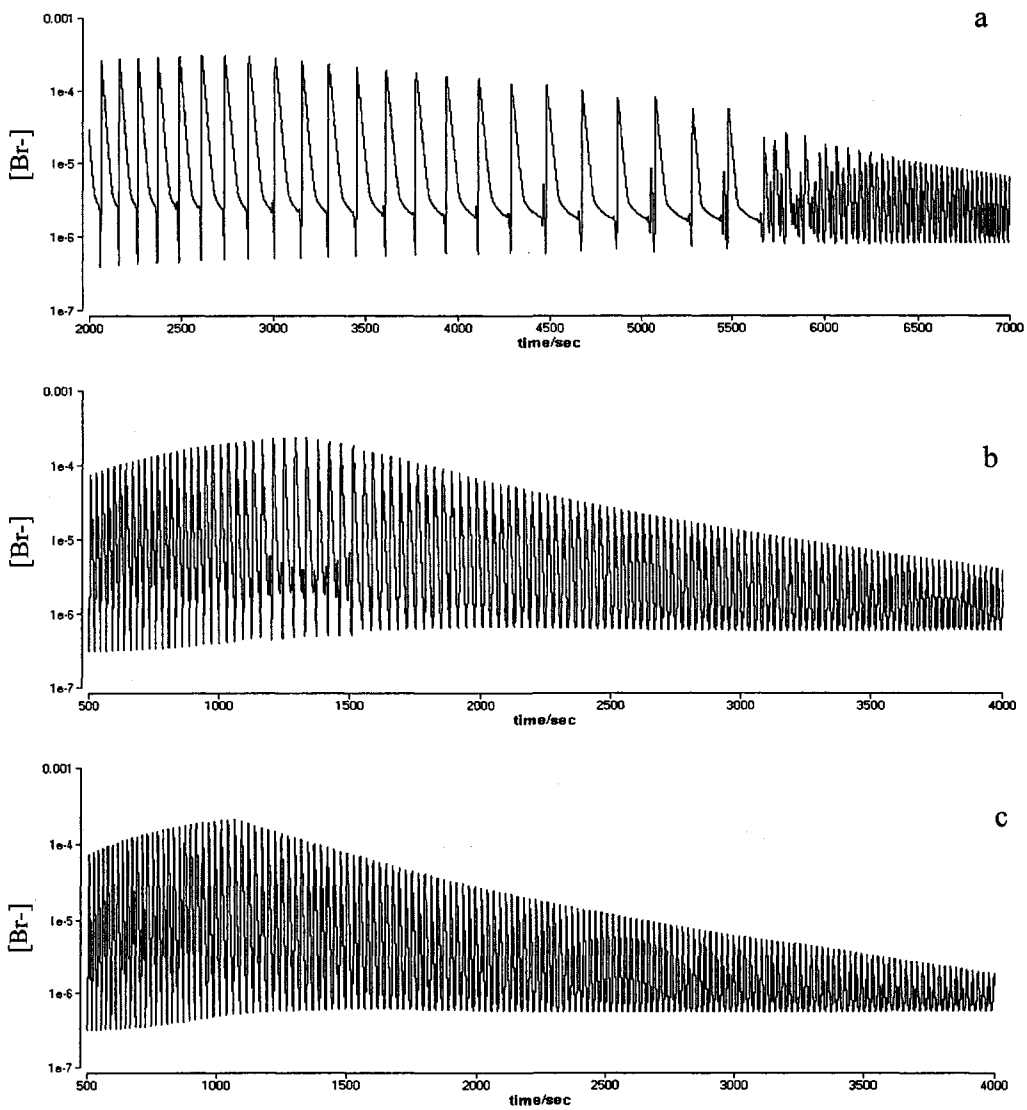

Figure 3.3

Similar influences were observed in figure 3.4 when the rate constants k_{19} was characterized (a) k_{19} =0.2 (b) k_{19} = 3.0

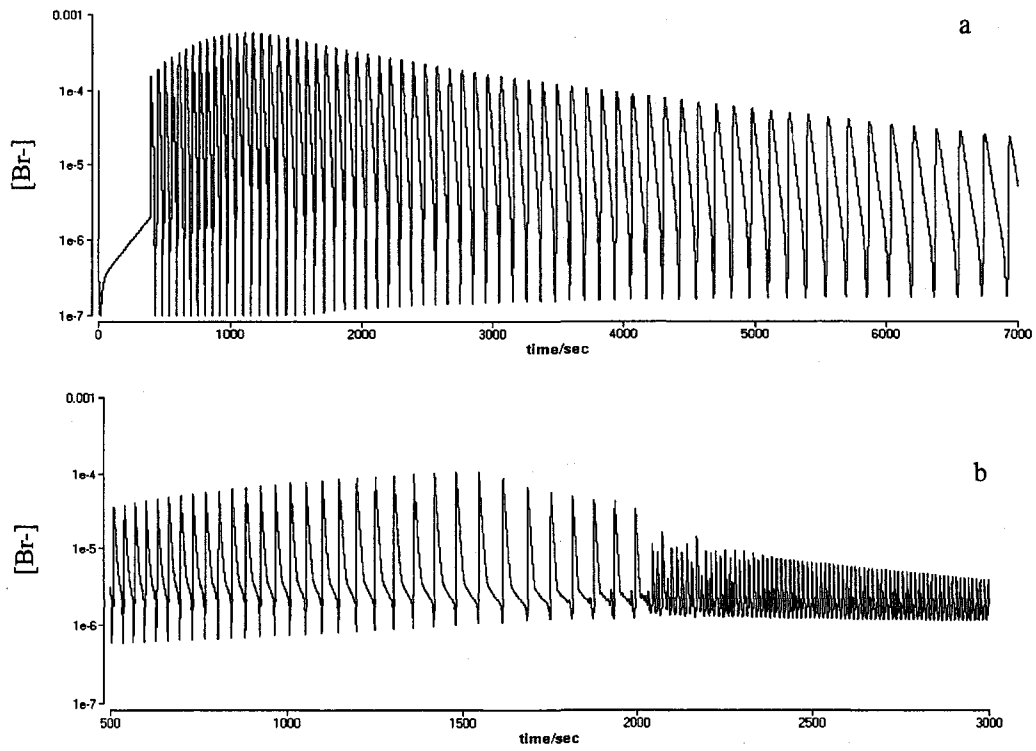

Figure 3.4

The influence of rate constants k_{15}, k_{21}, and k_{29} is characterized respectively in figure 3.5 (a) $k_{15}=1.0\times10^{11}$, (b) $k_{21}=3.0\times10^{8}$, and (c) $k_{29}=5.0\times10^{8}$. Figure 3.5 (a) shows that when the rate constant k_{15} is decreased to 1.0×10^{11} from the value used in table 3.1, complex oscillations cannot be observed anymore; however when k_{15} is above the value 1.0×10^{11}, complex oscillations can always be observed. This indicates that there is a threshold for the rate constant k_{15}. Similar to k_{15}, rate constants k_{21} and k_{29} have a threshold value too. Figures 3.5 (b) and (c) indicate that when these two rate constants are increased from their original values to 3.0×10^{8} for k_{21} and 5.0×10^{8} for k_{29}, the complex oscillations could not be observed anymore.

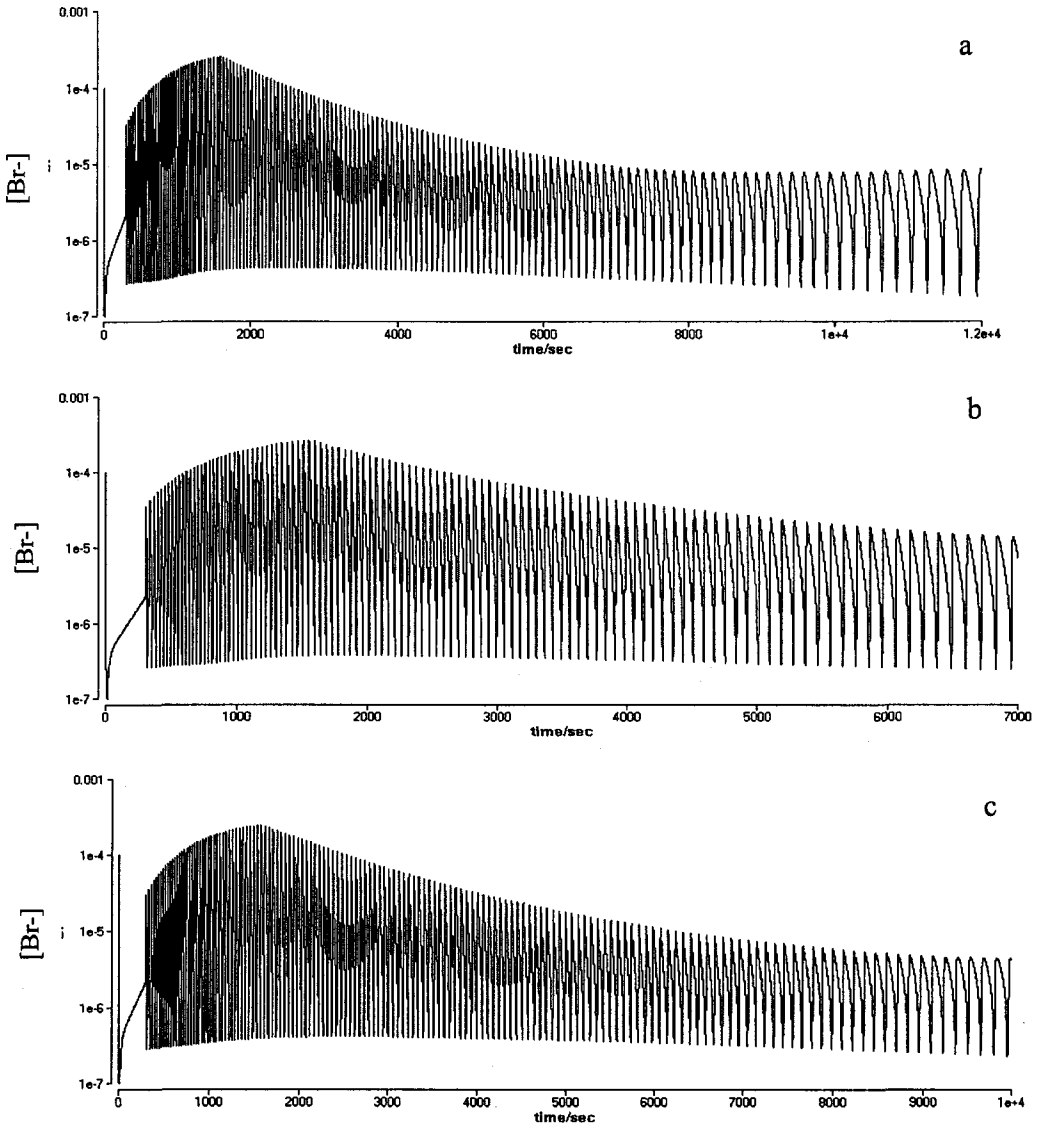

Figure 3.5

As discussed earlier, an essential difference between the FKN mechanism and the model proposed by Strizhak and co-workers is that the later considered reactions between ferroin/ferriin and HOBr, Br_2, $HBrO_2$, etc.[7,14] To examine the importance of those new steps in the development of complex oscillations, we have respectively adjusted rate

constants k_{22}, k_{23}, k_{24}, k_{25}, and k_{26}. These calculations illustrate that variation of k_{22} has significant effects on complex oscillations. Indeed, complex oscillations could be obtained only when k_{22} is within a proper range. Figure 3.6 shows the simulations when k_{22} is out of this range (a) k_{22} = 5 (b) k_{22} = 0.1. It is obvious that when k_{22} is beyond this proper range the numerical simulations do not match the experimental observations.

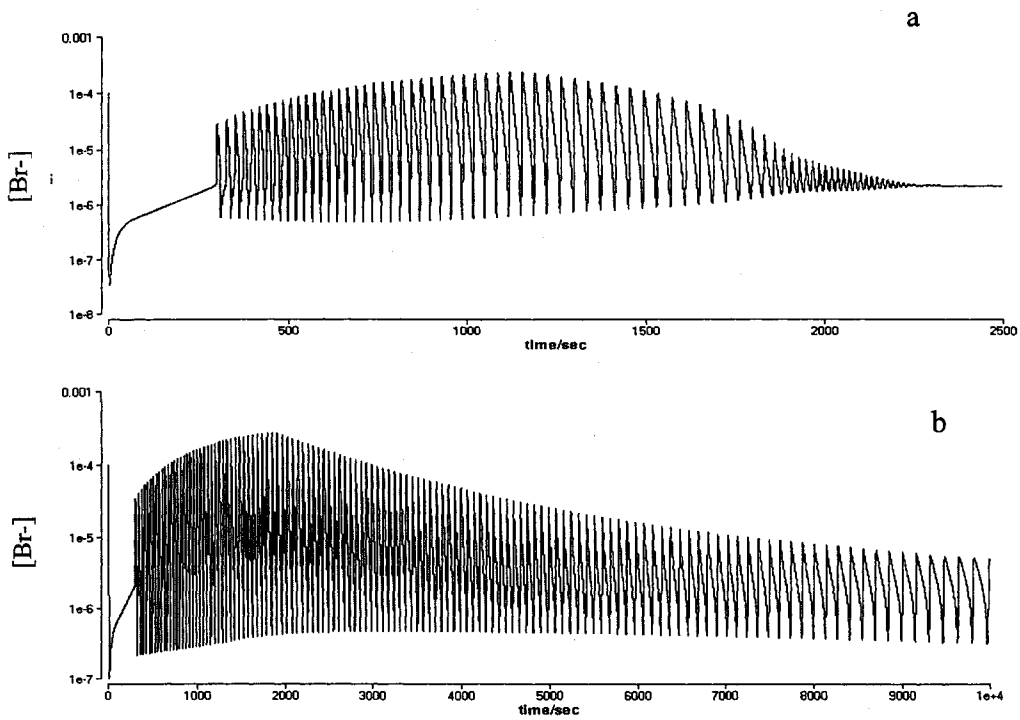

Figure 3.6

However, when k_{23}, k_{24}, and k_{26} were changed to 0, which corresponded to excluding those reactions from the proposed mechanism, there was no change at all in the complex oscillation pattern. Figure 3.7 shows the oscillations obtained when k_{23}, k_{24}, and k_{26} are set to zero: (a) k_{23} =0, (b) k_{24} =0 and (c) k_{26} =0. This simulation result indicates that reactions 23, 24 and 26 do not play an essential role in the development of complex oscillations.

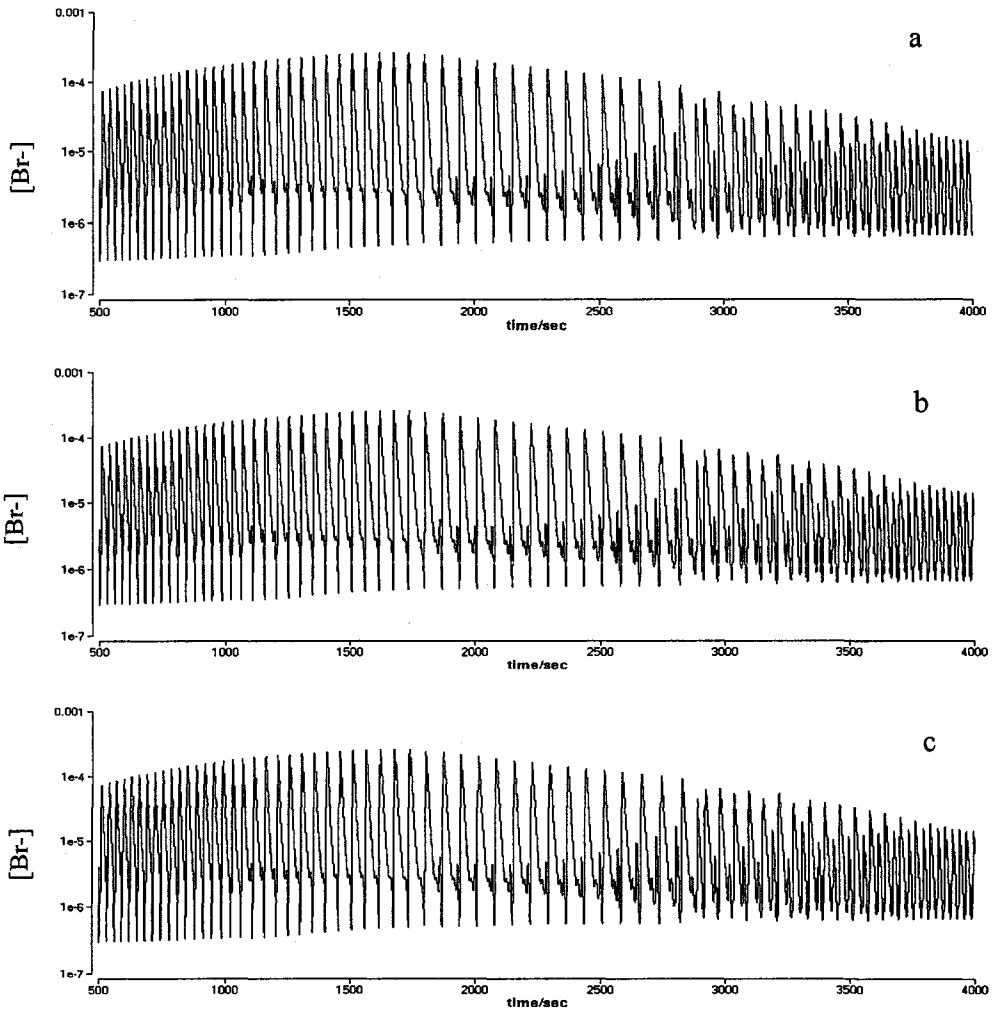

Figure 3.7

However, when k_{25} was adjusted to 0, complex oscillations became slightly simpler as shown in figure 3.8

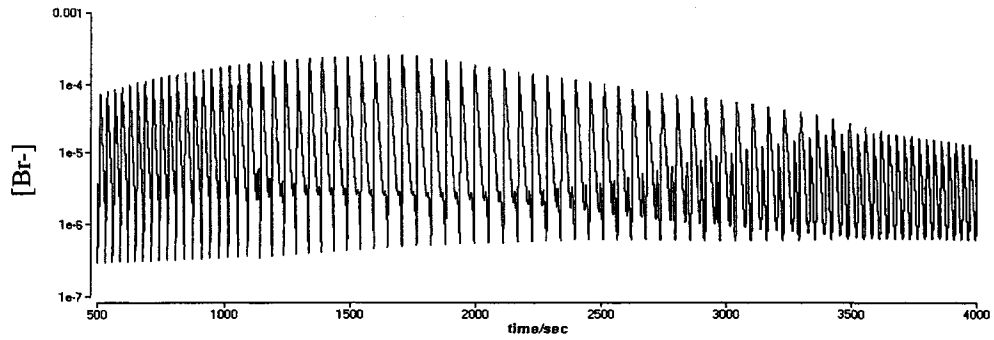

Figure 3.8

3.3 Conclusions:

In this study, the ferroin-catalyzed BZ reaction in a closed system was investigated numerically. Simulations with a model developed initially by Strizhak and co-workers have successfully reproduced the transient complex oscillations observed in our experiments.[95] The bifurcation sequence in the modeling also appears to consist of two regimes, in which the first part of period-doubled oscillations disappears simultaneously as a result of varying reaction parameters, i.e., decreasing BrO_3^- concentration. Unfortunately, in this simulation no simple oscillations (i.e., one peak per period) was obtained between the two bifurcation regimes, despite adjusting rate constants as well as initial values of all reactants over a broad range.

Numerical simulations conducted in this study also illustrated that eliminating the following three reaction steps from the model listed in Table 3.1 had no influence on transient complex oscillations:

23. $2Fe(phen)_3^{2+} + HBrO_2 + 2H^+ \rightarrow 2Fe(phen)_3^{3+} + HOBr + H_2O$

24. $2\,Fe(phen)_3^{2+} + HOBr + H^+ \rightarrow 2Fe(phen)_3^{3+} + Br^- + H_2O$

26. $2Fe(phen)_3^{3+} + 2\,Br^- \rightarrow 2\,Fe(phen)_3^{2+} + Br_2 + H^+$

Therefore, the mechanism proposed by Strizhak and co-workers could be simplified into a model consisting of only 26 steps.

Table 3.1

No.	Reaction	Rate constant
1	$Br^- + BrO_3^- + 2H^+ \rightarrow HOBr + HBrO_2$	1.28
2	$HOBr + HBrO_2 \rightarrow Br^- + BrO_3^- + 2H^+$	3.3
3	$HBrO_2 + Br^- + H^+ \rightarrow 2HOBr$	1.6×10^6
4	$2HOBr \rightarrow HBrO_2 + Br^- + H^+$	2×10^{-5}
5	$HOBr + Br^- + H^+ \rightarrow Br_2 + H_2O$	1.84×10^9
6	$Br_2 + H_2O \rightarrow HOBr + Br^- + H^+$	2
7	$2HBrO_2 \rightarrow BrO_3^- + HOBr + H^+$	3000
8	$BrO_3^- + HOBr + H^+ \rightarrow 2HBrO_2$	6.0×10^{-9}
9	$BrO_3^- + HBrO2 + H^+ \rightarrow 2BrO_2^{\cdot} + H_2O$	40
10	$2BrO_2^{\cdot} + H_2O \rightarrow BrO_3^- + HBrO_2 + H^+$	4.2×10^7
11	$MA + Br_2 \rightarrow BrMA + Br^- + H^+$	28.65
12	$MA + HOBr \rightarrow BrMA + H_2O$	8.2
13	$BrMA + HOBr \rightarrow$ product	0.1
14	$2BrMA^{\cdot} + H_2O \rightarrow BrMA + BrTTA$	1×10^8
15	$BrMA^{\cdot} + BrO_2^{\cdot} + H_2O \rightarrow HBrO_2 + BrTTA$	5×10^{11}
16	$BrMA^{\cdot} + MA^{\cdot} + H_2O \rightarrow MA + BrTTA$	1×10^9
17	$MA^{\cdot} + BrO_2^{\cdot} \rightarrow$ product	5×10^9
18	$MA^{\cdot} + BrO_3^- + H^+ \rightarrow BrO_2^{\cdot} +$ product	32
19	$BrTTA \rightarrow Br^- +$ product	1
20	$BrMA^{\cdot} + BrO_3^- + H^+ \rightarrow BrO_2^{\cdot} + BrTTA$	32
21	$Fe^{2+} + BrO_2^{\cdot} + H^+ \rightarrow Fe^{3+} + HBrO_2$	7×10^7
22	$2\,Fe^{2+} + BrO_3^- + 3H^+ \rightarrow 2\,Fe^{3+} + HBrO_2 + H_2O$	0.256
23	$2\,Fe^{2+} + HBrO_2 + 2H^+ \rightarrow 2\,Fe^{3+} + HOBr + H_2O$	1.6
24	$2\,Fe^{2+} + HOBr + H^+ \rightarrow 2\,Fe^{3+} + Br^- + H_2O$	5×10^{-3}
25	$2\,Fe^{2+} + Br_2 + H^+ \rightarrow 2\,Fe^{3+} + 2Br^-$	100
26	$2\,Fe^{3+} + 2\,Br^- \rightarrow 2\,Fe^{2+} + Br_2 + H^+$	See reference 13
27	$Fe^{3+} + MA \rightarrow Fe^{2+} + MA^{\cdot} + H^+$	1×10^{-2}
28	$Fe^{3+} + BrMA \rightarrow Fe^{2+} + BrMA^{\cdot} + H^+$	20
29	$Fe^{2+} + BrMA^{\cdot} + H^+ \rightarrow Fe^{3+} + BrMA$	5×10^7

Note: The concentration of $[H^+] = 0.8M$ and $[H_2O_2] = 55.56M$ are included in the rate constants.

Chapter4. Complex Oscillations in the Ferroin-BZ-1,4-CHD Oscillator

The Belousov-Zhabotinsky (BZ) reaction is one of the best understood chemical oscillators,[69-77] and has been frequently employed as a model system to gain insight into various nonlinear spatiotemporal behaviors.[78-82] For example, spatially extended BZ reactions catalyzed by ferroin or ruthenium have been investigated extensively in the past two decades, which led to observations of various pattern formation.[58, 64, 83] The classic BZ reaction is the oxidation and bromination of organic substrates, malonic acid (MA), by acidic bromate in the presence of metal ion catalyst. When MA is replaced by a different organic substrate or when two or more substrates are present simultaneously, the BZ reaction is found to exhibit quite different nonlinear behavior, including the occurrence of complex oscillations and/or dramatic changes in the frequency and amplitude of oscillation.[84-87] In this study, we investigated the oscillatory behavior of the ferroin-catalyzed BZ reaction in the presence of a second substrate, 1,4-cyclohexanedione (1,4-CHD).

As reported in the literature,[35] 1,4-CHD alone is capable of forming a chemical oscillator with bromate in an acidic environment. Therefore, in addition to a new route of regenerating the reduced metal catalysts (i.e. ferroin), the presence of 1,4-CHD in the ferroin-MA-bromate reaction also implements new autocatalytic nonlinear feedbacks via reactions of hydroquinone and bromine dioxide radicals. As a result, the mixed BZ system studied here consists of two bromate oscillators that are coupled together through such reagents as bromine dioxide radicals, ferroin/ferriin, bromine, etc. Forming a

coupled oscillatory system is an essential difference between this study and earlier investigations of the BZ reactions using two or more organic substrates, [84-87] in which kinetic effects are mainly caused by competitions on the regeneration of ferroin and Br^-. As is shown in the following, the presence of coupled nonlinear feedbacks leads to the occurrence of non-oscillatory evolution and bursting phenomena.

4.1 Experimental Procedures

All reactions were carried out in a thermostated cylindrical glass vessel, where temperature was controlled at (25.0 ± 0.1) °C by a circulating water bath (Fisher Scientific). The volume of the reaction mixture was kept constant at 30.0 mL throughout this study. There was about a 1-cm gap between the solution and the bottom of a Teflon lid. To avoid the influence of oxygen, nitrogen gas was continuously flowed into the gap at a speed of about 0.05 L/min. To examine whether flowing inert gases above the solution surface affects the reaction kinetics, for example, via inducing the loss of volatile species such as bromine, etc., argon was supplied at a much lower flow rate and no difference in the behavior was recorded. Reactions were followed by a platinum electrode coupled with a $Hg|Hg_2SO_4|K_2SO_4$ reference electrode. A personnel computer, interfaced through a PowerLab/4SP instrument (ADInstruments), was used to collect Pt potentials. For experiments illuminated by light, a fiber-optic halogen lamp (Fisher Scientific, Model DLS-100HD, 150W) with dual bifurcated fibers and continuously variable light levels was used as the light source. The two optical fibers were positioned at the opposite sides of the cylindrical glass reactor and were about 1 cm away from the external wall of the glass reactor. The light intensity was measured with an optical photometer from

Newport.

No temperature change was observed when the reaction mixture was illuminated by light, indicating that the observed effects were caused by photochemical reactions. Stock solutions of $NaBrO_3$ (Aldrich, 99%; 1.0 M), malonic acid (Aldrich, 98%; 0.8 M), and H_2SO_4 (Aldrich, 98%; 3 M) were prepared in double-distilled water. Ferroin ($Fe(phen)_3^{2+}$), 0.025 M, was prepared with $FeSO_4 \cdot 7H_2O$ (Aldrich) and 1,10-phenanthroline (Aldrich) according to a 1:3 stoichiometric relationship. 1,4-CHD (Aldrich, 98%) was directly dissolved in the reaction mixture. Bromate solution was added to the reaction solution after 1,4-CHD had dissolved completely. All chemicals used here were commercial grade and were used without further purification. Influences of initial concentrations of 1,4-CHD, MA, BrO_3^-, and ferroin on the reaction dynamics have been studied, in which their concentrations were adjusted respectively within the following ranges: 0.015-0.08 M (1,4-CHD), 0.075-0.25 M (MA), 0.07-0.09 M (BrO^{3-}), and 3.0×10^{-4}-7.0×10^{-4} M (ferroin).

4.2 Experimental Results and Discussions:

Figure 4.1 presents seven time series of the mixed BZ reaction conducted at different initial concentrations of 1,4-CHD: (a) 0.008M, (b) 0.010M, (c) 0.012M, (d)0.015M, (e) 0.02M, (f) 0.025M, and (g) 0.03M. Other reaction conditions are $[H_2SO_4]$ = 0.4 M, [MA] = 0.085 M, $[Fe(phen)_3^{2+}] = 4.0\times10^{-4}$ M, and $[BrO_3^-]$ = 0.08 M.

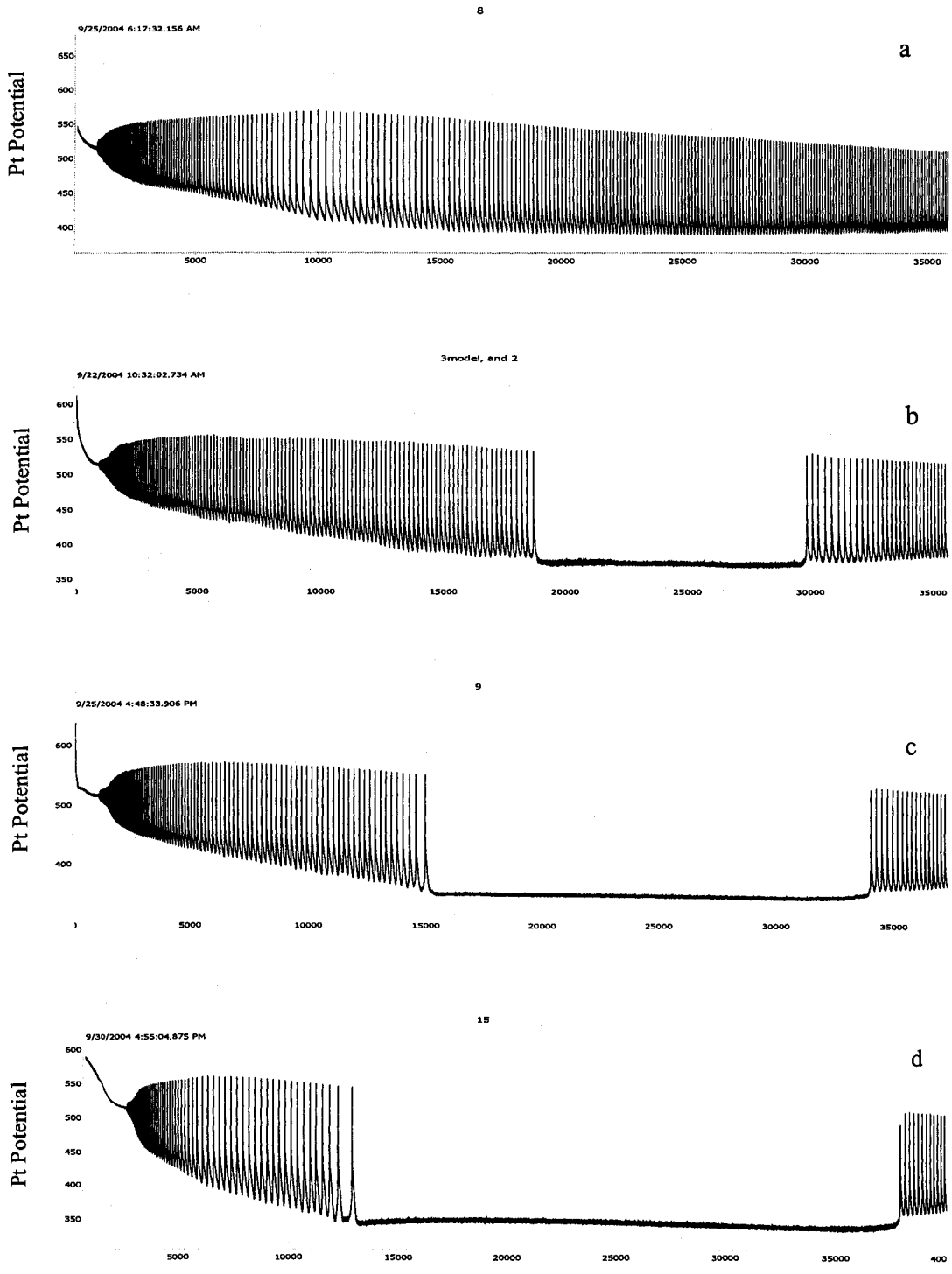

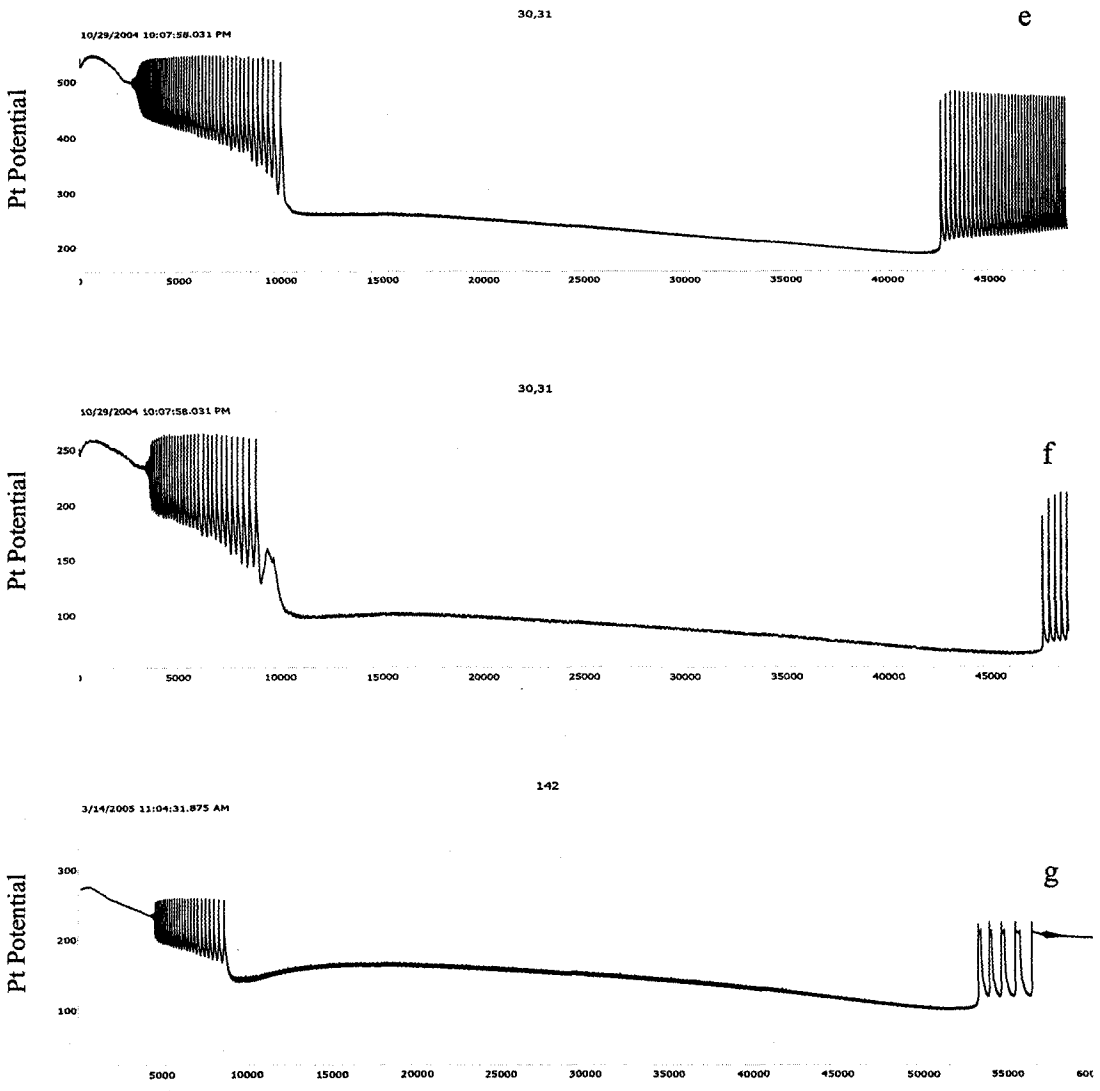

Figure 4.1

As is shown in the figure, there is a long induction time (>700 s), which grows as 1,4-CHD concentration is increased. In the absence of 1,4-CHD, the induction time is shorter than 80 s. During the induction period, the color of the reaction solution is blue, indicating that the system is in the oxidized state (i.e., high $Fe(phen)_3^{3+}$concentration). In Figure 4.1a, only a small amount of 1,4- CHD is added, modulations in the frequency of

oscillation can be seen at around 10000 s after mixing all reactants together. As 1,4-CHD concentration is increased, more dramatic changes in the reaction behavior appear in Figure 4.1b, in which a long quiescent period develops in the middle of the oscillatory window. Such a behavior resembles sequential oscillations reported in earlier investigations.[51] The non-oscillatory evolution commenced earlier and lasted longer if 1,4-CHD concentration was increased still (see Figure 4.1c), suggesting that 1,4-CHD plays an important role in the development of the sequential oscillations. In Figure 4.2, the length of the non-oscillatory period is plotted as a function of the initial concentration of 1,4-CHD, in which the period of the non-oscillatory window increases nearly linearly with 1,4-CHD concentration.

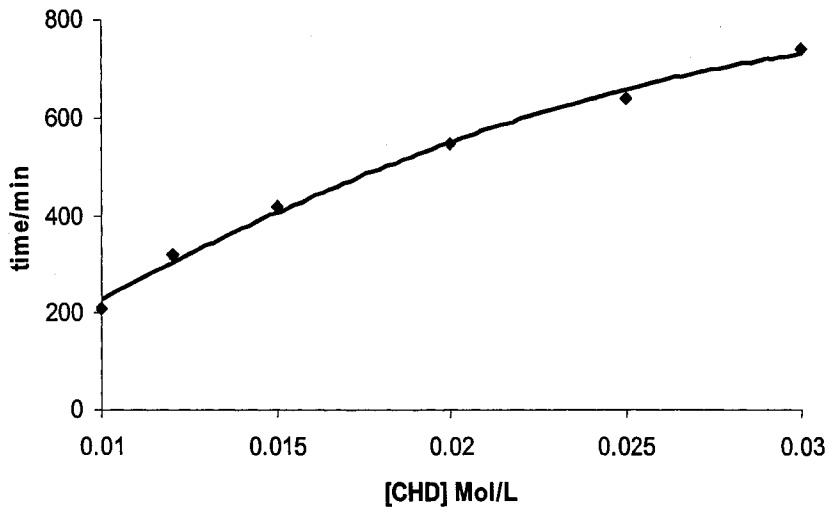

Figure 4.2

It is important to point out that as 1,4-CHD concentration is increased, both the first and the second group of oscillations last for a shorter period of time and their amplitudes

also become smaller. When 1,4-CHD concentration is increased to 0.03 M as shown in figure 4.1(g), only four peaks with an extremely slow oscillation frequency are obtained in the second oscillatory window.

The above influences of 1,4-CHD on the reaction behavior could arise from two sources: (1) 1,4-CHD competes with MA to react with ferriin, bromine, etc., and (2) the 1,4-CHD oscillator competes with the classic BZ oscillator for the autocatalyst, bromine dioxide radicals.

(1) $CHD + 2Fe(phen)^{3+} \rightarrow H_2Q + 2\ Fe(phen)^{2+} + 2H^+$

$MA + Fe(phen)^{3+} \rightarrow MA\bullet + Fe(phen)^{2+} + H^+$

(2) $H_2Q + BrO_2\bullet \rightarrow Q + HBrO_2$

$Fe(phen)^{2+} + BrO_2\bullet + H^+ \rightarrow HBrO_2 + Fe(phen)^{3+}$

If competitions for bromine dioxide radicals played an important role in inducing the non-oscillatory evolution, similar effects of increasing 1,4-CHD concentration should be achieved by decreasing the concentration of ferroin. In Figure 4.3, time series of the mixed BZ reaction are shown at $[Fe(phen)_3^{2+}]$: (a) 3.0×10^{-4} M, (b) 4.0×10^{-4}M, (c) 5.0×10^{-4}M, and (d) 6.0×10^{-4}M. Other reaction conditions are $[H_2SO_4]$ = 0.4M, [MA] = 0.085 M, [1,4-CHD] = 0.01 M, and $[BrO_3^-]$ = 0.08 M. This figure shows that increasing ferroin concentration does exhibit opposite effects as increasing 1,4-CHD concentration on the development of sequential oscillations. Therefore, as suggested earlier, competitions of the two bromate-based oscillators through the autocatalytic processes appear to play an essential role in the occurrence of sequential oscillations.

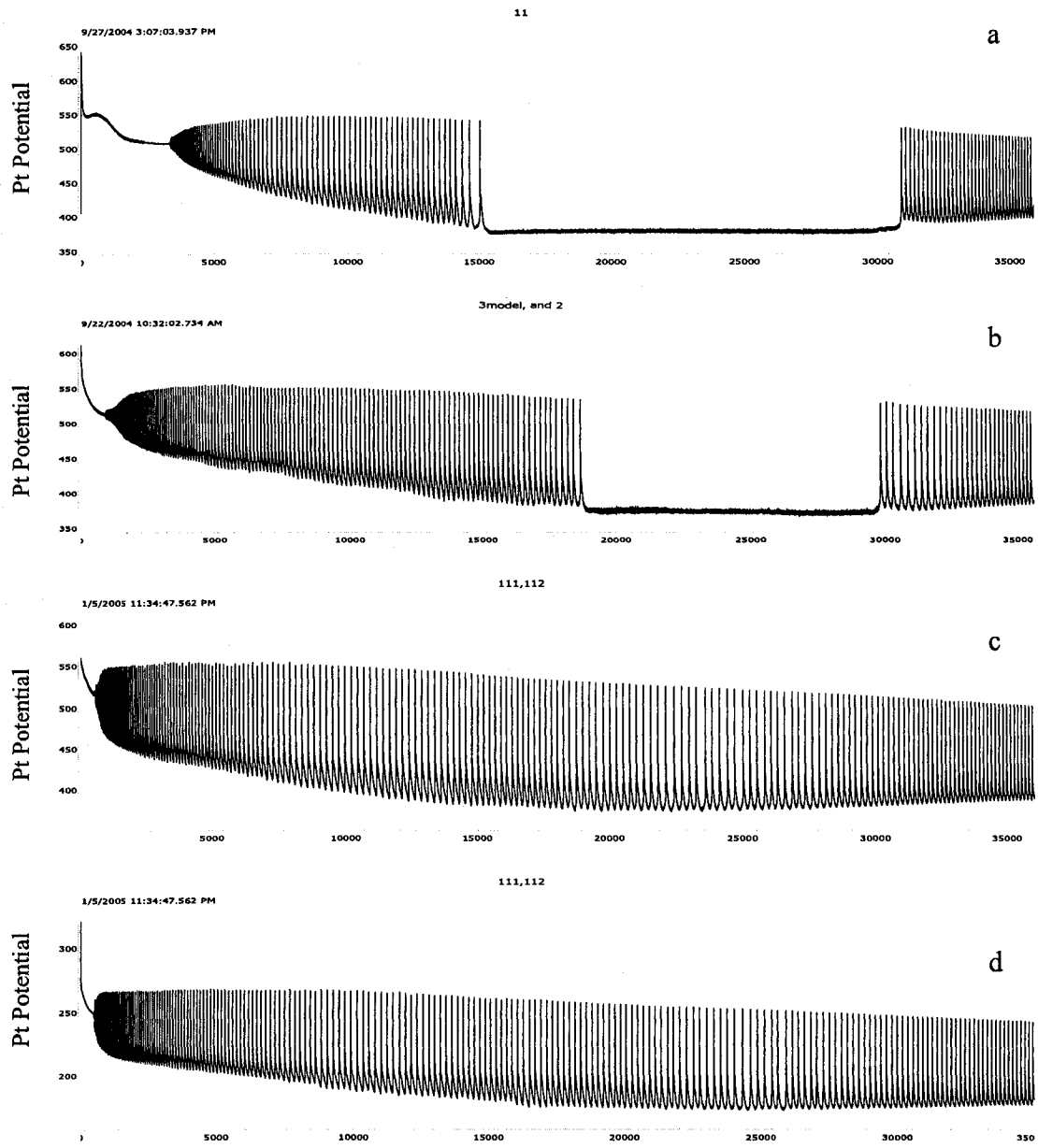

Figure 4.3

Figure 4.4 presents a phase diagram of the reaction dynamics in the ferroin-1,4-CHD concentration plane, in which three dynamic areas are observed: (I) simple oscillations, (II) bursting phenomena, and (III) sequential oscillations.

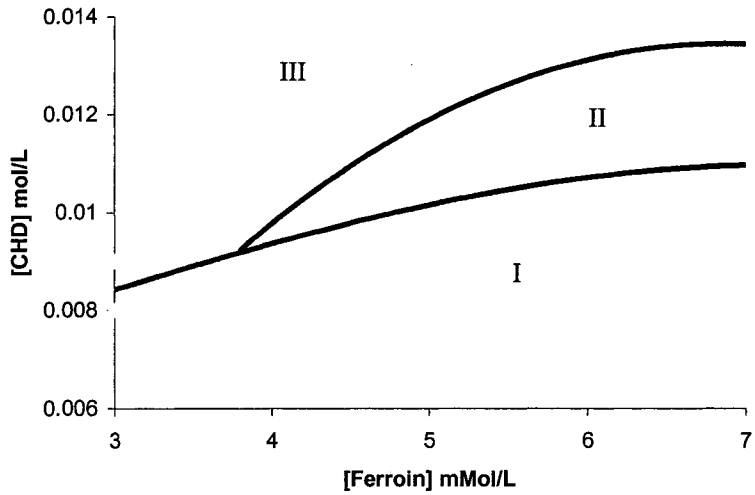

Figure 4.4

When the ratio of [1,4-CHD]/[ferroin] is low (i.e.,in region I), only one oscillatory window similar to those shown in Figures 4.1a is observed. The threshold ratio of [1,4-CHD]/[ferroin] for transitions from simple to complex oscillations is nearly constant over a broad range, indicating that the ratio of [1,4-CHD]/[ferroin] is more important than their absolute concentrations. However, as the concentration of ferroin moves to a higher region, the threshold concentration of 1,4-CHD appears to reach a plateau. In addition, at high ferroin concentration, increasing the concentration of 1,4-CHD will cause the system to exhibit bursting phenomena first (example is shown in figure 4.5b), and then the system moves to the parameter region where only sequential oscillations can be seen.

Figure 4.5 shows examples of (a) simple oscillations in region I (b) bust phenomena in region II (c) sequential oscillations in region III, respectively in the ferroin-1,4-CHD concentration plane:

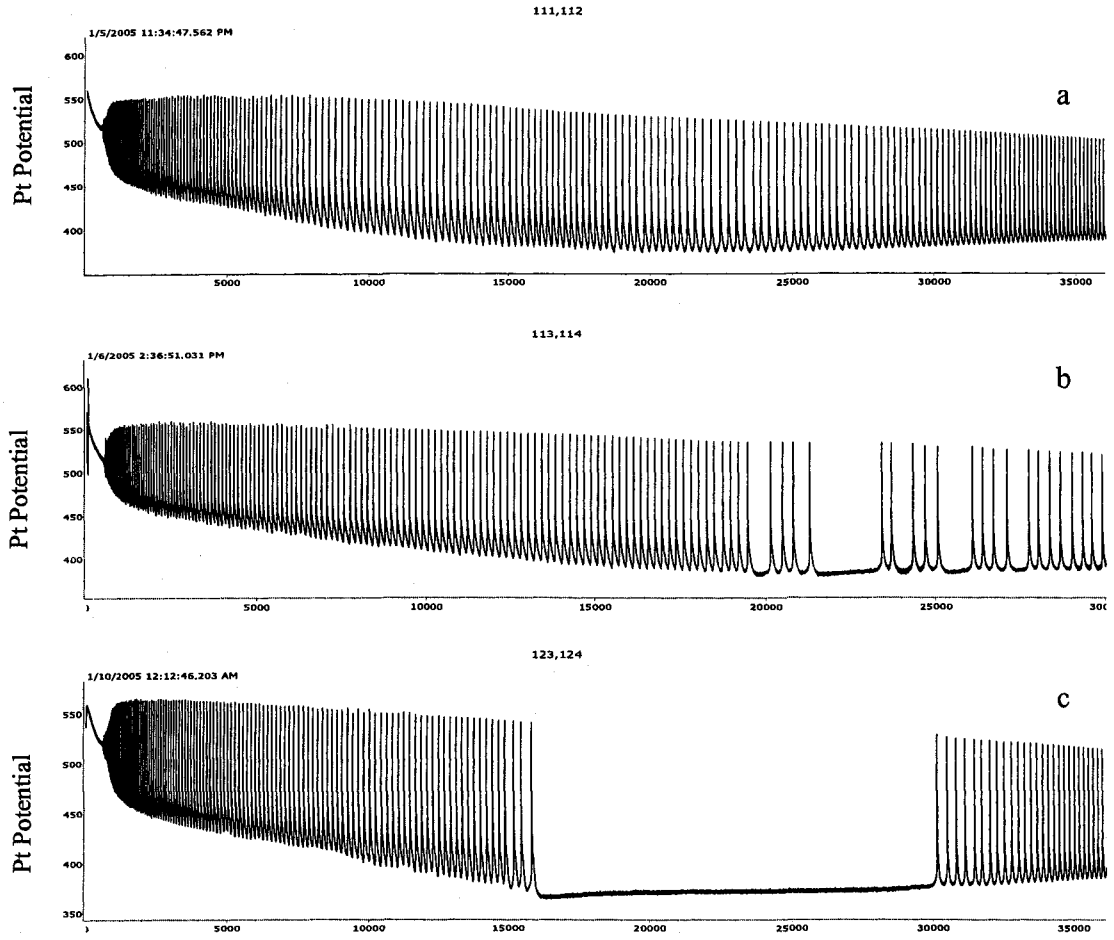

Figure 4.5

Figure 4.6 shows time series achieved under different initial concentration of MA: (a) 0.075M, (b) 0.085M, (c) 0.095M and (d) 0.105M.Other reaction conditions are $[H_2SO_4]$ = 0.4 M, 1,4-CHD = 0.01M, $[Fe(phen)_3^{2+}] = 4.0 \times 10^{-4}$ M, and $[BrO_3^-] = 0.08$ M.

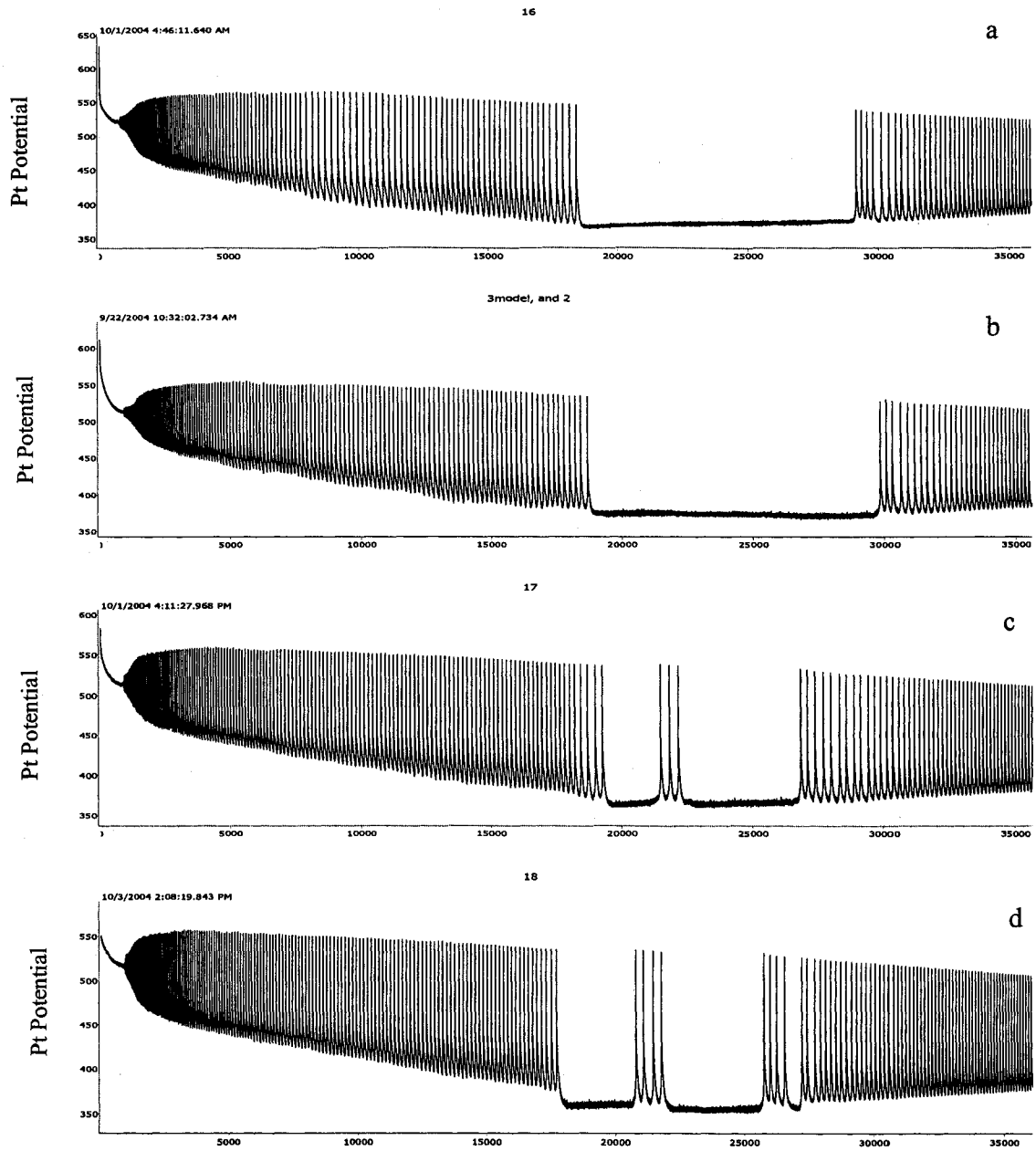

Figure 4.6

Notably, complex oscillations rather than sequential oscillations are observed in this series. This result illustrates that the effect of MA on the dynamics of the mixed BZ system is not as dramatic as that of 1,4-CHD. In other words, competitions between 1,4-CHD and MA for reagents such as bromine, ferriin, etc. are not critical in the

development of the non-oscillatory window. However, as the concentration of MA is increased to 0.095 M, a new complex phenomenon resembling bursting oscillations occurs within the non-oscillatory window. Bursting oscillations occur more frequently as the concentration of MA acid is increased further (see Figure 4.6d).

In Figure 4.7, complex behavior is characterized in the 1,4-CHD-MA concentration phase plane. Other reaction conditions are $[H_2SO_4]$ = 0.4 M, $[Fe(phen)_3^{2+}] = 4.0 \times 10^{-4}$ M, and $[BrO^{3-}]$ = 0.08 M. Three dynamic regions are observed. Only simple oscillations with one oscillatory window are observed in region I, whereas complex reaction behavior is seen in both region II (burst phenomena) and region III (sequential oscillations).

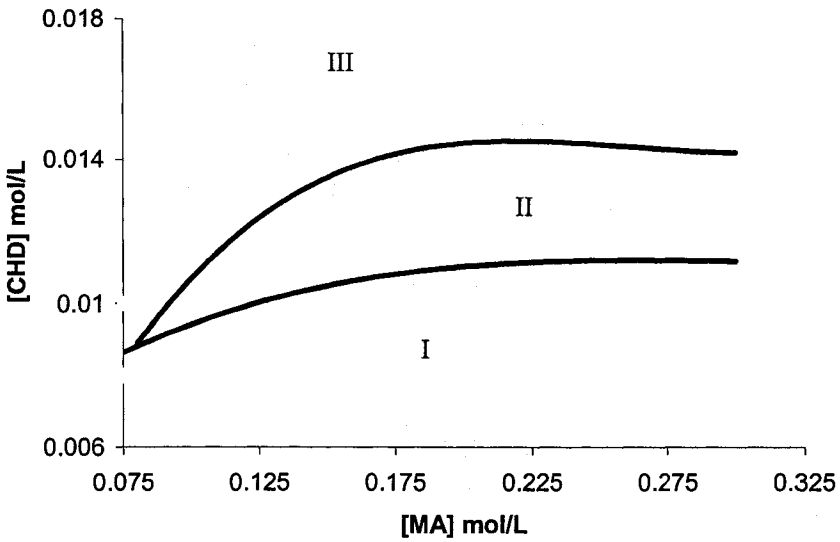

Figure 4.7

Figure 4.8 shows examples of: (a) simple oscillations in region I; (b) burst oscillations in region II; (c) sequential oscillations in region III, respectively, in the 1,4-CHD-MA concentration phase plane.

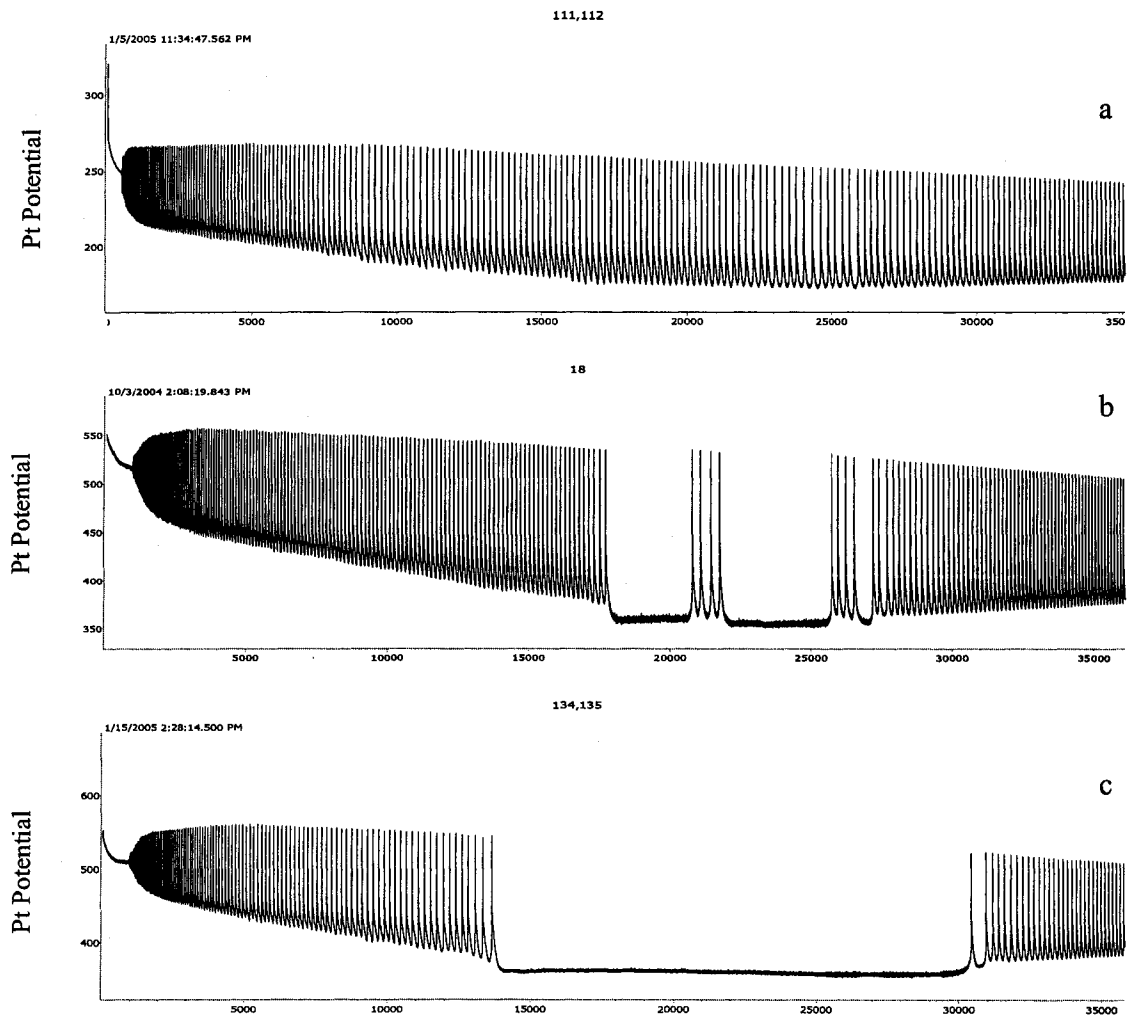

Figure 4.8

It is interesting to note that at low MA concentration, the threshold 1,4-CHD concentration required to induce complex oscillations also appears to increase proportionally with the initial concentration of MA. Whether such a relationship between [1,4-CHD] and [MA] arises from their competitions for ferroin or reactions with bromine remains to be understood. Nevertheless, the above phase diagram illustrates that interactions of 1,4-CHD and MA play an important role as well in the development of bursting phenomena, especially under low MA concentrations.

In addition to those reactants which are known to be involved in reactions competing with 1,4-CHD and/or the products of 1,4- CHD, bromate and sulfuric acid are also investigated in this study. Figure 4.9 presents two time series obtained under different initial concentrations of bromate: (a) 0.07 and (b) 0.09 M. All other reaction conditions are the same as those in Figure 4.1b, [1,4-CHD] = 0.01M, $[H_2SO_4]$ = 0.4 M, [MA] = 0.085 M, and $[Fe(phen)_3^{2+}] = 4.0\times10^{-4}$ M. Compared with the result shown in Figure 4.1b, the non-oscillatory window appeared earlier and lasted for a much longer time in Figure 4.9a as a result of the decreasing bromate concentration. On the other hand, when the concentration of bromate is increased, the nonoscillatory window disappears.

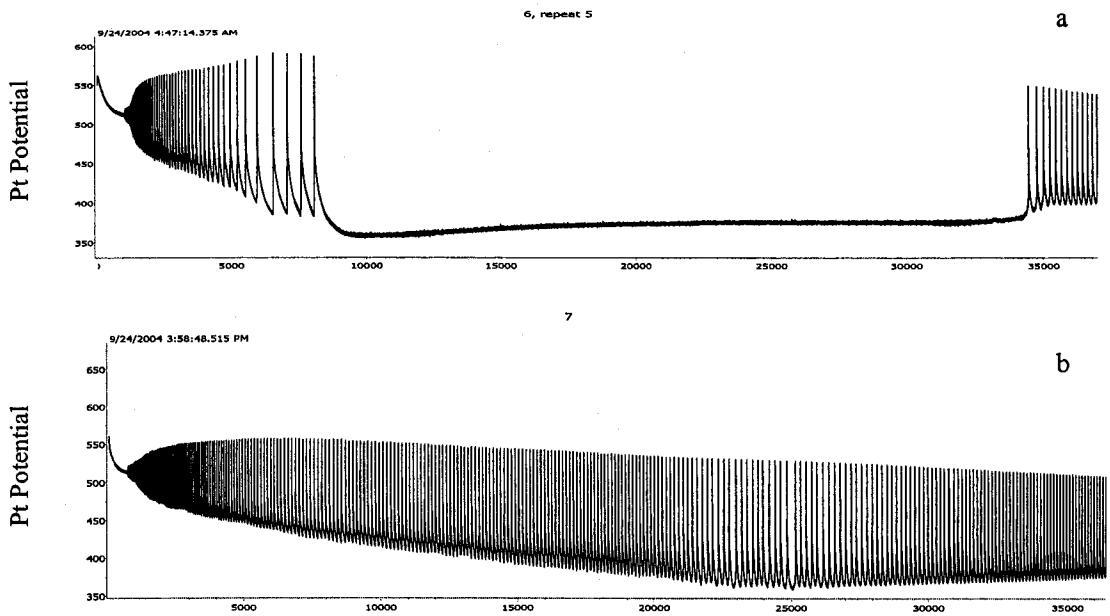

Figure 4.9

If the initial concentration of sulfuric acid is increased to 0.5 M with all other conditions the same as in Figure 4.1b, complex oscillations disappeares; on the other hand, if the sulfuric acid concentration is decreased to 0.3 M, the nonoscillatory window appears earlier and lasts for a longer period of time, similar to the effect of decreasing

bromate concentration. Figure 4.10 shows oscillations at different sulfuric acid concentrations.

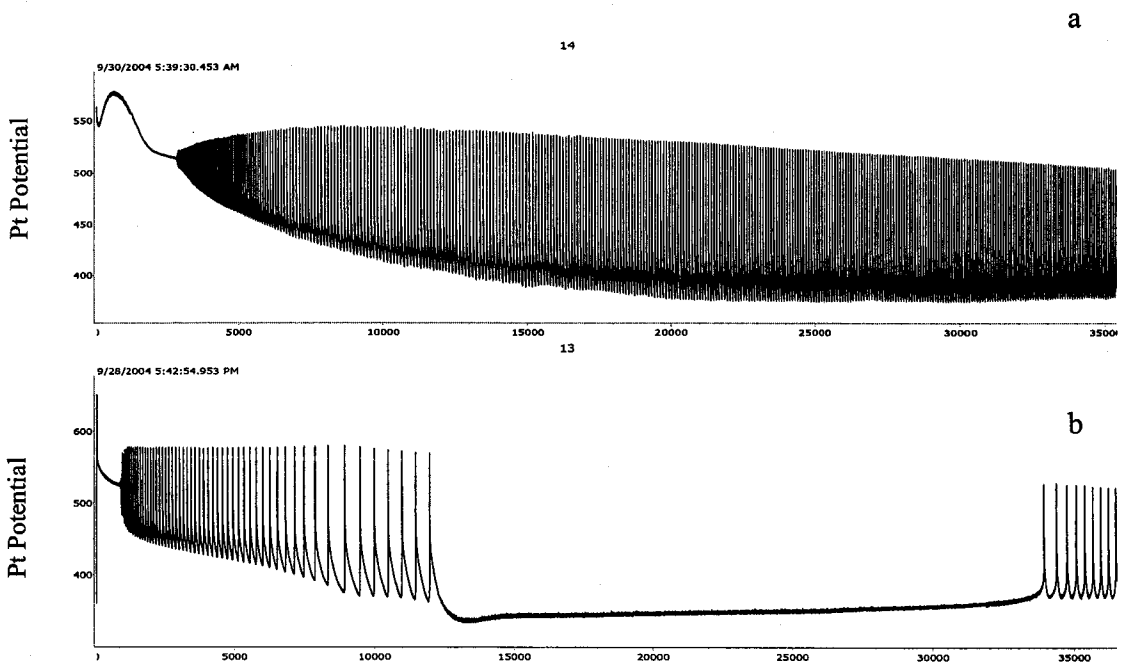

Figure 4.10

Earlier studies have demonstrated that the 1,4-CHD-bromate oscillator generally has a long induction time (>30 min).[16,35] Therefore, oscillations of the first oscillatory window are presumably governed by the classic BZ reaction mechanism. To shed light on properties of the nonoscillatory evolution and the second oscillatory window, illumination was employed as a means to perturb the mixed BZ reaction. According to existing literatures,[47,48, 88,89] the ferroin-catalyzed BZ reaction and the 1,4- CHD-bromate oscillator respond differently to light perturbation. Figure 4.13 presents the photoresponses of the ferroin-BZ oscillator (time series a) and the 1,4-CHD-ferroin-bromate oscillator (time series b).

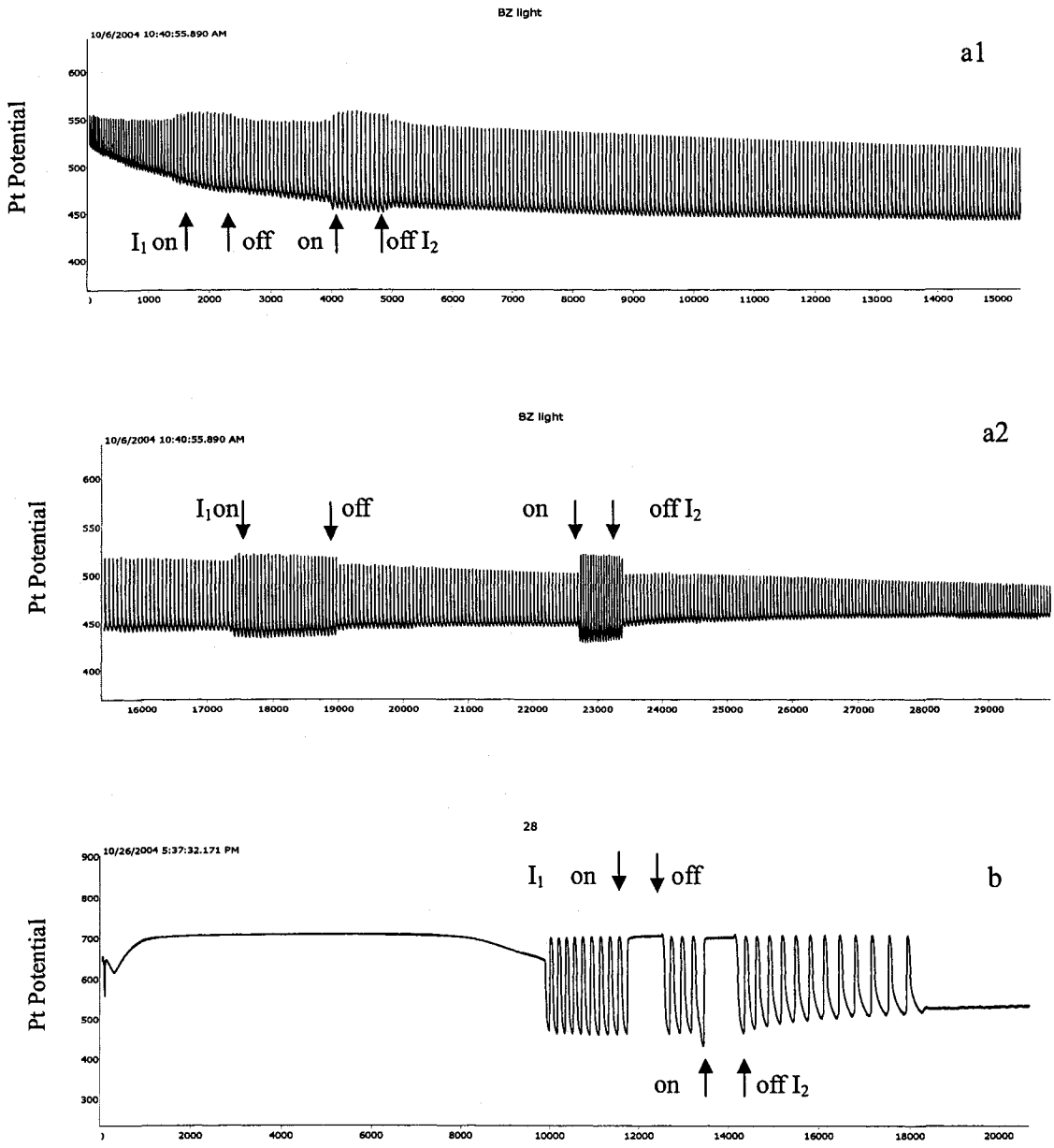

Figure 4.11

As are shown in Figures 4.11a and b, under the conditions studied here, the ferroin-catalyzed BZ reaction responds to illumination with significant increases in both the amplitude and frequency of oscillation. Furthermore, quenching is not achieved even when the intensity of the applied light is increased to 100mW/cm^2 (I_2). The above

constructive impacts of light could result from light-induced production of bromous acid and/or photoreduction of $Fe(phen)_3^{2+}$.[88] On the other hand, quenching behavior is observed in the 1,4-CHD-bromate-ferroin system when the applied light intensity exceeds 50 mW/ cm^2 (I_1). Importantly, the two bromate-driven oscillators studied here have opposite responses to illumination. Responses of the mixed BZ system to light perturbation are shown in Figure 4.12, in which the concentration of 1,4-CHD is varied: (a) 0.01M, (b) 0.02 M and (c) 0.03M

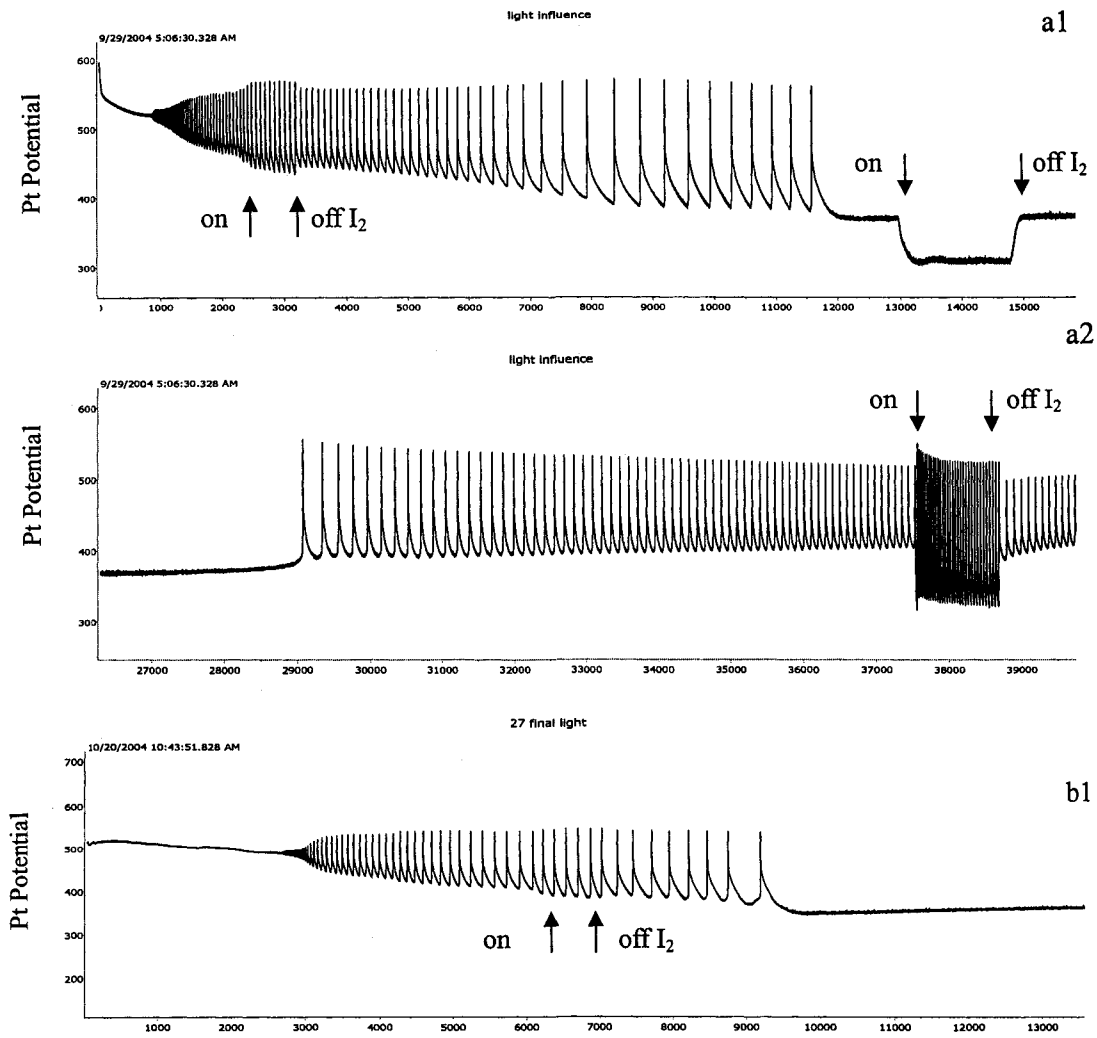

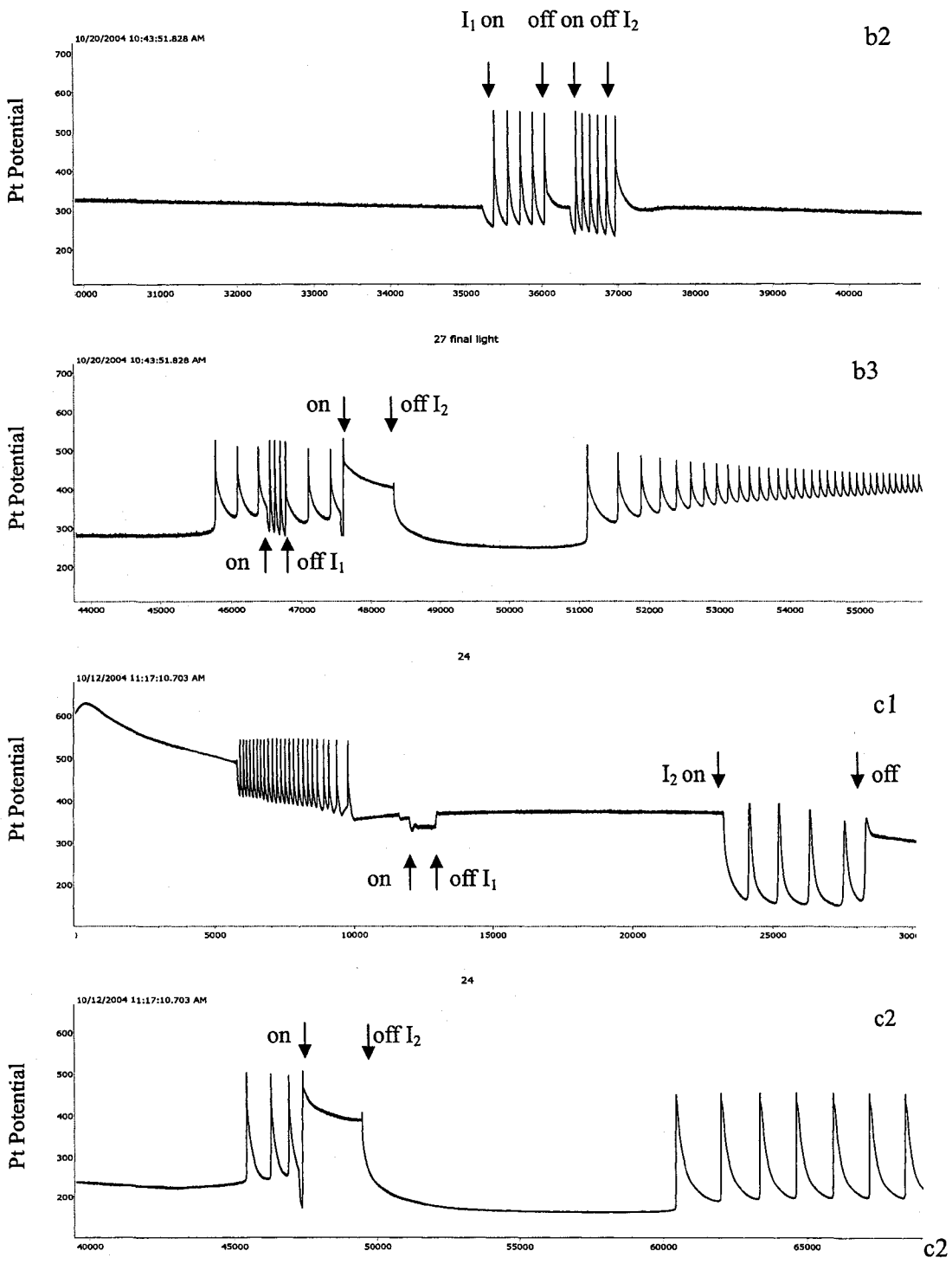

Figure 4.12

Figure 4.12a shows that when light was used to perturb the second oscillatory window, significant amplifications in the amplitude and frequency of oscillation took place. Those variations are similar to what occurred in Figure 4.11a. Notably, no quenching behavior was observed even after the light intensity was increased to 100 mW/ cm^2 (I_2). This result suggests that oscillations within the second oscillatory window are still dominated by the classic BZ reaction mechanism. Perturbations on the non-oscillatory window did not produce any interesting behavior, where no light-induced oscillations were observed.

As the initial concentration of 1,4-CHD was increased to 0.02 M, significant changes in photosensitivity took place at the latter stage of the non-oscillatory window, where light-induced oscillations were observed (see Figure 4.12b2). Frequencies of those light-induced oscillations increase with respect to the intensity of the applied light. Such a scenario is qualitatively the same as what was reported in the 1,4-CHD-bromate-ferroin reaction system.[47] As is shown in Figure 4.12 b3, within the second oscillatory window illumination with 50.0 mW/cm^2 (I_1) light was able to amplify both the amplitude and frequency of oscillation. Such a behavior is the same as what appeared in the classic BZ oscillator (see Figure 4.11a). However, as the light intensity is increased to 100 mW/cm^2 quenching phenomena are observed. Such qualitative changes in responses to light have been reported in the 1,4- CHD-bromate and the 1,4-CHD-bromate-ferroin systems,[47,48] but not in the classic ferroin-BZ reaction. When 1,4-CHD concentration is increased to 0.03M, (figure 4.11c) the light effect is more obvious. Light can intriger oscillations in early stage of nonoscillatory period, and at the secondary oscillation state the quenching effect by light is more dramatic. The above experiments thus suggest that, as the initial

concentration of 1,4-CHD is increased, the 1,4-CHD-bromate oscillator plays an increasingly important role in the non-oscillatory evolution and in the second oscillatory window.

4.3 Computational Results

The model is constructed by combining a mechanism proposed by Strizhak and co-workers for the ferroin-catalyzed BZ reaction[14] and a model developed by Koros and co-workers for the 1,4-CHD-bromate system.[16] The complete model (Table 4.1) consists of 43 reaction steps and 17 variables. Most of the rate constants are taken from literature without modification.[14,16,18] Figure 4.13 presents three time series calculated from the model, in which the initial concentration of 1,4-CHD is adjustedas the only variable: (a) 0.004, (b) 0.010, (c) 0.012 M, and (d) 0.015 M

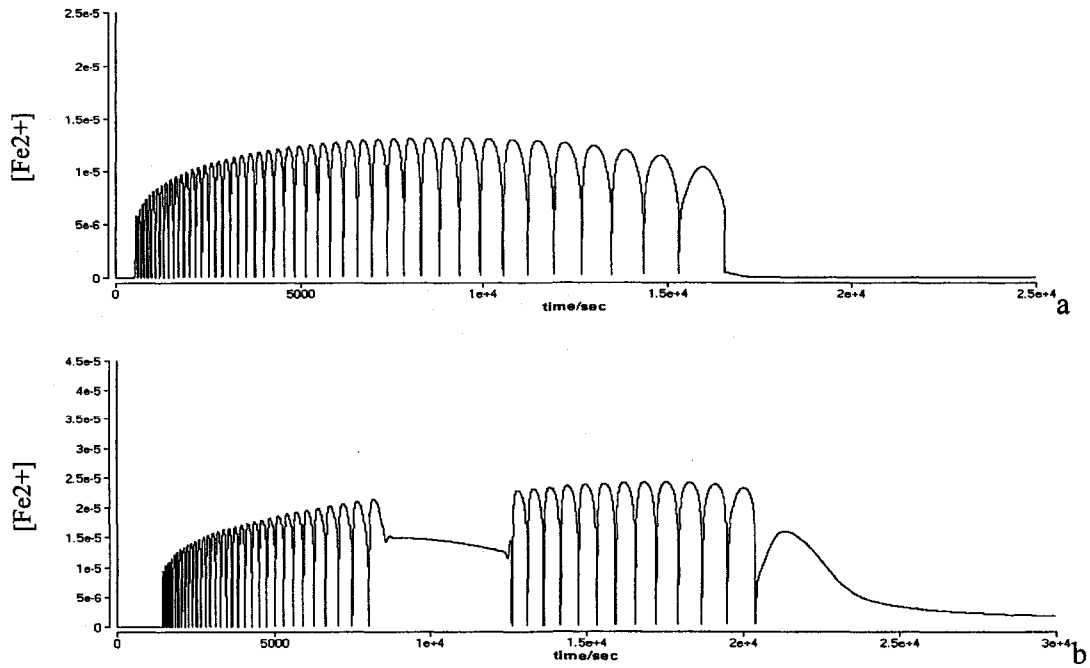

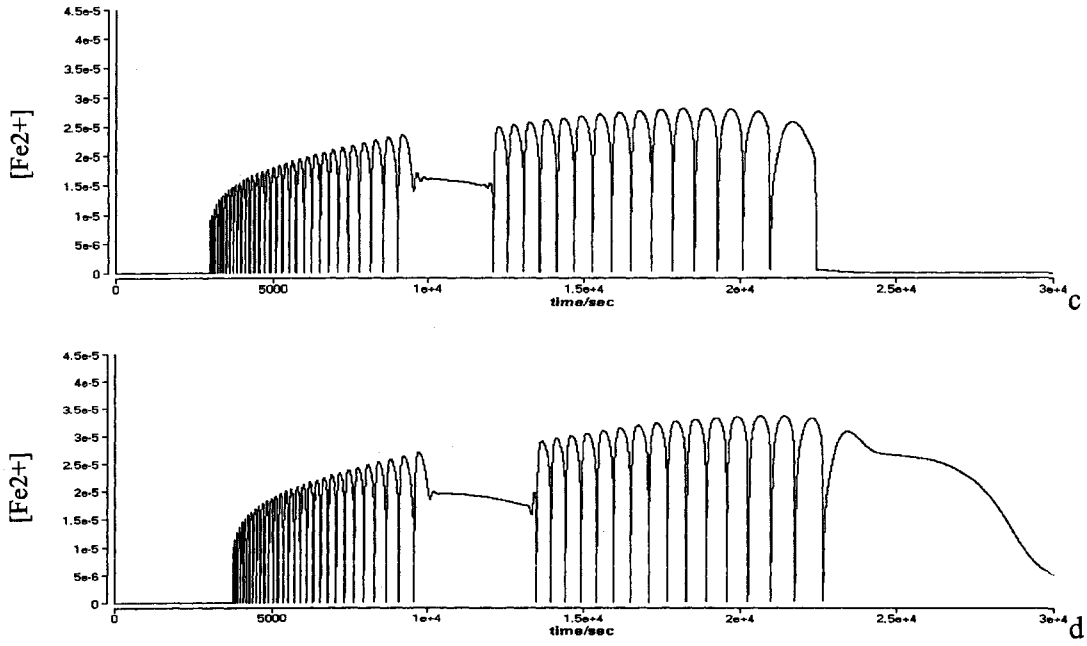

Figure 4.13

Similar to the experimental observation, there is only one oscillatory window when the concentration of 1,4-CHD is low. When [1,4-CHD] is increased to 0.010 M, a long period of non-oscillatory evolution occurs, separating the oscillations into two parts. This result supports that the complex oscillations seen in experiments arise from intrinsic reaction dynamics. Consistent with experimental observation, in the simulation the induction time of these spontaneous oscillations also increases with respect to 1,4-CHD concentration. While the model was able to qualitatively reproduce sequential oscillations induced by 1,4-CHD, influences of 1,4-CHD on the duration of the non-oscillatory evolution could not be reproduced. Specifically, further increasing 1,4-CHD concentration in the modeling (see Figure 4.13, parts b and c) does not prolong the non-oscillatory period as seen in experiments (see Figure 4.2).

To decipher the governing mechanisms in each reaction stage, during the simulation

process we temporarily eliminated one of the two suboscillators. These calculations show that, within the first oscillatory (5000 second) window, if concentrations of MA and BrMA are temporarily set to zero (i.e., to remove the ferroin-BZ oscillator), spontaneous oscillations stop immediately, (see figure 4.14a); however, temporarily setting concentrations of 1,4-CHD and BrCHD to zero, as is shown in figure 4.14b, does not affect those spontaneous oscillations. This illustrates that the first oscillatory window is indeed governed by the classic BZ oscillator.

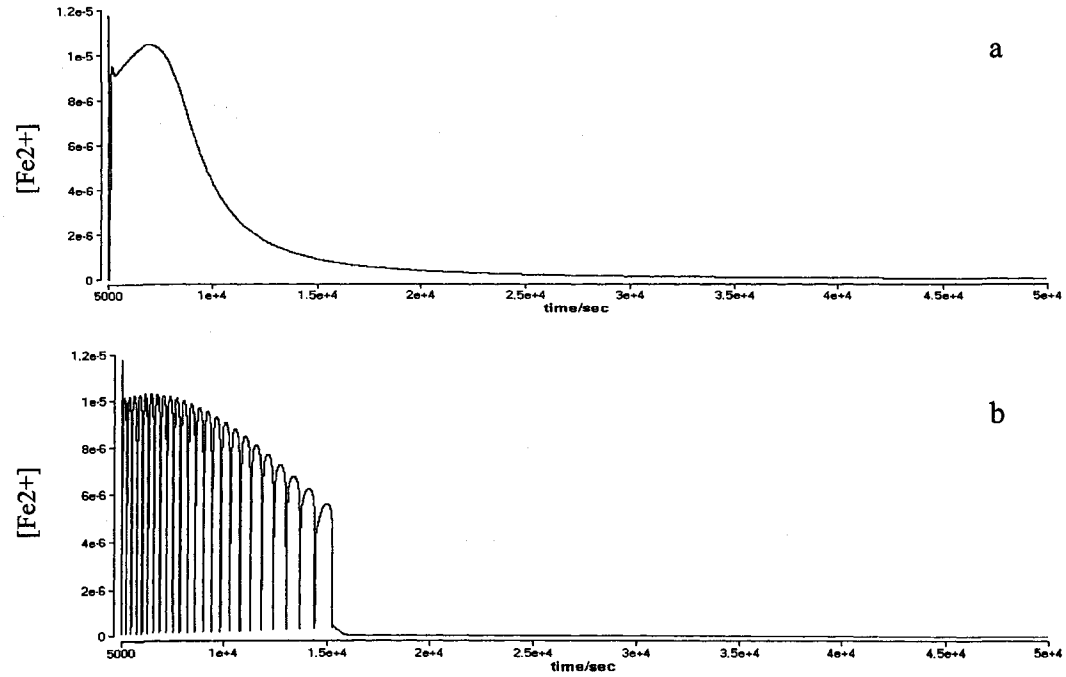

Figure 4.14

During the non-oscillatory period (9000 second), if concentrations of 1,4-CHD and BrCHD are set to zero, spontaneous oscillations reappear immediately (figure 4.15a),

illustrating that the 1,4-CHD-bromate reaction plays an essential role in the occurrence of the nonoscillatory window. If concentrations of MA and BrMA are temporarily set to zero within the non-oscillatory window, no spontaneous oscillations could appear unless the concentration of 1,4-CHD is increased slightly. Figure 4.15b shows the simulation result when the concentrations of MA and BrMA are set to zero and the concentration of CHD is slightly increased to 0.005M.

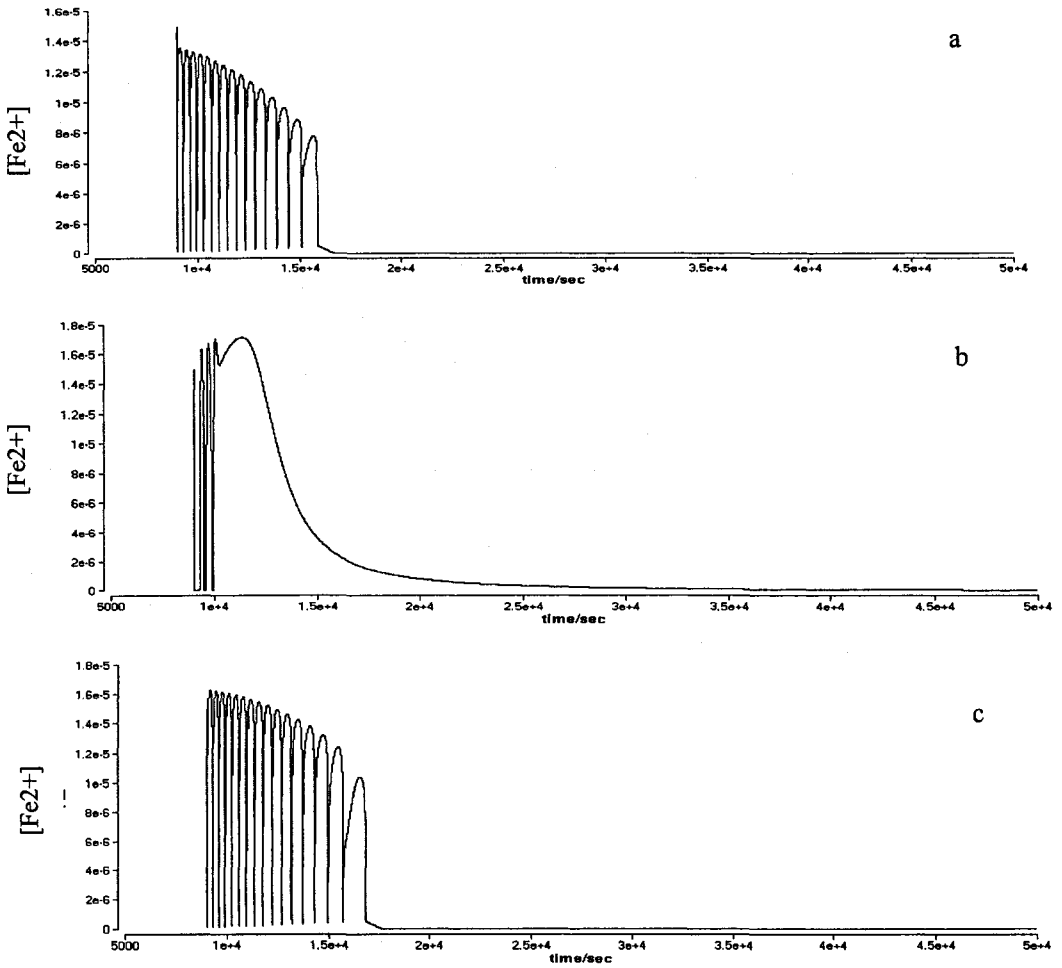

Figure 4.15

A close examination reveals that this is because most of the 1,4-CHD is converted to BrCHD during the first oscillatory window. Indeed, during the nonoscillatory window, temporarily setting BrCHD concentration to zero alone will be sufficient to revive oscillatory behavior (4.15c). This thus suggests that BrCHD dominates the production of bromide at a rate that is sufficient to quench oscillatory behavior. Reaction behavior at 10000 second (figure 4.16) and 12000 second (figure 4.17) during the nonoscillatory window are also characterized. In both figures, (a) is the simulation result when 1,4-CHD and BrCHD concentrations are set to zero,and (b) is the simulation when the BrMA and MA are set to zero and CHD concentration are increased to 0.005M. These studies indicate that 1,4-CHD, BrCHD, MA and BrMA play a similar role at different time within the non-oscillatory window.

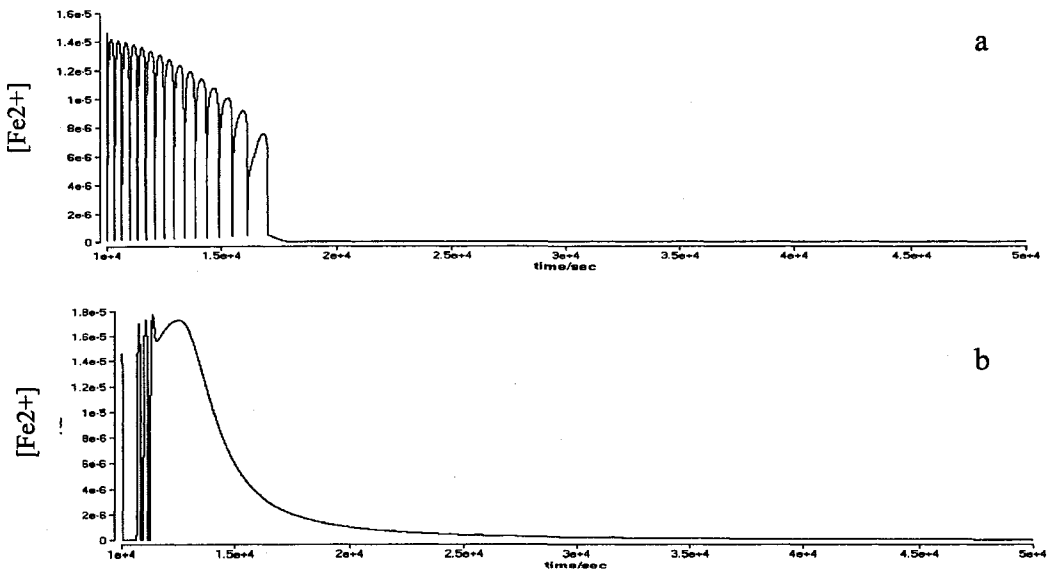

Figure 4.16

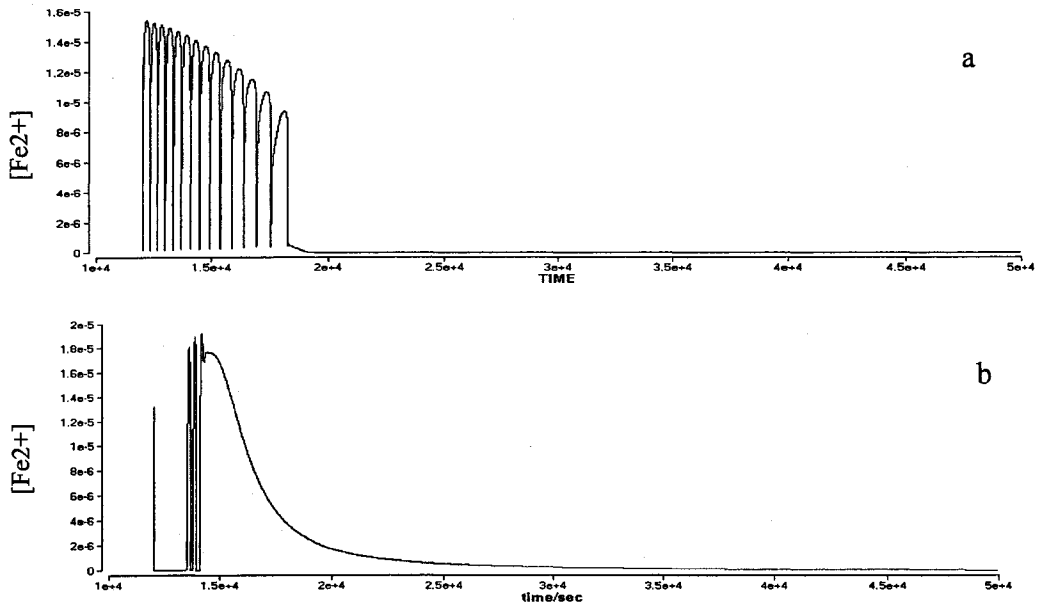

Figure 4.17

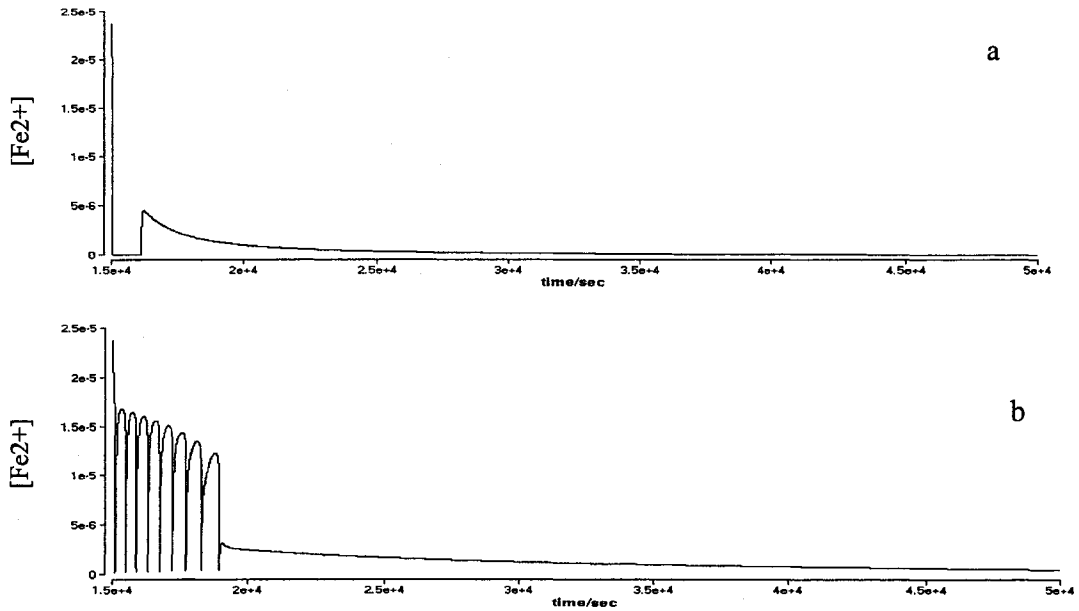

Figure 4.18

Within the second oscillatory window, spontaneous oscillations stop when concentrations of MA and BrMA are set to zero (i.e. eliminating the classic BZ reaction) (figure 4.18a);on the other hand, when concentrations of 1,4-CHD and BrCHD are set to

zero, oscillatory behavior lasts for a little longer time (shown in figure 4.18b). This indicates that the classic BZ reaction still plays an essential role in the second oscillatory window, but the presence of BrCHD exerts important influences on the oscillatory behavior. This conclusion is consistent with the experimental observation that the second oscillatory window exhibits subtle responses to light perturbation, in which BrCHD may lead to additional production of Br^- and consequently result in light-induced quenching phenomena.

4.4. Conclusions

This chapter investigates the nonlinear dynamics of a mixed ferroin-BZ reaction system, in which there are two organic substrates, namely, 1,4-CHD and MA. As opposed to the vast majority of previous studies with mixed substrates,[84-87] in this study the second organic substrate, 1,4-CHD, not only participates in reactions which compete with the first substrate, but also introduces additional nonlinear feedbacks. As is shown in the Figures above, complex behaviors such as sequential oscillations and bursting phenomena are induced by the presence of the second substrate. The fact that concentrations of 1,4-CHD and ferroin exhibit opposite effects on the occurrence of a non-oscillatory window suggests that the coupling of reactions R1-R3 plays an essential role in the development of complex reaction dynamics in the mixed system:

$$Fe(phen)_3^{2+} + BrO_2\bullet + H^+ \rightarrow Fe(phen)_3^{3+} + HBrO_2 \qquad (R1)$$

$$H_2Q + BrO_2\bullet + H^+ \rightarrow H_2Q\bullet + HBrO_2 \qquad (R2)$$

$$H_2Q\bullet + BrO_2\bullet + H^+ \rightarrow Q + HBrO_2 \qquad (R3)$$

Where hydroquinone (H_2Q) is a product of 1,4-CHD. Together with reaction 9 in Table

4.1, reactions (R1), (R2), and (R3) form two coupled autocatalytic feedbacks.

Dolnik and co-workers have demonstrated in the ferrocyanide-iodate-sulfite reaction that coupling the nonlinear feedback step could lead to the control of the frequency, amplitude, and existence of oscillations.[90] This study demonstrates that not only modulations in the frequency and amplitude of oscillation, but even complicated dynamical behavior can be achieved by coupling nonlinear feedbacks. It is interesting to note that the occurrence of complex oscillations also appears to depend on the ratio of the two organic substrates [1,4-CHD]/[MA], especially at low concentration of [MA], implying that couplings through linear processes also play an important role in the mixed BZ reaction. Both photoperturbation experiments and numerical simulations suggest that the 1,4-CHD-bromate reaction plays a critical role during the non-oscillatory evolution. At higher initial concentration of 1,4-CHD, behavior of the second oscillatory window is greatly affected by the 1,4-CHD-bromate oscillator, as evidenced by the subtle dependence of the photosensitivity on light intensity.

The unique photosensitivity, the presence of complex temporal dynamics, and the visible periodic color changes in this mixed BZ reaction make it an attractive model system for exploring novel spatiotemporal behavior, in particular pattern formation under perturbed nonlinear dynamics. Among existing studies of the coupled chemical oscillators, the coupled system was usually constructed via coupling two identical chemical systems operated at different reaction conditions.[91,92] In this study, the coupled system was formed via a combination of different oscillatory reactions (i.e. through "internal" couplings). Results obtained here thus shall be important for understanding the occurrence of complex dynamics in coupled nonlinear media.

Table 4.1

No.	Reaction	Rate constant
	A. Reactions between bromine-containing compounds	
1	$Br^- + BrO_3^- + 2H^+ \rightarrow HOBr + HBrO_2$	*0.1
2	$HOBr + HBrO_2 \rightarrow Br^- + BrO_3^- + 2H^+$	3.3
3	$HBrO_2 + Br^- + H^+ \rightarrow 2HOBr$	1.6×10^6
4	$2HOBr \rightarrow HBrO_2 + Br^- + H^+$	2×10^{-5}
5	$HOBr + Br^- + H^+ \rightarrow Br_2 + H_2O$	1.84×10^9
6	$Br_2 + H_2O \rightarrow HOBr + Br^- + H^+$	2
7	$2HBrO_2 \rightarrow BrO_3^- + HOBr + H^+$	3000
8	$BrO_3^- + HOBr + H^+ \rightarrow 2HBrO_2$	6.0×10^{-9}
9	$BrO_3^- + HBrO2 + H^+ \rightarrow 2BrO_2^{\cdot} + H_2O$	40
10	$2BrO_2^{\cdot} + H_2O \rightarrow BrO_3^- + HBrO_2 + H^+$	4.2×10^7
	B. Reactions with the participation of bromine-containing compounds and malonic acid derivatives	
11	$MA + Br_2 \rightarrow BrMA + Br^- + H^+$	28.65
12	$MA + HOBr \rightarrow BrMA + H_2O$	8.2
13	$BrMA + HOBr \rightarrow$ product	0.1
14	$2BrMA^{\cdot} + H_2O \rightarrow BrMA + BrTTA$	1×10^8
15	$BrMA^{\cdot} + BrO_2^{\cdot} + H_2O \rightarrow HBrO_2 + BrTTA$	5×10^9
16	$BrMA^{\cdot} + MA^{\cdot} + H_2O \rightarrow MA + BrTTA$	1×10^9
17	$MA^{\cdot} + BrO_2^{\cdot} \rightarrow$ product	5×10^9
18	$MA^{\cdot} + BrO_3^- + H^+ \rightarrow BrO_2^{\cdot} +$ product	32
19	$BrTTA \rightarrow Br^-$ + product	1
20	$BrMA^{\cdot} + BrO_3^- + H^+ \rightarrow BrO_2^{\cdot} + BrTTA$	32
	C. Reactions with the participation of the catalyst	
21	$Fe^{2+} + BrO_2^{\cdot} + H^+ \rightarrow Fe^{3+} + HBrO_2$	5×10^8
22	$Fe^{2+} + BrO_3^- + 3H^+ \rightarrow 2\ Fe^{3+} + HBrO_2 + H_2O$	0.256
23	$2\ Fe^{2+} + HBrO_2 + 2H^+ \rightarrow 2\ Fe^{3+} + HOBr + H_2O$	1.6
24	$2\ Fe^{2+} + HOBr + H^+ \rightarrow 2\ Fe^{3+} + Br^- + H_2O$	5×10^{-3}
25	$2\ Fe^{2+} + Br_2 + H^+ \rightarrow 2\ Fe^{3+} + 2Br^-$	100
26	$2\ Fe^{3+} + 2\ Br^- \rightarrow 2\ Fe^{2+} + Br_2 + H^+$	See reference 13
27	$Fe^{3+} + MA \rightarrow Fe^{2+} + MA^{\cdot} + H^+$	1×10^{-2}
28	$Fe^{3+} + BrMA \rightarrow Fe^{2+} + BrMA^{\cdot} + H^+$	20
29	$Fe^{2+} + BrMA^{\cdot} + H^+ \rightarrow Fe^{3+} + BrMA$	2×10^9
	D. Reactions with CHD	
30	$H_2Q + 2\ BrO_2^{\cdot} \rightarrow 2HBrO_2 + Q$	2×10^6
31	$H_2Q + Br_2 \rightarrow Q + 2\ Br^-$	1×10^4
32	$H_2Q + H^+ + BrO_3^- \rightarrow Q + HBrO_2 + H_2O$	1.6×10^{-2}
33	$H_2Q + HOBr \rightarrow Q + Br^- + H^+ + H_2O$	6×10^5
34	$H_2Q + 2\ Fe^{3+} \rightarrow 2\ Fe^{2+} + Q + 2H^+$	6×10^3
35	$CHD + H^+ \rightarrow CHDE + H^+$	2.1×10^{-4}
36	$CHDE + H^+ \rightarrow CHD + H^+$	5.2×10^2
37	$CHDE + Br_2 \rightarrow BrCHD + H^+ + Br^-$	2.8×10^9
38	$CHD + HBrO_2 \rightarrow H_2Q + HOBr + H_2O$	5
39	$BrCHD + H^+ \rightarrow CHED + Br^- + 2\ H^+$	5×10^{-5}
40	$CHED + H^+ \rightarrow H_2Q + H^+$	$*8 \times 10^{-5}$
41	$CHD + BrO_3^- + H^+ \rightarrow H_2Q + HBrO_2 + H_2O$	1.6×10^{-5}
42	$2\ Fe^{3+} + CHD \rightarrow 2Fe^{2+} + H_2Q + 2H^+$	*0.03
43	$2\ Fe^{3+} + BrCHD \rightarrow Q + Br^- + 3\ H^+ + 2Fe^{2+}$	0.051

Note: The concentration of $[H^+] = 0.8M$ and $[H_2O] = 55.56M$ are included in the rate constants.

Chapter 5. Complex Oscillations in the Cerium-BZ-1,4-CHD Oscillator

In the study conducted in chapter 4, 1,4-CHD was introduced to the ferroin-catalyzed BZ reaction as a second substrate. Because 1,4-CHD alone is capable of forming a chemical oscillator with bromate in an acidic environment, the presence of 1,4-CHD not only implements the same kinds of perturbations as other second substrates do in literature, it also introduced a new autocatalytic feedback competing with the classic BZ oscillations for bromine dioxide radicals. The occurrence of complex oscillations in such a coupled oscillatory system has been attributed to competitions between ferroin and hydroquinone for bromine dioxide radicals and between 1,4-CHD and MA.

In this chapter, we investigated influences of 1,4-CHD on the nonlinear dynamics of the cerium-catalyzed BZ reaction. It is motivated by the fact that metal catalyst ferroin/ferriin and Ce^{4+}/Ce^{3+} have quite different redox potentials, which result in opposite changes in the rates of the reaction between metal catalyst and bromine dioxide radicals and the reaction of MA and the oxidized metal catalyst. More specifically, the higher redox potential of Ce^{4+}/Ce^{3+} weakens the strength of Ce^{3+} in competing with hydroquinone for bromine dioxide radicals, while the reaction of MA and Ce^{4+} is consolidated. If a balanced interaction between the autocatalytic oxidation of metal catalyst and the recovery of the reduced metal catalyst is essential for the development of complex oscillations, the ferroin- and cerium- catalyzed BZ reactions would lay on the opposite sides of a teeterboard. As a result, interesting dynamical behavior could be observed in this coupled bromate oscillator. As is shown in the following, the coupled

cerium-catalyzed BZ reaction does exhibit some new dynamical properties such as the distinct effect of cerium compared to ferroin on the appearance of complex oscillations and the symmetric geometry of the boundary separating simple and complex oscillations in the cerium-1,4-CHD phase plane and in the MA-1,4-CHD concentration plane.

5.1. Experimental procedures:

All the reactions were carried out in a thermostated glass beaker, where temperature was controlled at (25.0 ± 0.1)°C by a circulating water bath (Fisher Scientific). The volume of the reaction solution was kept constant at 30.0ml throughout this study. Reactions were monitored by a platinum electrode coupled with a $Hg|Hg_2SO_4|K_2SO_4$ reference electrode. A polyvinyl chloride lid was placed on the top of the reactor to hold the two electrodes. The potential was recorded with a personnel computer connected through a PowerLab/4SP instrument (ADInstruments). Stock solutions of 0.6M $NaBrO_3$ (Aldrich, 99%), 0.8M malonic acid (Aldrich, 98%), 3.0M sulfuric acid (Aldrich, 98%), 0.025M $(Ce)_2(SO_4)_3$ (Aldrich, 97%) were prepared with double-distilled water. 1, 4-CHD was directly dissolved in the reaction mixture. Nitrogen gas was continuously flowed through the top part of the reactor at a speed of about 0.05L/min to avoid the influence of oxygen. To reduce the amount of oxygen presented initially in the stock solutions, 1,4-CHD, sulfuric acid, malonic acid, cerium were mixed first in the reactor, and the mixture was stirred for 10 minutes under nitrogen environment. All chemicals were used in their commercial grade without further purification.

5.2 Experimental Results

Figure 5.1 presents time series of the cerium catalyzed BZ-CHD reaction observed at different 1, 4-CHD concentrations: (a) 0.0M, (b) 0.001M, (c) 0.002M, (d) 0.006M, (e)

0.007M, and (f) 0.008M. Other reaction conditions are: $[H_2SO_4] = 0.7M$, $[MA] = 0.085M$, $[BrO_3^-] = 0.08M$, and $[Ce^{3+}] = 4.0 \times 10^{-4}M$. Figures 5.1(a) and (b) show that without or with a small amount of 1, 4-CHD present in the coupled oscillation system, no complex oscillation can be observed. Similar to the ferroin catalyzed 1, 4-CHD-BZ system studied in chapter 4, when the concentration of 1, 4-CHD is increased further, more drastic changes in the oscillatory behavior take place. When the concentration of 1,4-CHD is increased to 0.002M, for example, burst phenomena appear. However, with the further increase of 1,4-CHD concentration, the system evolve back into simple oscillations. When the concentration of 1,4-CHD is above 0.007M, instead of the sequential oscillation seen in the ferroin-BZ-CHD system, other modes of complex oscillations took place. (figures 5.1 e, f). This series of experimental results illustrate that 1,4-CHD plays an important role in the development of complex oscillations in this mixed bromate-oscillator.

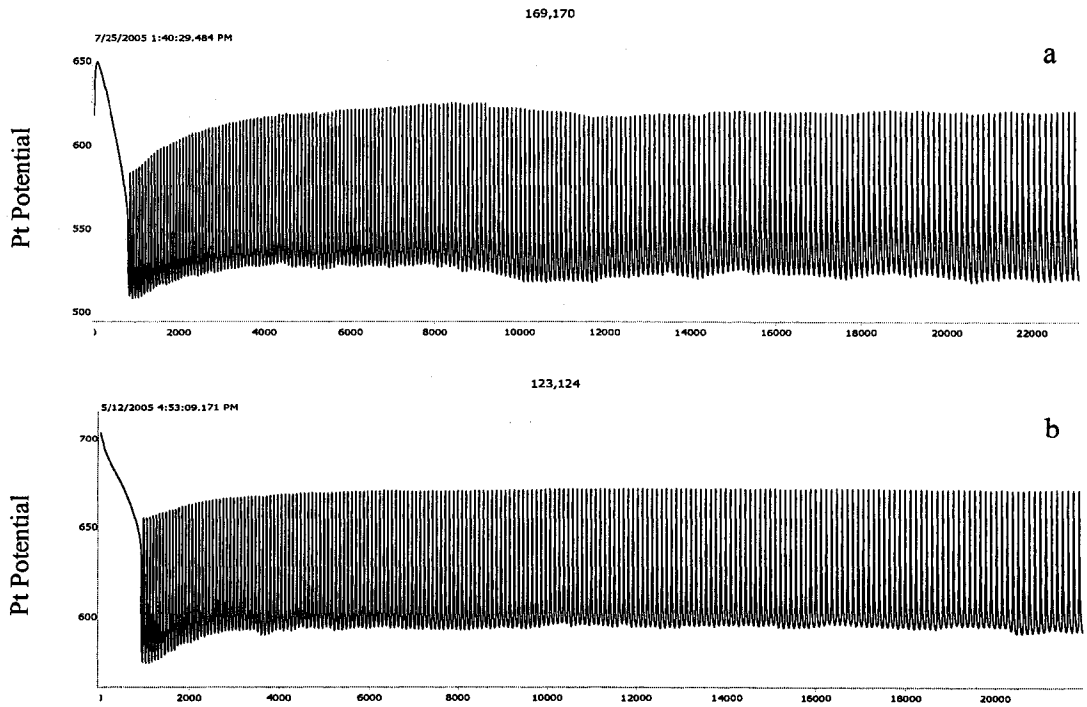

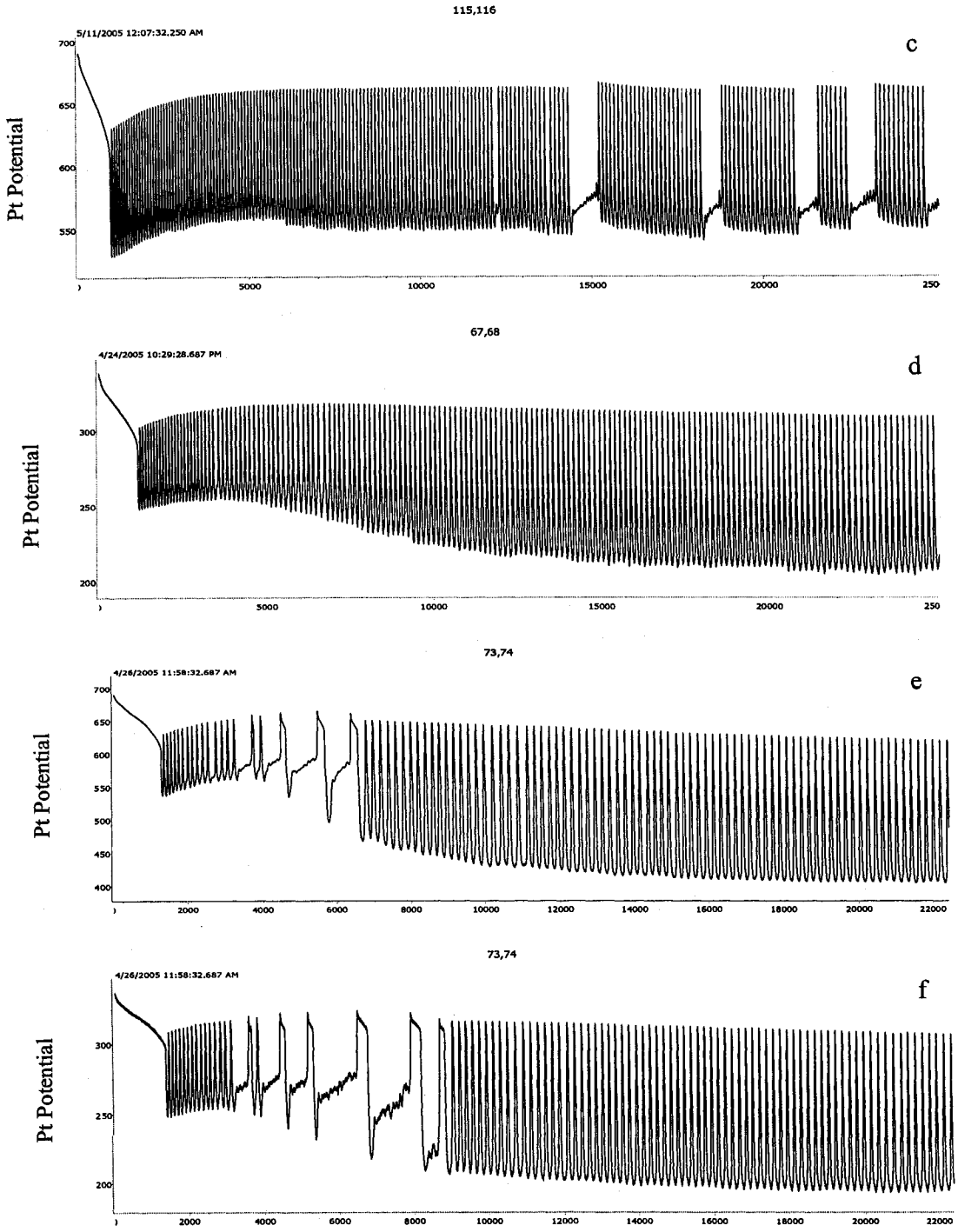

Figure 5.1

Figure 5.2 presents the length of the induction time as a function of 1,4-CHD concentration for the conditions used in figure 5.1. As shown in the figure, there was a long induction time which grows with the increase of 1,4-CHD concentration. During the induction time period, the reaction solution exhibits yellow color, indicating the system is at the oxidized state. This further suggested that the presence of a long induction time is due to the insufficient amount of Br^- being produced.

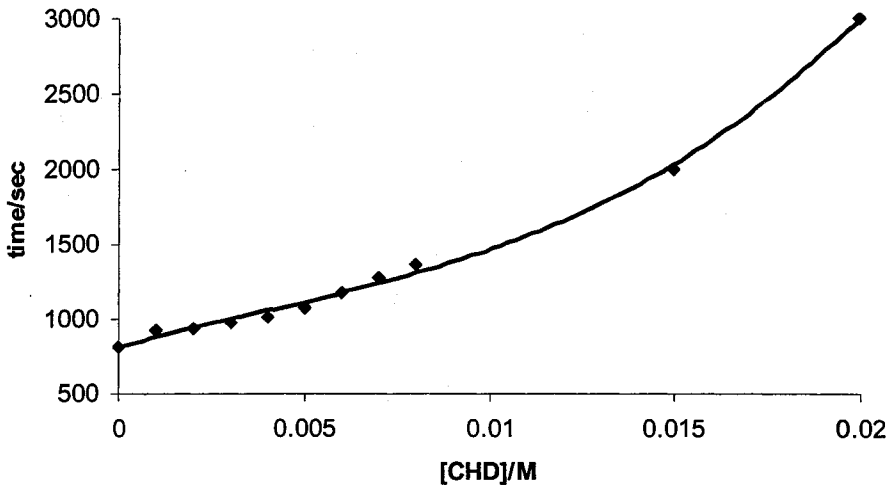

Figure 5.2

The influence of 1,4-CHD on the oscillatory behavior was also studied at a lower bromate concentration level. Figure 5.3 presents three time series at the bromate concentration of 0.04M, in which the 1,4-CHD concentration was changed as the only variable: (a) 0M, (b) 0.001M, (c) 0.002M.

The following experimental results indicate that at lower bromate concentration, the mixed oscillation system is more sensitive to the 1,4-CHD than that in higher bromate condition. When bromate concentration is 0.04M, the addition of 0.001M 1,4-CHD results in the burst phenomenon (5.3b), while at bromate concentration 0.08M, shown in

figure 5.1b, 0.001M 1,4-CHD does not have obvious influence on the oscillation behavior until the concentration of 1,4-CHD is increased up to 0.02M at which burst oscillations appear.

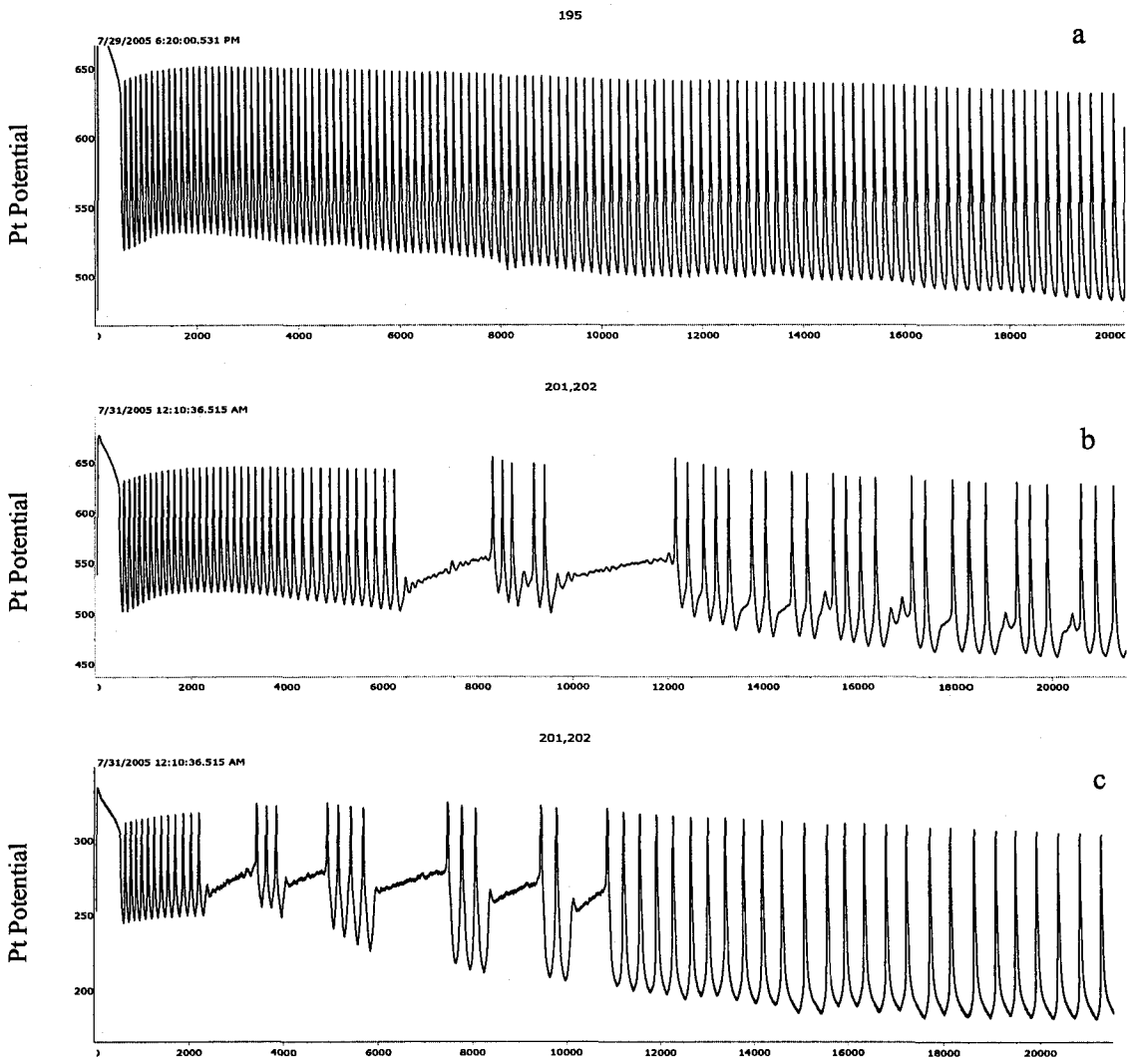

Figure 5.3

Figure 5.4 shows four time series of the mixed BZ reaction at different cerium concentrations: (a) 4.0×10^{-4}M, (b) 8.0×10^{-4}M, (c)1.0×10^{-3}M, and (d)1.2×10^{-3}M. Other

reaction conditions are: $[H_2SO_4]$ = 0.7M, [MA] = 0.085M, $[BrO_3^-]$ = 0.08M, and [1,4-CHD] = 0.005M.

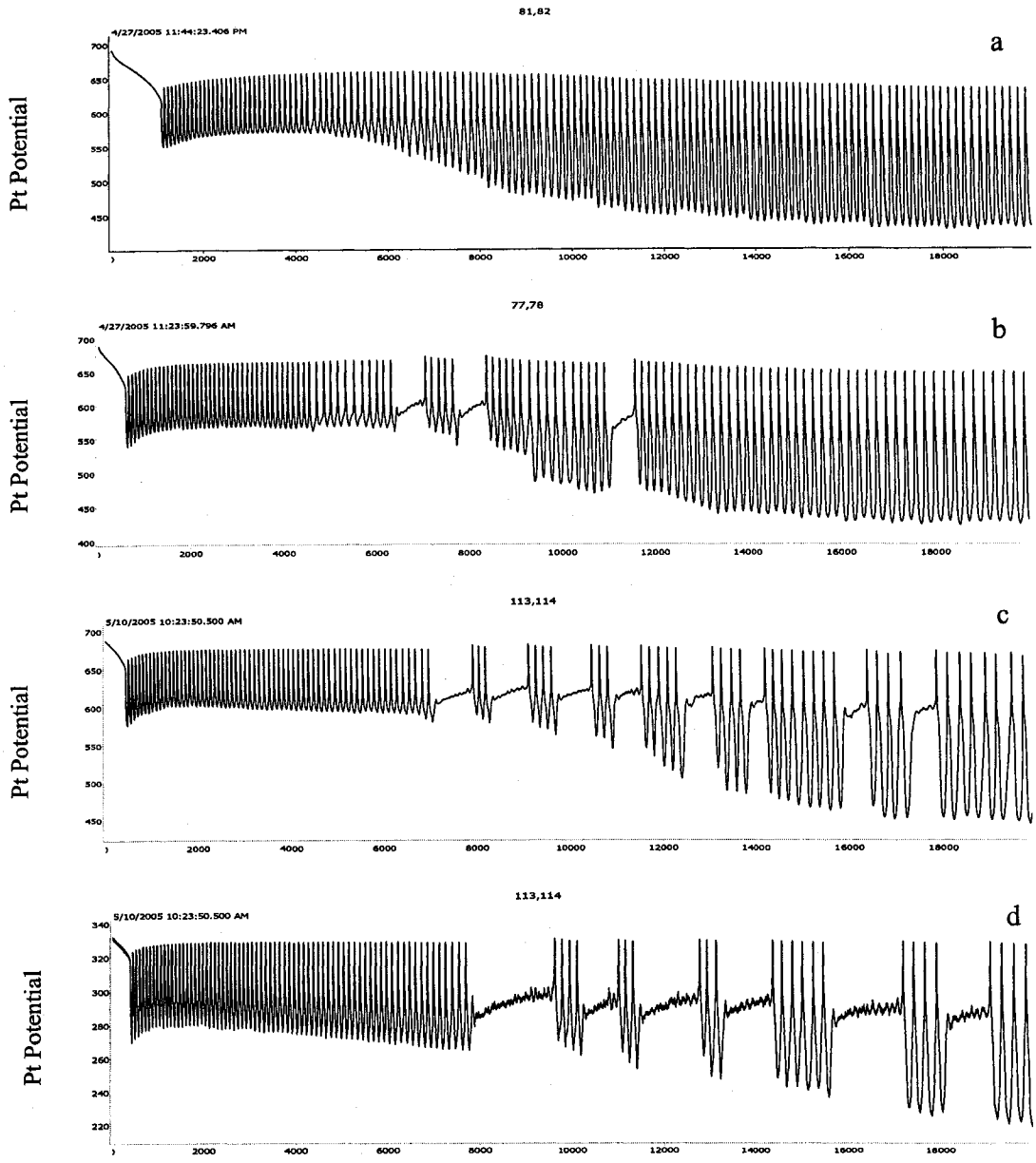

Figure 5.4

At low cerium concentration, only simple oscillations are observed. When the cerium concentration is increased to 8.0×10^{-4} M, burst phenomena are observed. The burst phenomena become more obvious as the cerium concentration is increased further. Even

after the concentration of cerium is increased to 1.6×10^{-3}M, burst phenomena can still been seen. Therefore, the catalyst cerium in this system played an distinct role with the ferroin on the development of complex oscillations in the mixed BZ-1,4-CHD system, in which the increase of ferroin concentration quenches the complex oscillations. Such a difference may be understood based on the redox potential difference between the Ce(IV)/Ce(III) and ferriin/ferroin couple. The oxidation rate of the metal catalyst by the BrO_3^-/ BrO2· couple depends on the redox potential of themselves. Since the redox potential of Ce(IV)/Ce(III) (1.44 V) is much higher than the ferriin/ferroin couple, the oxidization rate of cerium(III) by bromine dioxide radicals to cerium (IV) therefore is much slower than that of ferroin. On the other hand the reduction rate of Ce(IV) by malonic acid will be faster than that of ferroin at analogous conditions.

$$Ce^{4+} + e^- \longrightarrow Ce^{3+} \qquad E^\circ = 1.44\ V$$

$$Fe^{3+} + e^- \longrightarrow Fe^{2+} \qquad E^\circ = 1.06\ V$$

Figure 5.5 presents the induction time of those spontaneous oscillations as a function of cerium concentration. This result indicates that the induction time decreases with respect to the increase of cerium concentration. Comparing figure 5.5 with figure 5.2, one can see that 1,4-CHD and cerium play an opposite role in the occurrence of the induction time, which represents useful information for the further understanding of the competition between this two species for bromine dioxide radical.

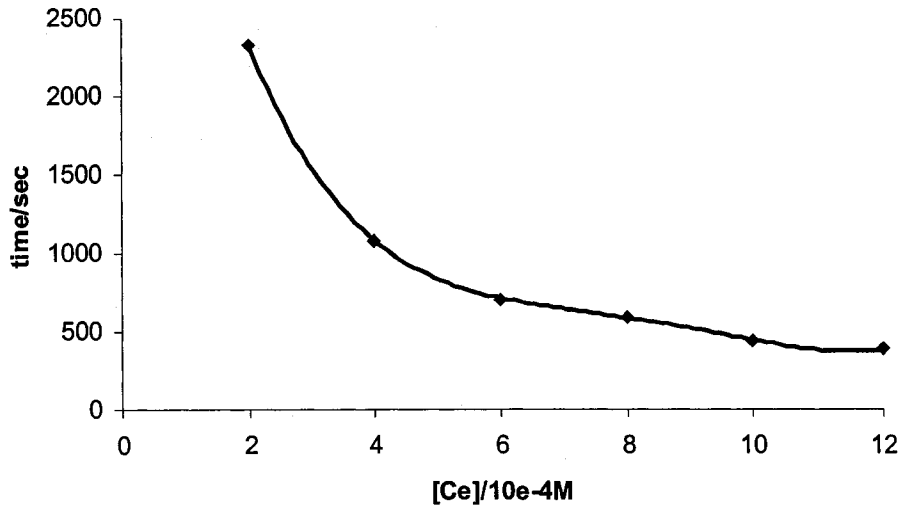

Figure 5.5

Figure 5.6 presents the influence of cerium concentration on the oscillatory behavior at 1,4-CHD concentration equal to 0.006M. The concentration of cerium is (a) 1.0×10^{-4}M, (b) 2.0×10^{-4}M, (c) 4.0×10^{-4}M, and (d) 8.0×10^{-4}M. Other reaction conditions are the same as those in figure 5.4. Similar to the series in figure 5.4, the increase of cerium concentration induces the transition of the system from simple to burst phenomenon. However, at low cerium condition, more interesting phenomena such as mixed mode oscillations, and dual frequency oscillations were observed.(see figure 5.6 (a) and (b)) When cerium concentration is 1.0×10^{-4}M, there is a long induction time before the appearance of mixed mode oscillations. When the cerium concentration is increased to 2.0×10^{-4}M, dual frequency oscillations appear, where the low frequency oscillations only last about 4000 seconds then the system evolves into high frequency simple oscillations. In this series, the induction time also monotonically decreases with respect to the increase of cerium concentration.

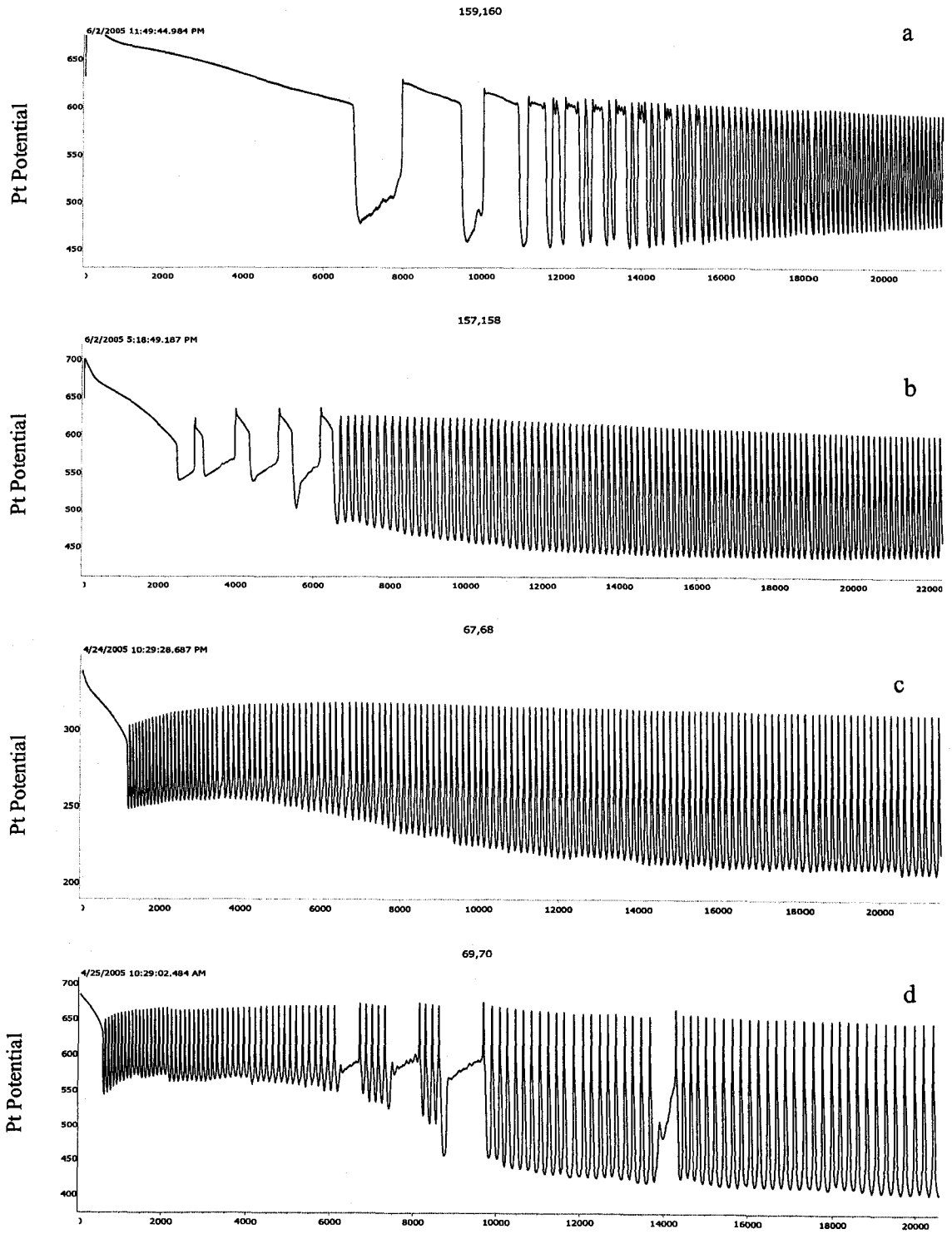

Figure 5.6

Figure 5.7 presents three time series achieved at different initial concentrations of malonic acid: (a) 0.045M, (b) 0.125M, and (c) 0.285M. Other reaction conditions are $[H_2SO_4] = 0.7M$, $[Ce^{3+}] = 4.0 \times 10^{-4}$ M, $[BrO_3^-] = 0.08M$, and [1,4-CHD] = 0.005M.

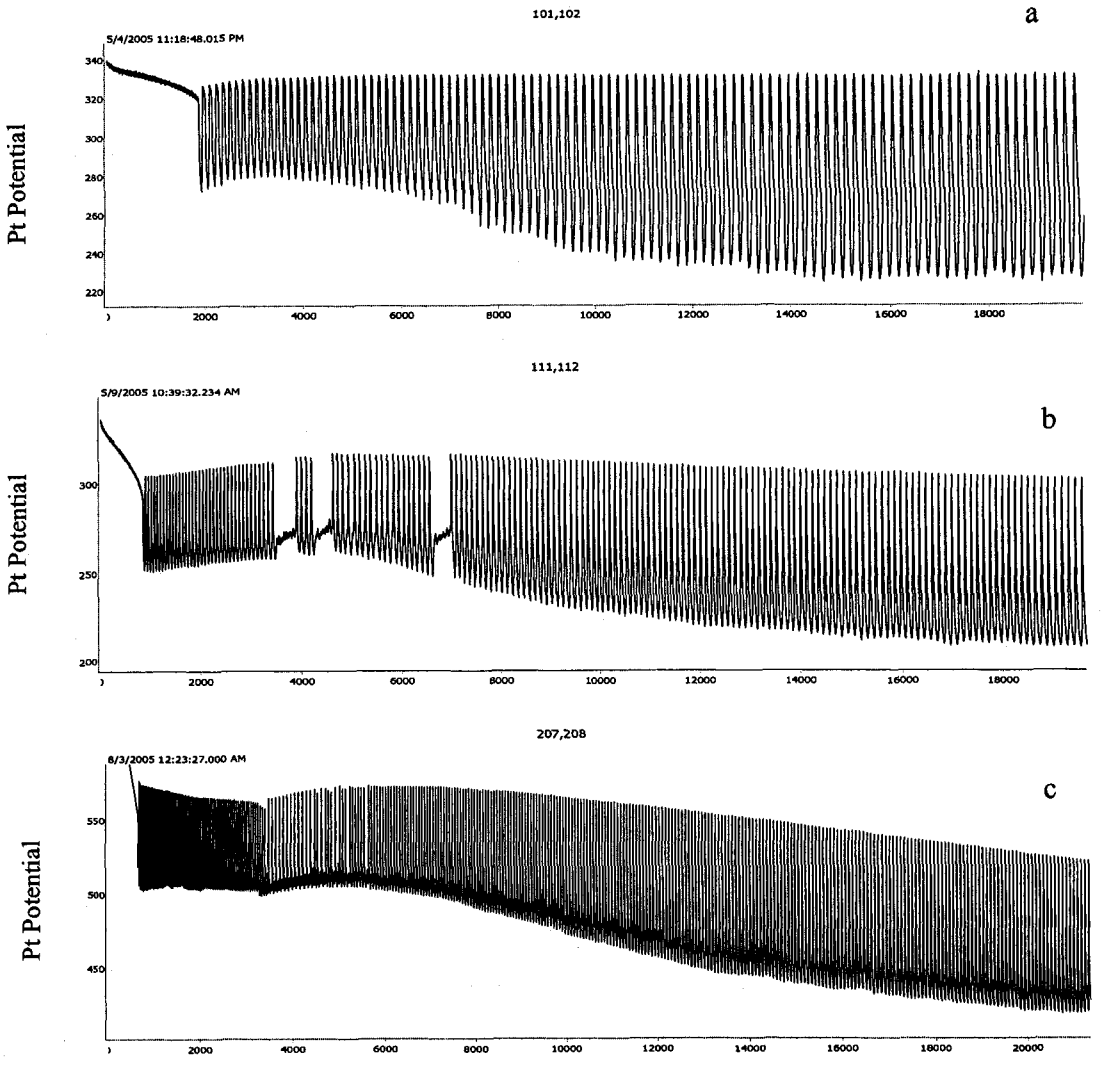

Figure 5.7

At the low malonic acid concentration condition, MA does not play an essential role in the development of complex oscillations.(see figure 5.7a) When malonic acid concentration is increased to 0.125M, burst oscillations appear, which have also been observed at similar malonic acid condition in the ferroin-catalyzed 1,4-CHD-BZ reaction system. When malonic acid concentration is increased to 0.285M, the oscillation frequency is increased dramatically, and period-doubling oscillations take place. These results indicate that malonic acid plays a similar role in both the ferroin- and cerium-catalyzed BZ oscillators.

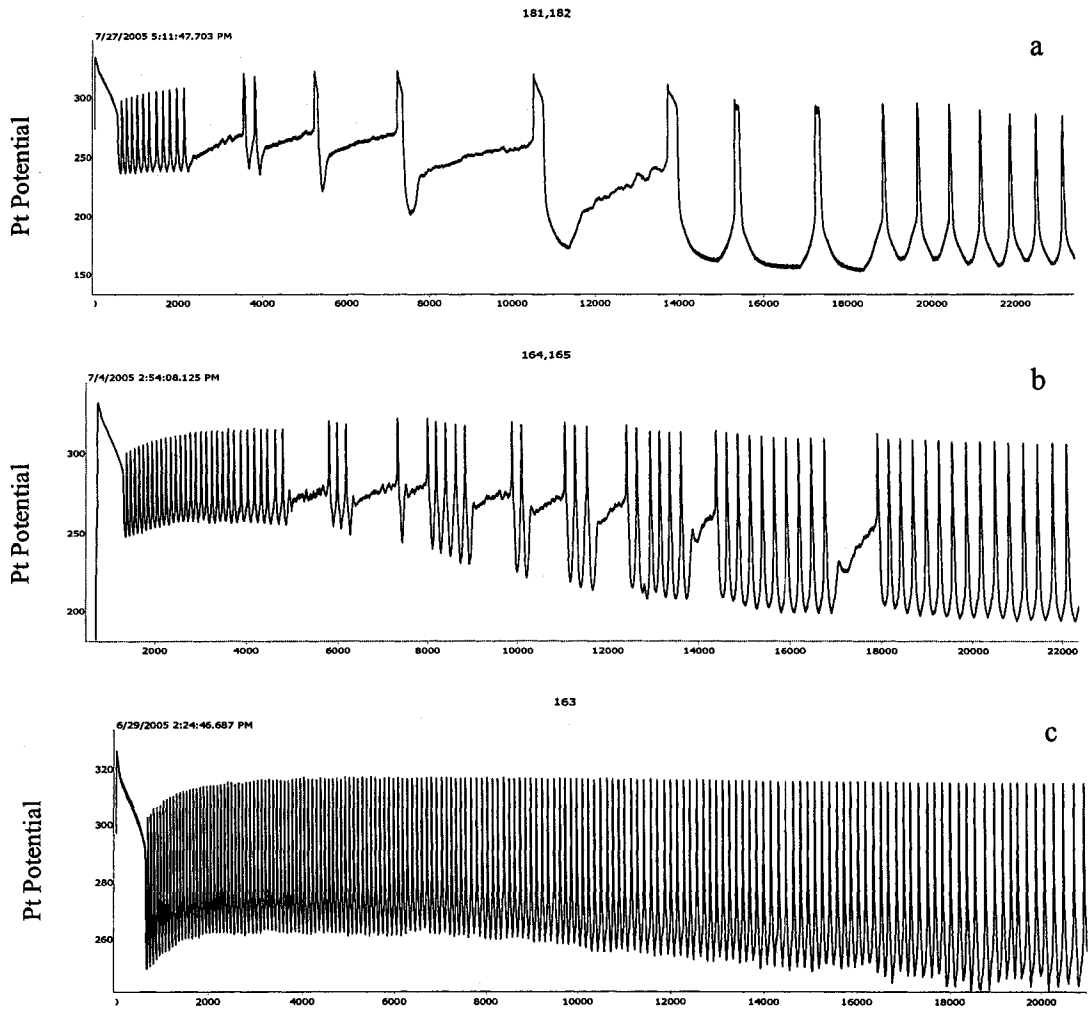

Figure 5.8

Figure 5.8 presents three time series obtained at different bromate concentration: (a) 0.04M, (b) 0.06M, and (c) 0.1M. Other reaction conditions are the same as these used in figure 5.4b. The system undergoes transformation from complex to simple oscillations as the bromate concentration is increased. For example when the bromate concentration is increased to 0.1M, complex oscillations disappear completely. Similar result was also observed in the ferroin-BZ-1,4-CHD system, implicating that bromate plays a similar role in both systems. Comparing with the result shown in figure 5.4(b), which is obtained under a lower bromate concentration, oscillations in figure 5.7(c) are more complicated, and last for a longer time.

Figure 5.9a presents a phase diagram of the reaction dynamics in the Cerium-1,4-CHD concentration plane. Three dynamic areas are observed there: (I) simple oscillations, (II) bursting phenomena, and (III) complex oscillations. The reaction conditions are: $[H_2SO_4] = 0.7M$, $[MA] = 0.085$ M, and $[BrO_3^-] = 0.08M$. When the concentration of 1,4-CHD or cerium is low, only simple oscillations can be observed. When concentrations of 1,4-CHD and cerium are increased to above a certain level (region II), burst phenomena are observed. For 1,4-CHD concentration between 0.003M and 0.006M, burst phenomena are observed even after the concentration of cerium is increased to 1.2×10^{-3}M. Notably, in the cerium-1,4-CHD phase plane, the boundary separating simple and complex oscillations is symmetric, implying that competitions between cerium and 1,4-CHD for bromine dioxide radical have played an essential role in the development of complex oscillations.

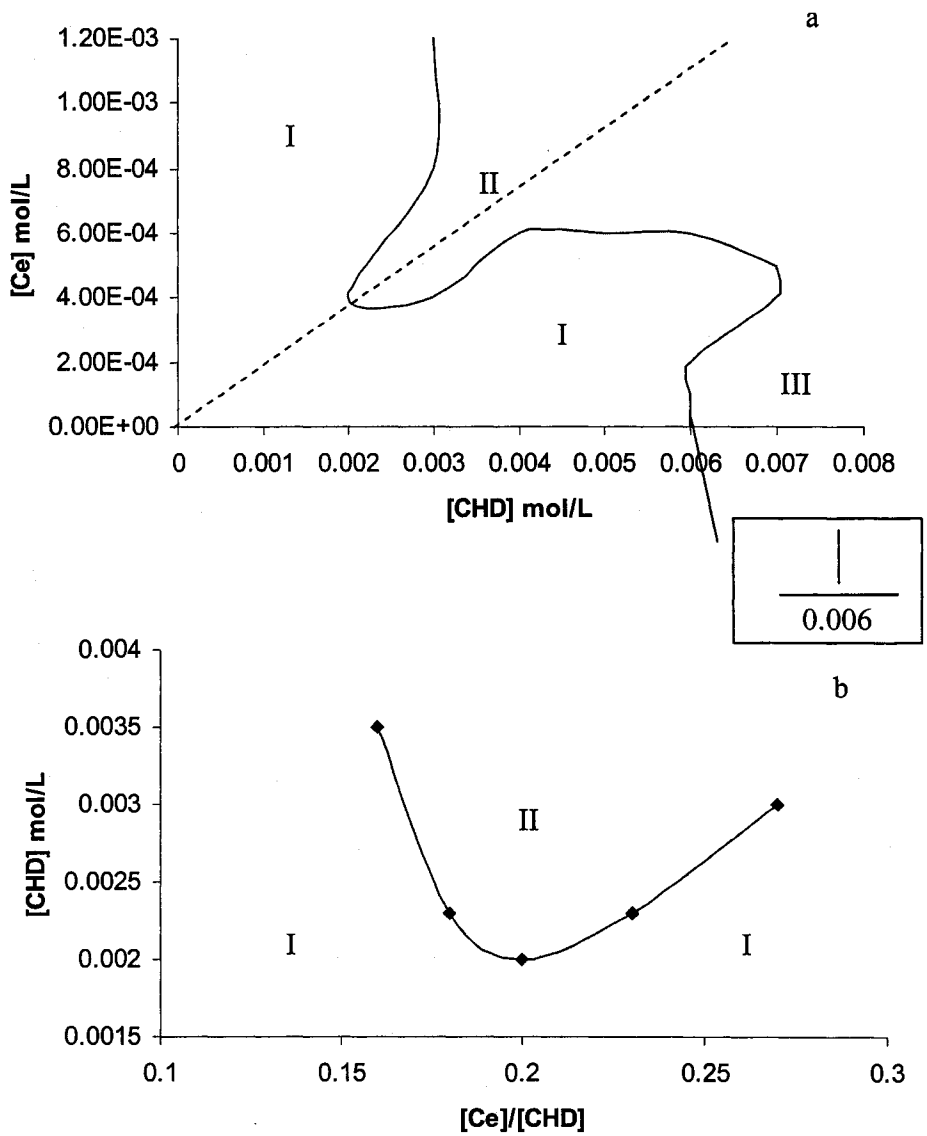

Figure 5.9

In figure 5.9b the reaction dynamics is characterized by plotting the concentration of 1,4-CHD versus the ratio of cerium and 1,4-CHD. Region II presents complex oscillations, while region I presents simple oscillations. This figure clearly illustrates that the occurrence of complex oscillations depends on the concentration ratio of cerium and 1,4-CHD. In other words the competition between this two species plays a very important

role in the oscillatory behavior. As is shown in figure when the ratio is 0.2, very small amount of 1,4-CHD can cause burst phenomena, while farther away from this state more 1,4-CHD is needed to cause dramatic changes in the oscillatory behavior.

It is important to point out that in figure 5.9a when the cerium concentration is between 4.0 $\times 10^{-4}$M and 6.0 $\times 10^{-4}$M the system undergoes a transition from simple to complex and then back to simple oscillatory behavior as the concentration of 1,4-CHD is increased. In order to conform the above interesting phenomena, one more series of experiments at the concentration of cerium 5.0 $\times 10^{-4}$ M are carried out and the results are shown in figure 5.10. The 1,4-CHD concentration is varied gradually as: (a) 0.001M, (b) 0.002M, (c) 0.005M, and (d) 0.008M. Other reaction conditions are the same as those used in figure 5.1. Transition from simple to burst, burst back to simple, and then simple to more complex oscillations are observed again in series.

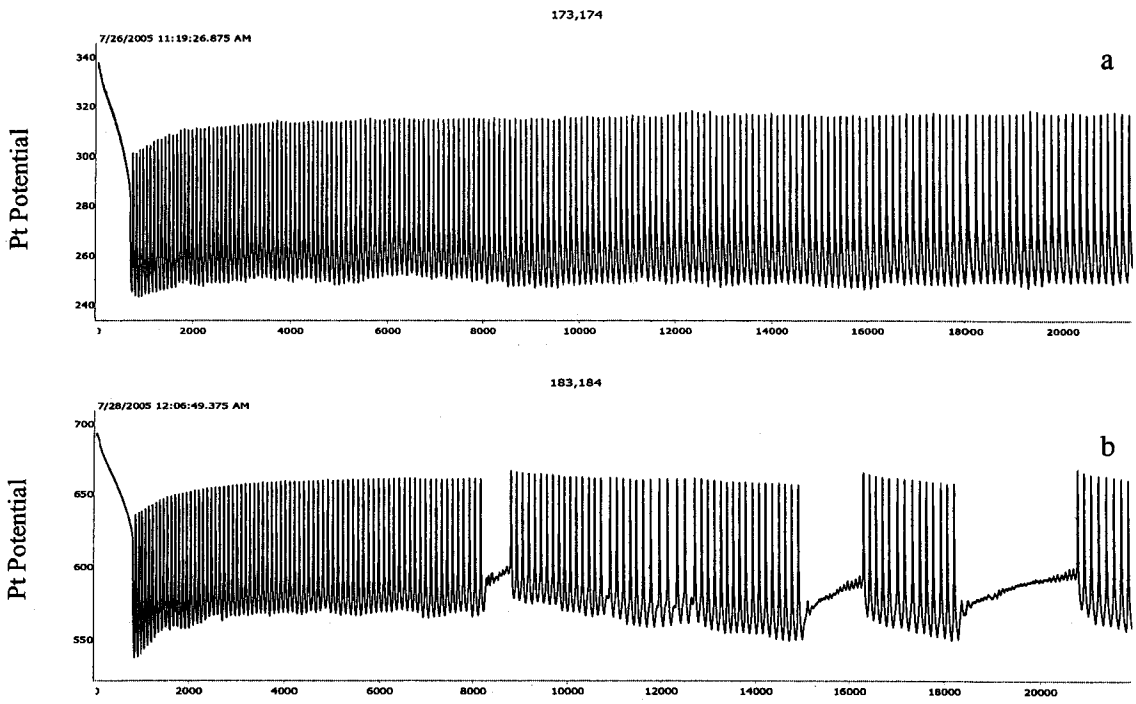

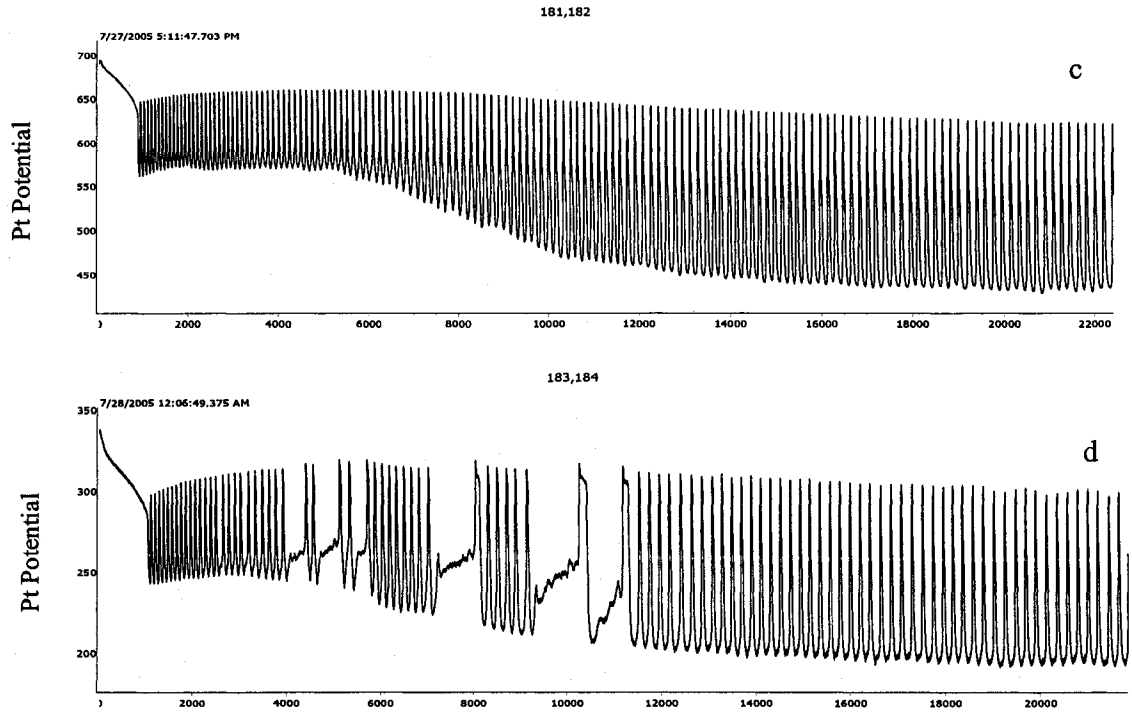

Figure 5.10

Example of typical oscillatory behaviors in different regions of the Ce-1,4-CHD phase diagram are presented in figure 5.11: (a) simple oscillations in region I, (b) burst phenomena in region II, and (c) complex oscillations in region III.

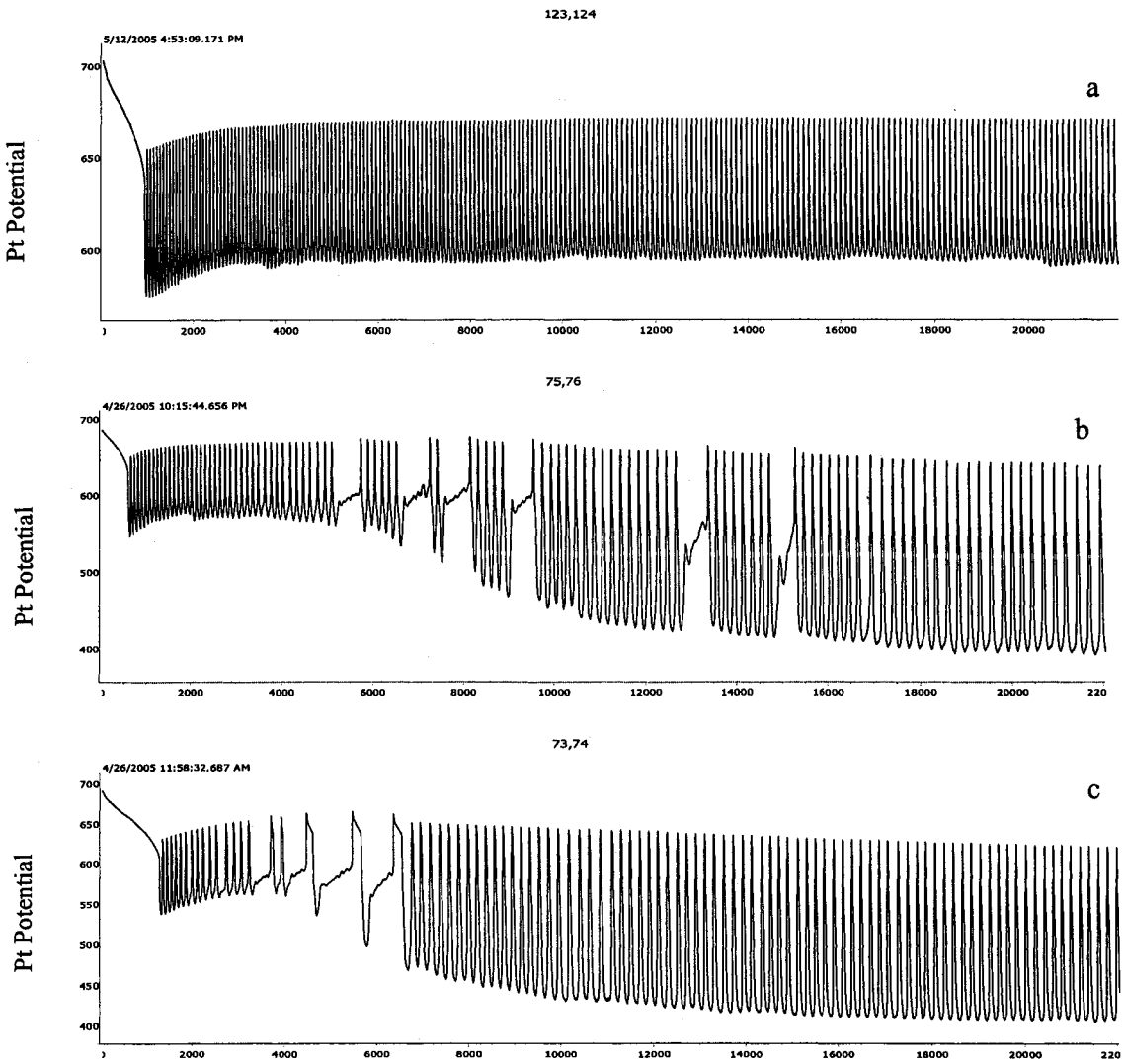

Figure 5.11

Figure 5.12 presents four series of the induction time as a function of cerium concentration at different 1,4-CHD concentrations 0.003M, 0.004M, 0.005M, 0.006M, and 0.007M. As the cerium concentration is increased, the induction time decreases monotonically. Moreover, the series obtained at a higher 1, 4-CHD concentration always stays on top of the ones obtained at the lower 1, 4-CHD concentration. This is consistent

with the result that the induction time increases with respect to the increase of 1,4-CHD concentration.

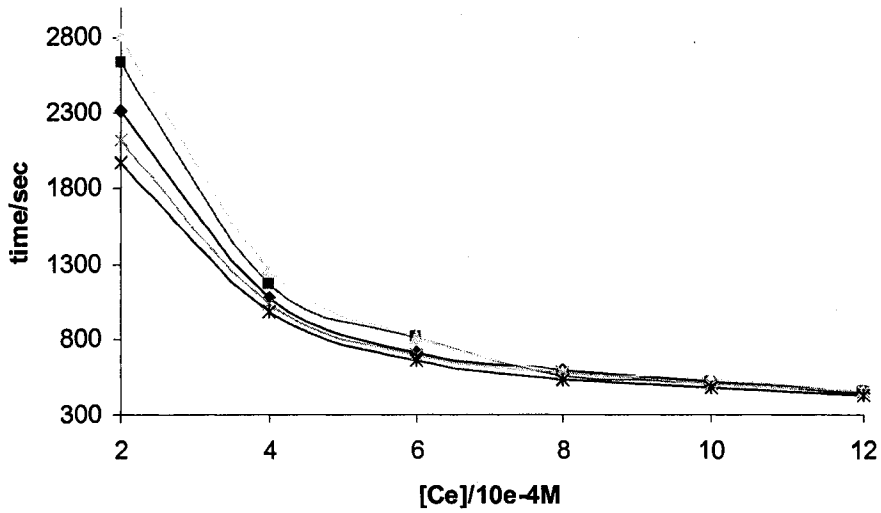

Figure 5.12

Complex oscillations are also characterized in the 1,4-CHD-MA concentration plane. (see figure 5.13a) Reaction conditions are: $[H_2SO_4]$ = 0.7M, [Ce] = 4×10^{-4} M, and $[BrO_3^-]$ = 0.08M. There are four dynamic regions in this phase diagram: (I) simple oscillations, (II) bursting phenomena, (III) complex oscillations, and (IV) non-oscillatory area. It is necessary to point out that in this phase diagram, there is a nonoscillatory region IV at very low concentrations of malonic acid. This result indicates that in the region around the original, the classic BZ reaction plays an important role in the oscillatory behavior since decreasing malonic acid to this region can be approximately treated as eliminating the classic BZ reaction. It is also interesting to point out that we did not find the nonoscillatory region in the Ce-1,4-CHD concentration phase plane.

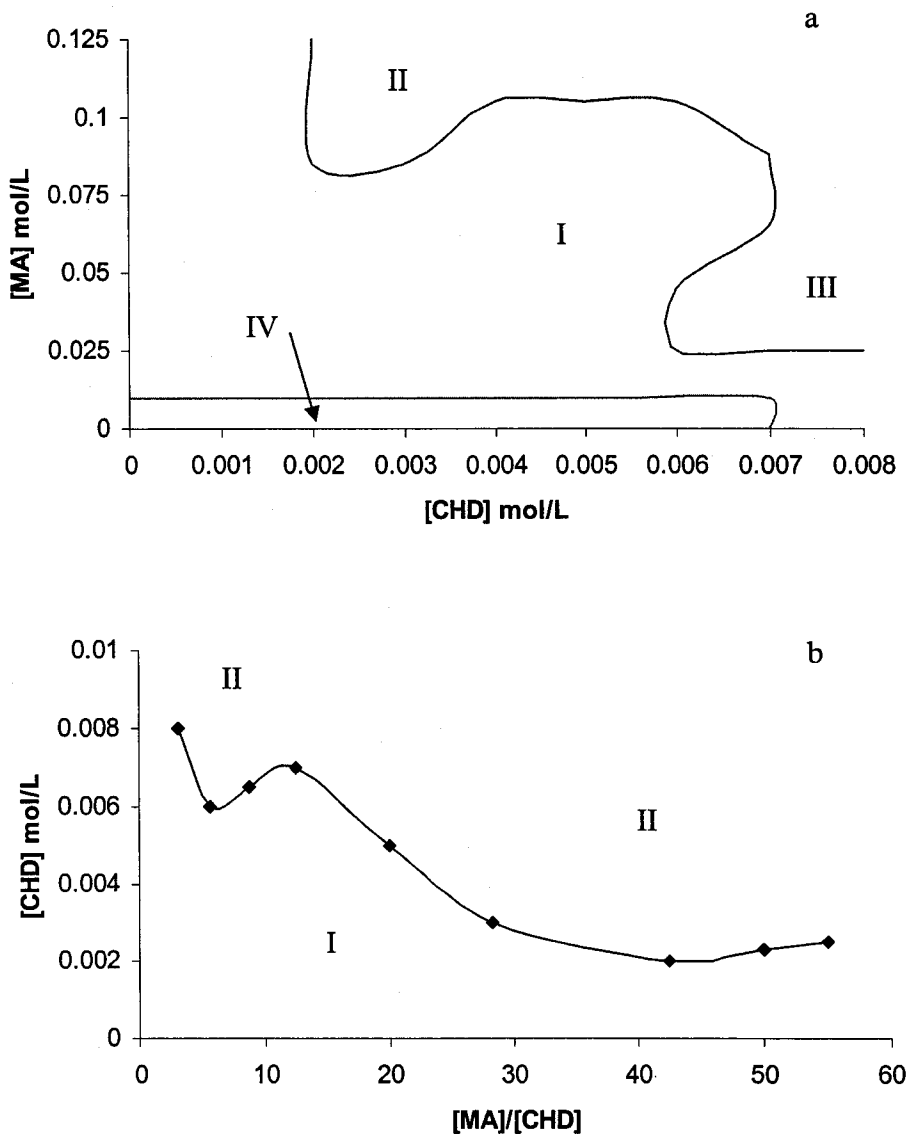

Figure 5.13

In figure 5.13b, the reaction dynamics is characterized by plotting the concentration of 1,4-CHD versus the ratio of malonic acid and 1,4-CHD. Different from what was seen on the Ce-1,4-CHD concentration plane, there are two minima in this figure. This figure illustrate at high ratio of [MA]/[CHD], the system is much more sensitive to the variation of 1,4-CHD concentration. On the other hand, at the low [MA]/[1,4-CHD] ratio the

competition between malonic acid and 1,4-CHD is also very important to the development of complex oscillations.

Typical oscillations in different regions of Ce-1,4-CHD phase plane are shown in figure 5.14: (a) simple oscillations in region I, (b) burst phenomena in region II, and (c) complex oscillations in region III.

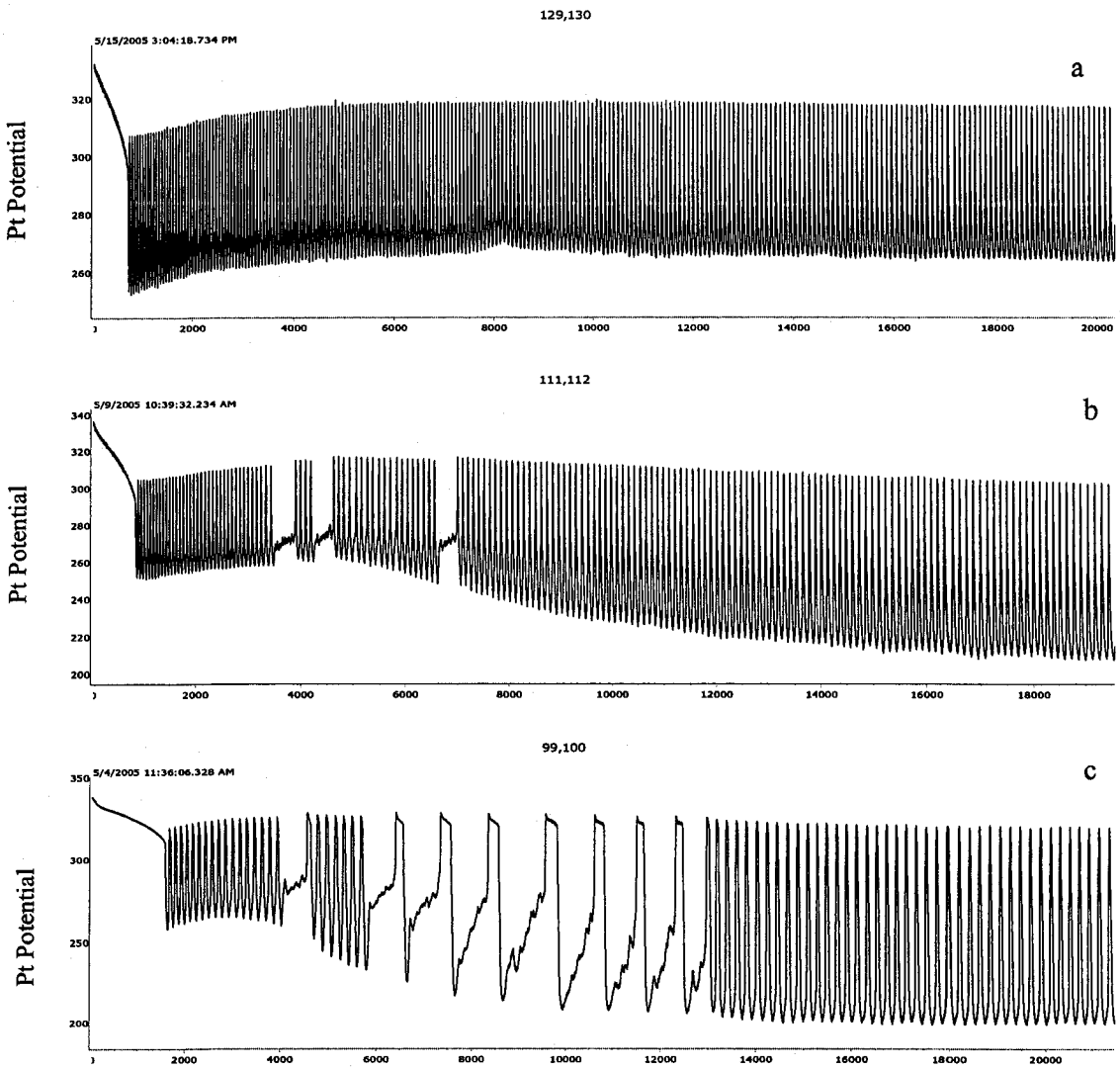

Figure 5.14

Figure 5.15 presents five series of the induction time plotted as a function of the concentration of malonic acid at [1,4-CHD]: 0.003M, 0.004M, 0.005M, 0.006M and 0.007M. The induction time becomes shorter as the malonic acid concentration increases. The series obtained at higher 1,4- CHD concentration has a longer induction time than those conducted at low 1,4-CHD concentration.

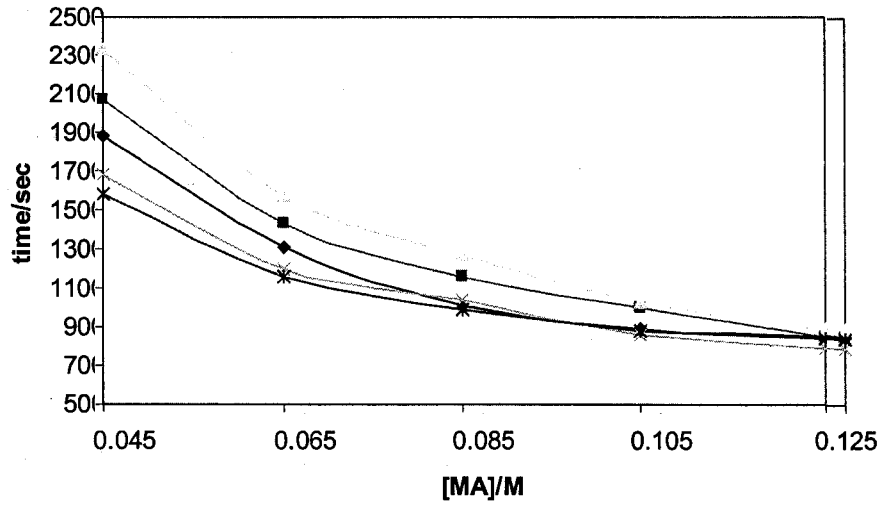

Figure 5.15

To shed light on properties of these complex oscillations, illuminations are employed to perturb the mixed BZ reaction. According to existing literatures, the cerium-catalyzed BZ reaction is not sensitive to light perturbation, while both positive and negative effects of light on the 1,4-CHD bromate oscillations have been reported.[47-49] Responses of the mixed BZ reaction to light perturbation are shown in figure 5.16, in which the perturbation is conducted at different time periods: (a) initial oscillations, (b) burst oscillations, and (c) non-oscillatory period (d) secondary oscillations

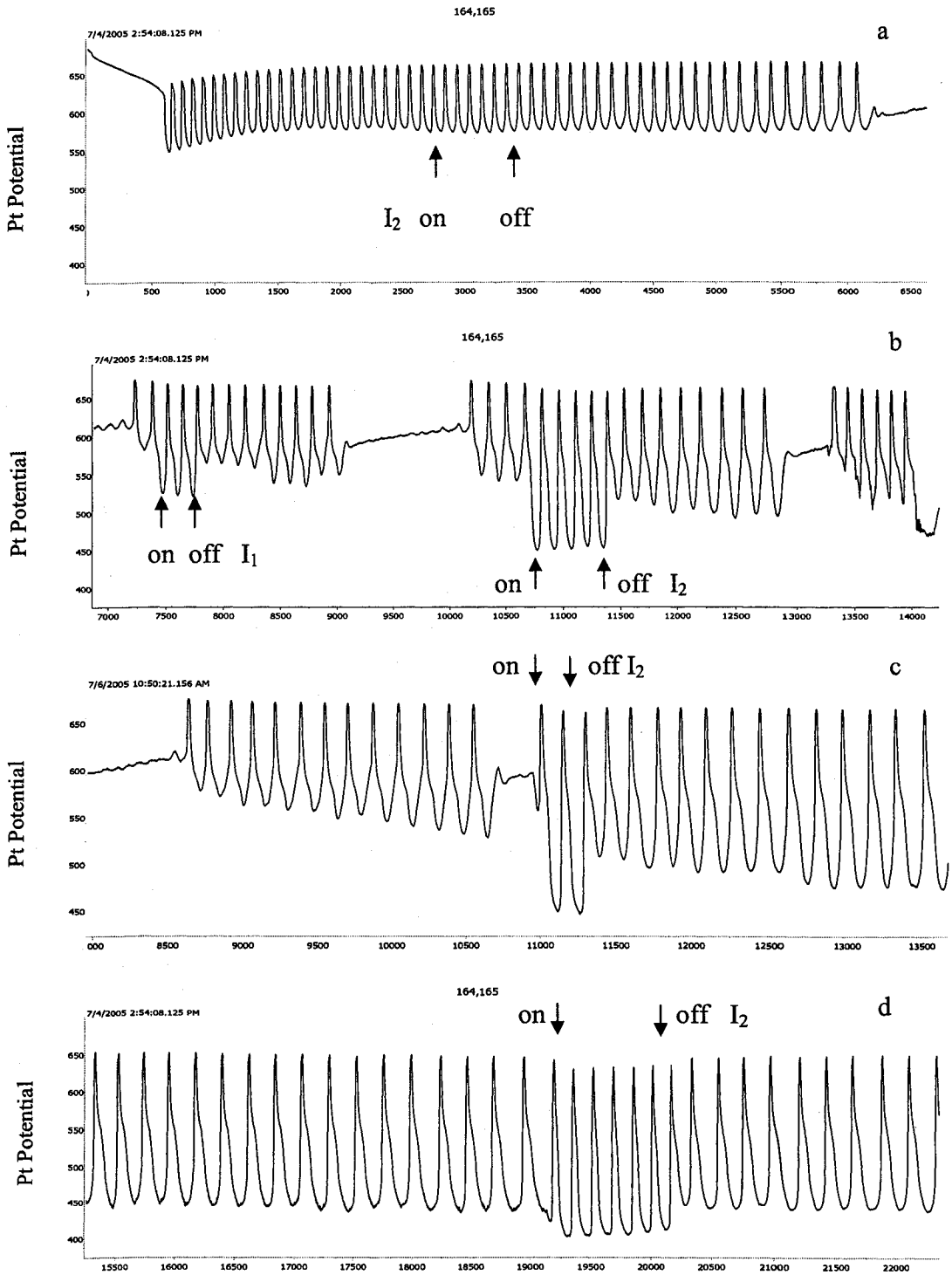

Figure 5.16

Reaction conditions here are the same as that in figure 5.4(b). Figure 5.16(a) shows that when light is applied to perturb the initial simple oscillations, there is no obvious

influence even though the light intensity is increased to 100mW/cm^2. This experimental result suggests that these initial oscillations are controlled by the cerium-BZ reaction, due to their similar responses to light. Figure 5.16(b) presents light perturbation at I_1 = 50mW/cm^2, and I_2 = 100mW/cm^2 conducted respectively, during the complex oscillations. Notably, light perturbation causes drastic changes on the amplitude of these oscillations. The amplitude of these light-induced oscillations increases with respect to the intensity of the applied light. It is interesting to point out that light can also trigger oscillations during the non-oscillation period between two burst (see figure 5.16 (c)). Since light has very similar effect as that in the 1,4-CHD-bromate oscillator, it suggests that 1,4-CHD system plays a prominent role during this reaction period. However, we did not observe any negative light effects on the mixed oscillator during this period, although different intensities of light were applied. Figure 5.16(d) shows the light perturbation on the secondary simple oscillations. The frequency of these oscillations is increased and the potential is shifted when the light is applied during this period. The potential shift in the 1,4-CHD-bromate oscillator upon light perturbations has been reported by our group[48]. The response to light observed during the secondary oscillations indicates that the 1,4-CHD bromate still play an important role during this period.

5.3 Computational Results:

The model is constructed by combining a model proposed by Gyorgyi and coworkers for the cerium-catalyzed BZ reaction[94] and a mechanism developed by Koros and coworkers for the 1,4-CHD bromate oscillator[18]. The new model consists of 33 reaction steps and 16 variables. All of the reaction rate constants are taken from the literature

without modification except that k_9 and k_{20} are decreased 10 times from their original values.

Figure 5.17 presents three time series calculated from the model listed in table 5.1, in which the initial cerium concentration is adjusted as the only variable: (a) 4.0×10^{-4} M, (b) 8.0×10^{-4} M, and (c) 1.0×10^{-3} M. Initial values of other reactants match those used in the experiments. Similar to the experiment observation, when cerium concentration is set to 4.0×10^{-4} M, only simple oscillations can be observed. When cerium concentration is increased to 8.0×10^{-4} M, burst phenomena occur. This result suggests that the complex oscillations seen in our experiments arise from the intrinsic dynamics. This series of simulation results qualitatively reproduce the experimental observations that an increase of cerium concentration gives rise to complex oscillations.

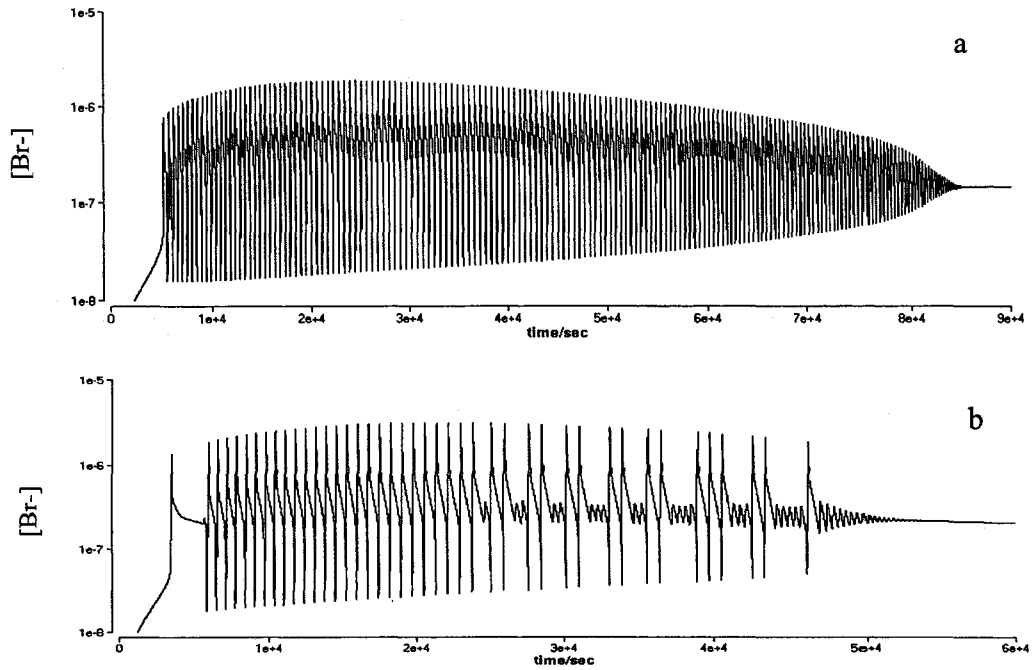

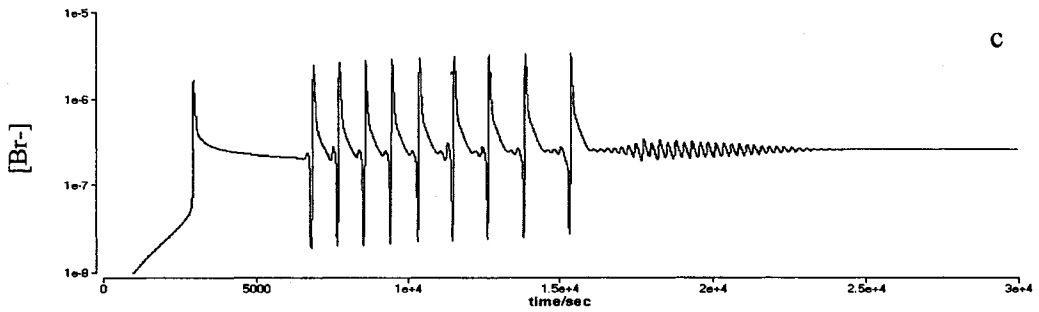

Figure 5.17

Our simulation also illustrates that the complex dynamic behavior of the mixed cerium-catalyzed BZ reaction is particularly sensitive to the rate constants k_9 and k_{20}, which in turn determines the competition between the catalyst cerium and hydroquinone (an intermediate product of 1,4-CHD) for the bromine dioxide radical. The burst phenomena could only be observed when the rate constant k_9 was set to be between 8300 and 9300, and the k_{20} was set to be between 5.6×10^{-4} and 6.1×10^{-4}.

R9 $\quad Ce^{3+} + BrO_2 \cdot + H^+ \rightarrow HBrO_2 + Ce^{4+}$

R20 $\quad H_2Q + 2\,BrO_2 \cdot \rightarrow 2HBrO_2 + Q$

In order to provide insights into the 1,4-CHD induced complex oscillations, numerical simulations at different 1,4-CHD concentrations are carried out. In the simulation, 1,4-CHD concentration is adjusted as: [CHD] (a) 0.0003M, (b) 0.001M, (c) 0.004M, and (d) 0.007M. Other reaction conditions are the same as those used in figure 5.10. Similar to the experimental observation, when the concentration of 1,4-CHD is very low or at zero, only simple oscillations appear. When the concentration of 1,4-CHD is increased to 0.001M, burst oscillations are observed. When the 1,4-CHD concentration is further increased, the system undergoes a transition from burst to simple oscillations. Increase of 1,4-CHD concentration leads to complex oscillations appear again.

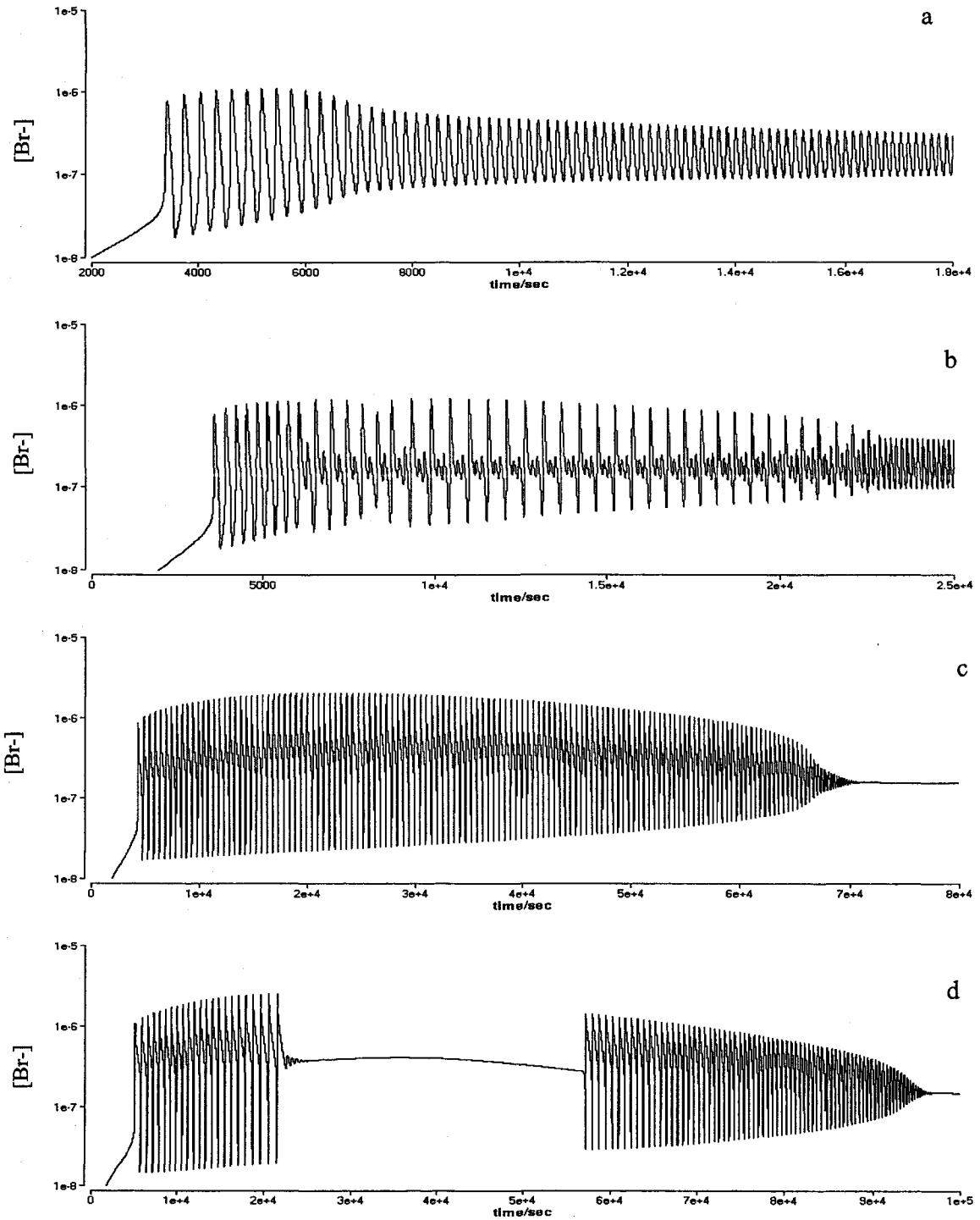

Figure 5.18

To shed light on the governing mechanism of each reaction stage, during the simulation process we temporarily eliminated one of the two suboscillators. Within the

first oscillation window (<5000 second), if the concentration of MA and BrMA are temporarily set to zero to remove the cerium-BZ oscillator, spontaneous oscillations stop immediately, as is shown in figure 5.19a. However, temporarily setting concentrations of 1,4-CHD and BrCHD to zero, as is shown in figure 5.19b, does not affect those spontaneous oscillations. This simulation result illustrates that these initial simple oscillations (before the burst) is governed by the classic BZ reaction.

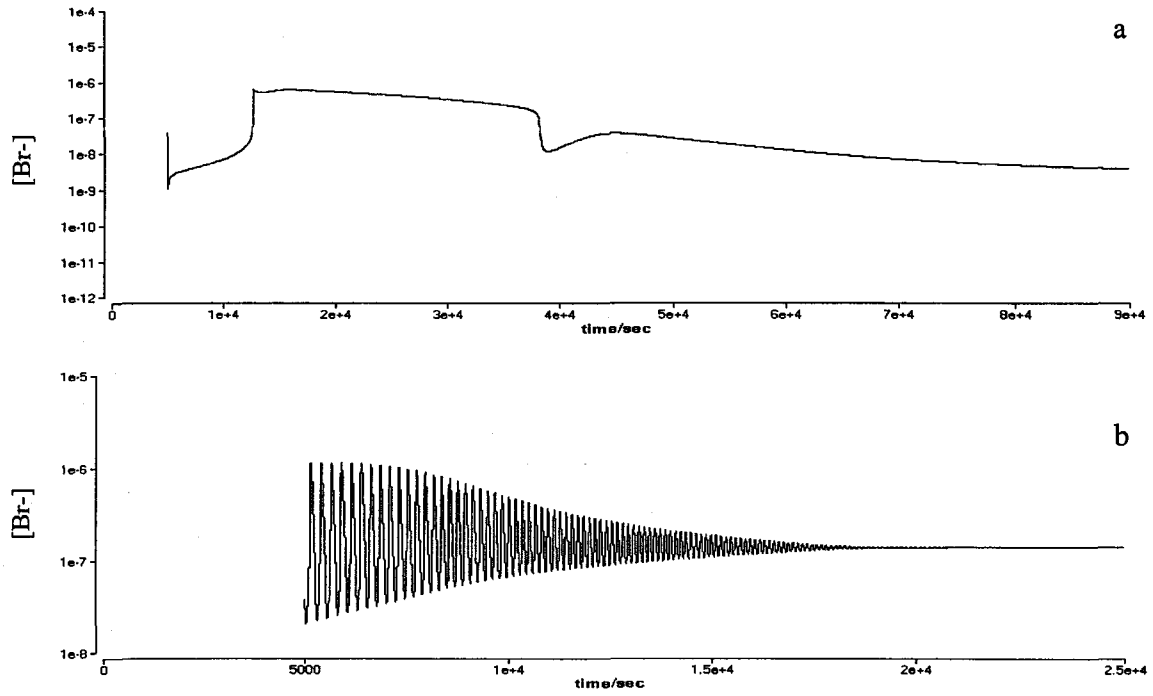

Figure 5.19

During the complex oscillations (around 15000 second), if concentrations of 1,4-CHD and BrCHD are set to zero, the complex phenomena disappear immediately (figure 5.20a), illustrating that the 1,4-CHD-bromate oscillator plays an essential role in the occurrence of the burst. Indeed, during the burst oscillations, temporarily setting BrCHD concentration to zero alone is sufficient to quench the burst to simple oscillations (5.20b). This suggests that BrCHD dominates the production of H_2Q at a rate that is high enough

to compete with the cerium for bromine dioxide radicals to give rise to the complex oscillations. Certainly, the production of Br^- from BrCHD may have also played an important role here. If the concentrations of MA and BrMA are temporarily set to zero in figure 5.20c, no spontaneous oscillations could appear.

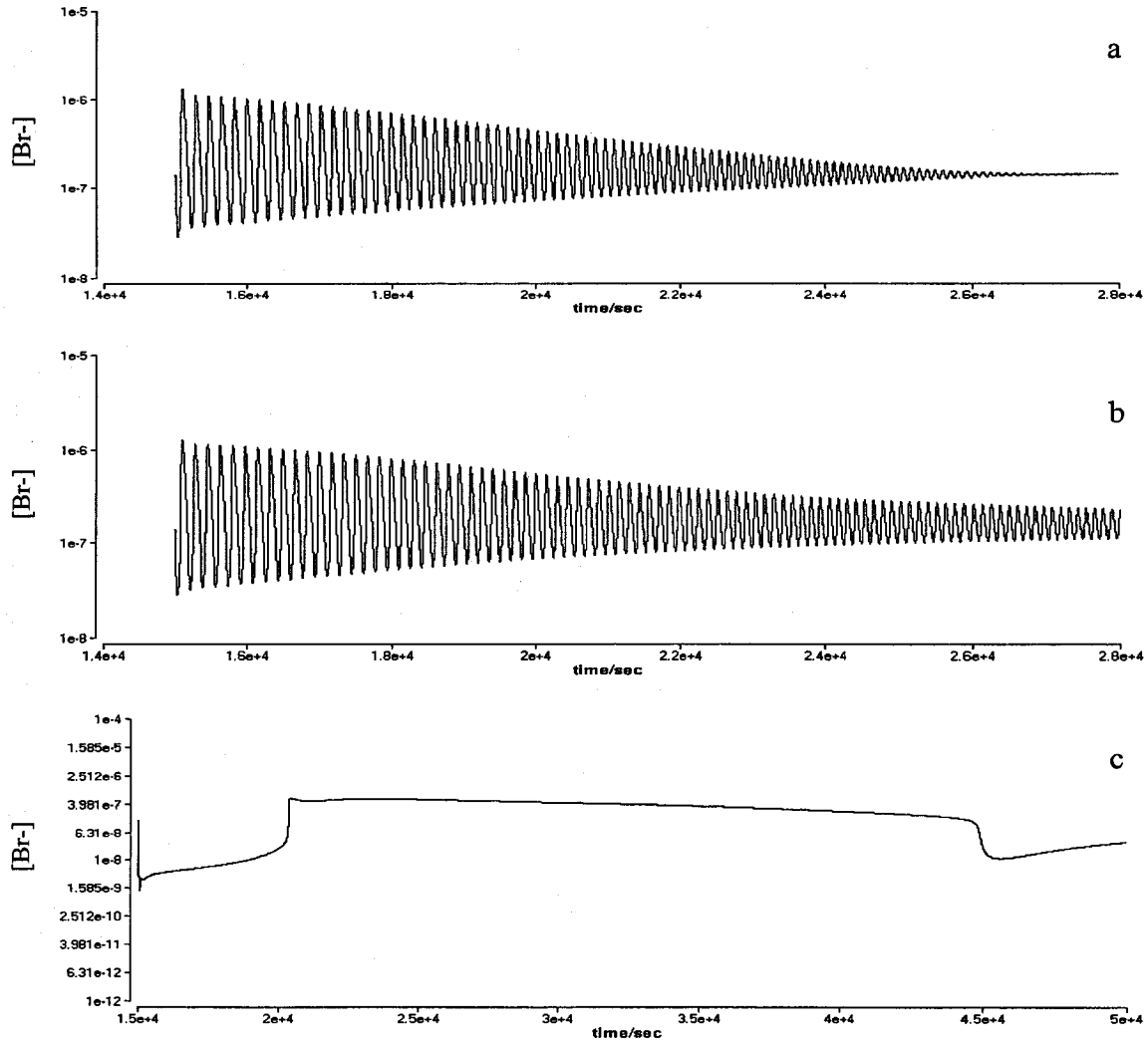

Figure 5.20

Within the second group of simple oscillations (after burst), spontaneous oscillations stop when concentrations of MA and BrMA are set to zero (eliminating the BZ reaction); while oscillatory behavior lasts for a little longer time shown in figure 5.21 b when the concentrations of 1,4-CHD and BrCHD are set to zero. This indicates that the BZ

reaction still plays an important role in the second oscillation window, but BrCHD exerts important influences on the oscillatory behavior. This conclusion is consistent with the experimental results that the second oscillation window exhibits responses to light perturbation.

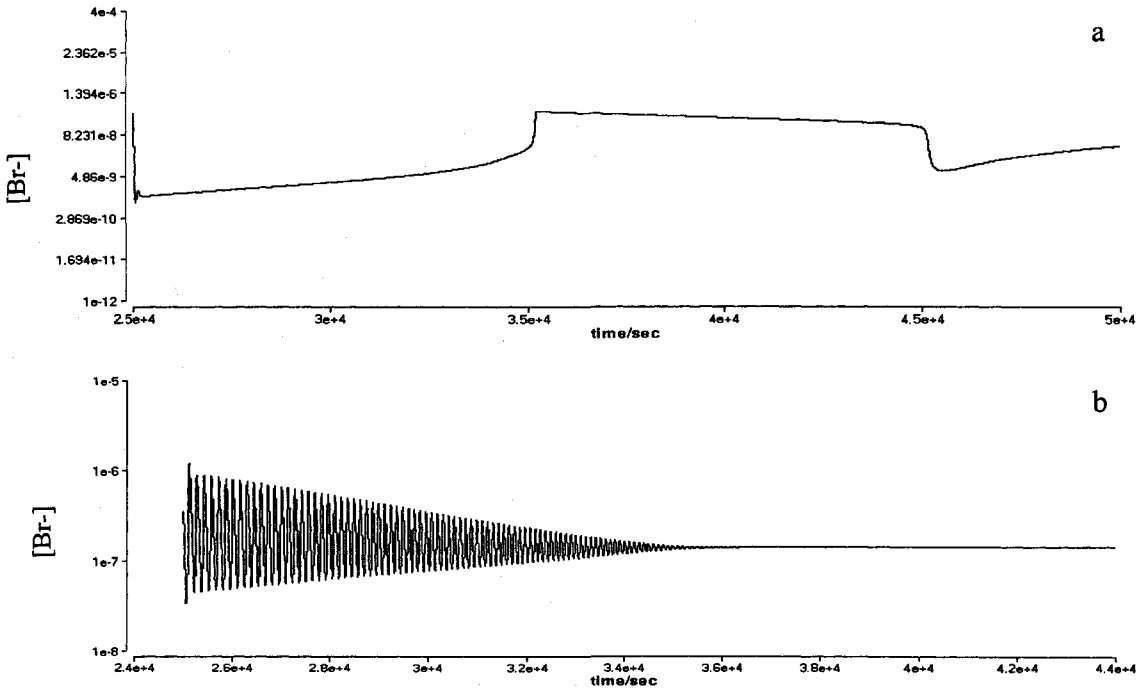

Figure 5.21

Figure 5.22 presents numerical simulations of the reaction dynamics in the Ce-CHD concentration plane (figure 5.9). Similar to figure 5.9, at low cerium concentration only simple oscillations appear. When the concentration of cerium is increased, the addition of 1,4-CHD causes the system evolve from simple to burst, and back to simple. When the 1,4-CHD is extremely high the system gives rises to more complicated oscillations. Yet, the calculated phase diagram shifts a little to the left, comparing with the experimental results shown in figure 5.9.

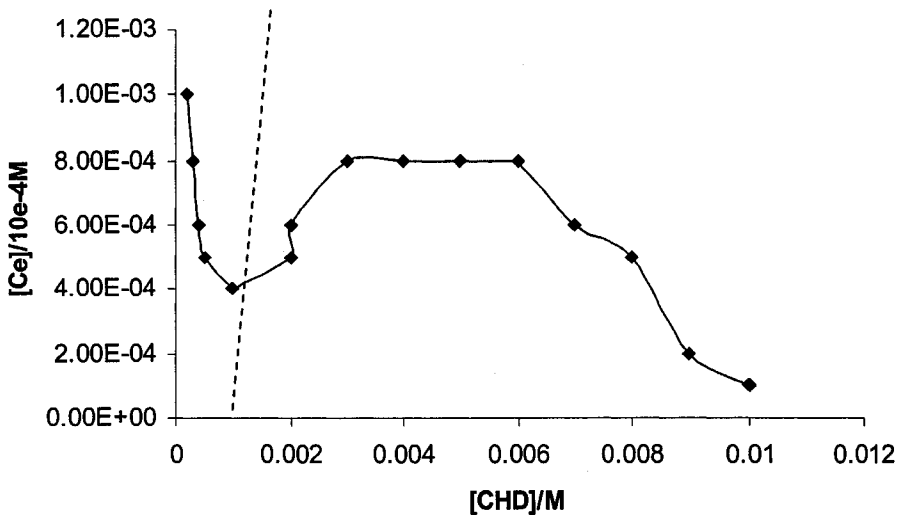

Figure 5.22

5.4 Conclusion:

In this study, the nonlinear dynamics of a mixed oscillation system, constructed by coupling the BZ reaction and the 1,4-CHD bromate oscillator was investigated. Different from our earlier study in which ferroin is used as the catalyst, cerium exhibits distinct effects to the ferroin on the development of complex oscillations. Complex oscillations including dual frequency oscillations, period doubled oscillations, bursting and mixed mode oscillations are observed in this study, which appears to be much richer than the nonlinear behavior exhibited by the ferroin-BZ-1,4-CHD system. Presumably such a difference is resulted from the difference in the redox potential of Ce^{4+}/Ce^{3+} and ferroin/ferriin.

Numerical simulations results indicate that the reaction 9 and reaction 20, which represent the competition between cerium and hydroquinone for the bromine dioxide radical, play an essential role on the development of complex oscillations.

$$Ce^{3+} + BrO_2^{\cdot} + H^+ \rightarrow HBrO_2 + Ce^{4+} \quad (R1)$$

$$H_2Q + 2\,BrO_2^{\cdot} \rightarrow 2HBrO_2 + Q \quad (R2)$$

The above two reactions form two coupled autocatalytic feedbacks in the mechanism listed in table 5.1. In complement to our earlier work, this study clearly demonstrated demonstrates that the competition via nonlinear feedback plays an important role in the observed complex oscillations (see figure 5.9). These results are particularly useful for the study of controlling nonlinear spatiotemporal dynamics.

Table 5.1 cerium catalyzed BZ-CHD mechanism

No.	Reaction	Rate constant
	A. Reactions between bromine-containing compounds	
1	$HOBr + Br^- + H^+ \rightarrow Br_2 + H_2O$	3.23×10^9
2	$Br_2 + H_2O \rightarrow HOBr + Br^- + H^+$	2
3	$HBrO_2 + Br^- + H^+ \rightarrow 2HOBr$	2.8×10^6
4	$Br^- + BrO_3^- + 2H^+ \rightarrow HOBr + HBrO_2$	0.314
5	$HOBr + HBrO_2 \rightarrow Br^- + BrO_3^- + 2H^+$	3.2
6	$2HBrO_2 \rightarrow BrO_3^- + HOBr + H^+$	3000
7	$BrO_3^- + HBrO2 + H^+ \rightarrow 2BrO_2\cdot + H_2O$	3.696
8	$2BrO_2\cdot + H_2O \rightarrow BrO_3^- + HBrO_2 + H^+$	4.2×10^7
9	$Ce^{3+} + BrO_2\cdot + H^+ \rightarrow HBrO_2 + Ce^{4+}$	*8500
10	$HBrO_2 + Ce^{4+} \rightarrow Ce^{3+} + BrO_2\cdot + H^+$	7000
	B. Reactions with the participation of bromine-containing compounds and malonic acid derivatives	
11	$MA + Br_2 \rightarrow BrMA + Br^- + H_2O$	40
12	$MA + HOBr \rightarrow BrMA + H_2O$	8.2
13	$MA + Ce^{4+} \rightarrow MA^- + Ce^{3+} + H^+$	0.3
14	$BrMA + Ce^{4+} \rightarrow Ce^{3+} + Br^- + \{products\}$	30
15	$MA\cdot + BrMA \rightarrow MA + Br^- + \{products\}$	24000
16	$MA\cdot + Br_2 \rightarrow BrMA + Br\cdot$	1.5×10^8
17	$MA\cdot + HOBr \rightarrow Br\cdot + \{products\}$	1×10^7
18	$2\ MA\cdot + \rightarrow MA + \{products\}$	3×10^9
19	$Br\cdot + MA \rightarrow Br^- + MA\cdot + \{products\}$	1×10^5
	C. Reactions with CHD	
20	$H_2Q + 2\ BrO_2\cdot \rightarrow 2HBrO_2 + Q$	$*6\times 10^5$
21	$H_2Q + Br_2 \rightarrow Q + 2\ Br^-$	1×10^4
22	$H_2Q + H^+ + BrO_3^- \rightarrow Q + HBrO_2 + H_2O$	0.028
23	$H_2Q + HOBr \rightarrow Q + Br^- + H^+ + H_2O$	6×10^5
24	$H_2Q + 2\ Ce^{4+} \rightarrow 2\ Ce^{3+} + Q + 2H^+$	100
25	$CHD + H^+ \rightarrow CHDE + H^+$	2.1×10^{-4}
26	$CHDE + H^+ \rightarrow CHD + H^+$	520
27	$CHDE + Br_2 \rightarrow BrCHD + H^+ + Br^-$	2.8×10^9
28	$CHD + HBrO_2 \rightarrow H_2Q + HOBr + H_2O$	5
29	$BrCHD + H^+ \rightarrow CHED + Br^- + 2\ H^+$	5×10^{-5}
30	$CHED + H^+ \rightarrow H_2Q + H^+$	1.9×10^{-4}
31	$CHD + BrO_3^- + H^+ \rightarrow H_2Q + HBrO_2 + H_2O$	2.8×10^{-5}
32	$2\ Ce^{4+} + CHD \rightarrow 2Ce^{3+} + H_2Q + 2H^+$	0.47
33	$2\ Ce^{4+} + BrCHD \rightarrow Q + Br^- + 3\ H^+ + 2Ce^{3+}$	0.51

Note: The concentration of $[H^+] = 1.4$ M and $[H_2O] = 55.56$M are included in the rate constants.

Chapter6. Summary and Perspectives

In this thesis, nonlinear dynamics of bromate-based oscillators are investigated. Our study illustrates that, despite that bromate-oscillators including the famous BZ reaction have been extensively investigated in the past three decades, there are still numerous new phenomena to be uncovered in these systems. For example, the co-existence of two bifurcation regimes in a closed ferroin-catalyzed BZ reaction was discovered in this study, which provided a set of unique data to characterize existing BZ reaction mechanisms. Our simulations with a modified FKN mechanism illustrate that the reactions between ferroin and, $HBrO_2$, or HBrO, and the reactions between ferriin and Br^- are not essential in the development of complex oscillations. Therefore, the existing ferroin-BZ models could be reduced to simple ones via eliminating those unimportant steps.

In the following chapters, nonlinear behavior of the mixed oscillation system, constructed by adding 1,4-CHD into the BZ reaction, was investigated. Significantly, the reactant 1,4-CHD not only participates in reactions which compete with the substrate MA, but also introduces additional nonlinear feedbacks into the classic BZ reaction. This is an essential difference between our study and earlier studies of BZ reactions using two or more organic substrates. Various complex oscillatory behaviors such as burst phenomena and sequential oscillations are observed in the new system, which can be qualitatively interpreted based on the competitions between ferroin and 1,4-H_2Q for the bromine dioxide radicals. Our experiments are supported by numerical simulations conducted with the FKN model modified via including reactions between metal catalyst and 1,4-CHD and 1,4-CHD derivatives.

In order to gain further insights into the competitions between the metal catalyst and 1,4-H_2Q for bromine dioxide radicals, 1,4-CHD is also introduced into the cerium-catalyzed BZ reaction, in which complex oscillations such as burst oscillations, mixed-mode oscillations, and dual frequency oscillations are observed. Due to the difference in their redox potentials, Ce^{3+} /Ce^{4+} and ferroin/ferriin exhibit distinct effects on the development of complex oscillations. These complex oscillatory behaviors are better reproduced by numerical simulations, supporting that the FKN mechanism is fairly effective to account for the oscillatory behaviors in the cerium-catalyzed BZ reaction.

Perturbed nonlinear dynamics has garnered a great deal of attention in the last decade due to their potential applications in catalysis, biology and information processing etc. Among existing studies on perturbed nonlinear dynamics, an external driven forcing is usually introduced. In complement to those existing studies, this research investigates the dynamics of an internally coupled chemical system, which illustrates that the interaction via nonlinear feedbacks presents an effective approach of inducing dramatic changes in the dynamical behavior.

In addition to those complex oscillations seen in this study, we anticipate that novel pattern formation could be observed in the spatially extended 1,4-CHD-ferroin-BZ system. In particular, the improved photosensitivity due to the presence of 1,4-CHD shall make the new system an attractive model for studying nonlinear dynamics because it allows one to conveniently introduce spatiotemporal perturbations.

Appendix:

1. Reaction Rate Equations Corresponding to the Kinetic Mechanism in Table 3.1:

$d[Br]/dt = -k_1*Br*BrO_3+k_2*HOBr*HBrO_2-k_3*HBrO_2*Br+k_4*(HOBr)^2-k_5*HOBr*Br+ k_6*Br_2+k_{11}*MA*Br_2+k_{19}*BrTTA+k_{24}*Fe_2*HOBr+2*k_{25}*Fe_2*Br_2-2*(k_{26}+ks_{26}*Br) *(0.0005-Fe_2)*Br$

$d[Br_2]/dt=k_5*HOBr*Br-k_6*Br_2-k_{11}*MA*Br_2-k_{25}*Fe_2*Br_2+(k_{26}+ks_{26}*Br)*(0.0005-Fe_2) *Br$

$d[HOBr]/dt = k_1*Br*BrO_3-k_2*HOBr*HBrO_2+2*k_3*HBrO_2*Br-2*k_4*(HOBr)^2 - k_5*HOBr*Br + k_6*Br_2 + k_7*(HBrO2)^2 - k_8*BrO_3*HOBr - k_{12}*MA*HOBr - k_{13}*BrMA*HOBr + K_{23}*Fe_2*HBrO_2 - k_{24}*Fe_2*HOBr$

$d[HBrO_2]/dt = k_1*Br*BrO_3 - k_2*HOBr*HBrO_2 - k_3*HBrO_2*Br+k_4*(HOBr)^2 - 2*k_7*(HBrO2)^2 + 2*k_8*BrO_3*HOBr - k_9*BrO_3*HBrO_2 + k_{10}*(BrO2)^2 + k_{15}*BrMAr*BrO_2 + k_{21}*Fe_2*BrO_2 + k_{22}*Fe_2*BrO_3 - k_{23}*Fe_2*HBrO_2$

$d[BrO_2]/dt = 2*k_9*BrO_3*HBrO_2 - 2*k_{10}*(BrO_2)^2 - k_{15}*BrMAr*BrO_2 - k_{17}*MAr*BrO_2 + k_{18}*MAr*BrO_3 + k_{20}*BrMAr*BrO_3 - k_{21}*Fe_2*BrO_2$

$d[BrO_3]/dt = -k_1*Br*BrO_3 + k_2*HOBr*HBrO_2 + k_7*(HBrO2)^2 - k_8*BrO_3*HOBr - k_9*BrO_3*HBrO_2 + k_{10}*(BrO_2)^2 - k_{18}*MAr*BrO_3 - k_{20}*BrMAr*BrO_3 - k_{22}*Fe_2*BrO_3$

$d[BrTTA]/dt = k_{14}*(BrMAr)^2 + k_{15}*BrMAr*BrO_2 + k_{16}*BrMAr*MAr - k_{19}*BrTTA + k_{20}*BrMAr*BrO_3$

$d[MA]/dt = -k_{11}*MA*Br_2 - k_{12}*MA*HOBr + k_{16}*BrMAr*MAr - k_{27}*(0.0005-Fe_2)*MA$

$d[MAr]/dt = -k_{16}*BrMAr*MAr-k_{17}*MAr*BrO_2-k_{18}*MAr*BrO_3+k_{27}*(0.0005-Fe2)*MA$

$d[BrMA]/dt = k_{11}*MA*Br_2 + k_{12}*MA*HOBr - k_{13}*BrMA*HOBr + k_{14}*(BrMAr)^2 - k_{28}*(0.0005-Fe_2)*BrMA + k_{29}*Fe_2*BrMAr$

$d[BrMAr]/dt = -2*k_{14}*(BrMAr)^2 - k_{15}*BrMAr*BrO_2 - k_{16}*BrMAr*MAr - k_{20}*BrMAr*BrO_3 + k_{28}*(0.0005-Fe_2)*BrMA - k_{29}*Fe_2*BrMAr$

$d[Fe_2]/dt =-k_{21}*Fe_2*BrO_2-2*Fe_2*(k_{22}*BrO_3+k_{23}*HBrO_2+k_{24}*HOBr+k_{25}*Br_2)+ 2*(k_{26}+ks_{26}*Br)*(0.0005-Fe_2)*Br + k_{27}*(0.0005-Fe_2)*MA + k_{28}*(0.0005-Fe_2)*BrMA -k_{29}*Fe_2*BrMAr$

2. Reaction Rate Equations Corresponding to the Kinetic Mechanism in Table 4.1

d/dt(Br)=-k1*Br*BrO3+k2*HOBr*HBrO2-k3*HBrO2*Br+k4*$(HOBr)^2$-k5*HOBr*Br
+k6*Br2+k11*MA*Br2+k19*BrTTA+k24*Fe2*HOBr+2*k25*Fe2*Br2-
2*(k26+ks26*Br)*(0.0004-Fe2)*Br+2*k31*H2Q*Br2+k33*H2Q*HOBr
+k37*CHDE*Br2+k39*BrCHD+k43*(0.0004-Fe2)*BrCHD

d/dt(Br2)=k5*HOBr*Br-k6*Br2-k11*MA*Br2-k25*Fe2*Br2+(k26+ks26*Br)*(0.0004-
Fe2)*Br-k31*H2Q*Br2-k37*CHDE*Br2

d/dt(HOBr)=k1*Br*BrO3-k2*HOBr*HBrO2+2*k3*HBrO2*Br-2*k4*$(HOBr)^2$-
k5*HOBr*Br+k6*Br2+k7*$(HBrO2)^2$-k8*BrO3*HOBr-k12*MA*HOBr-
k13*BrMA*HOBr+K23*Fe2*HBrO2-k24*Fe2*HOBr-k33*H2Q*HOBr +
k38*CHD*HBrO2

d/dt(HBrO2)=k1*Br*BrO3-k2*HOBr*HBrO2-k3*HBrO2*Br+k4*$(HOBr)^2$-
2*k7*$(HBrO2)^2$+2*k8*BrO3*HOBr-k9*BrO3*HBrO2+k10*$(BrO2)^2$+
k15*BrMAr*BrO2+k21*Fe2*BrO2+k22*Fe2*BrO3-k23*Fe2*HBrO2
+2*k30*H2Q*BrO2+k32*H2Q*BrO3-k38*CHD*HBrO2+k41*CHD*BrO3

d/dt(BrO2)=2*k9*BrO3*HBrO2-2*k10*$(BrO2)^2$-k15*BrMAr*BrO2-k17*MAr*BrO2
+k18*MAr*BrO3+k20*BrMAr*BrO3-k21*Fe2*BrO2-2*k30*H2Q*BrO2

d/dt(BrO3)=-k1*Br*BrO3+k2*HOBr*HBrO2+k7*$(HBrO2)^2$-k8*BrO3*HOBr-
k9*BrO3*HBrO2+k10*$(BrO2)^2$-k18*MAr*BrO3-k20*BrMAr*BrO3-k22*Fe2*BrO3-
k32*H2Q*BrO3-k41*CHD*BrO3

d/dt(BrTTA)=k14*$(BrMAr)^2$+k15*BrMAr*BrO2+k16*BrMAr*MAr-k19*BrTTA
+k20*BrMAr*BrO3

d/dt(MA)=-k11*MA*Br2-k12*MA*HOBr+k16*BrMAr*MAr-k27*(0.0004-Fe2)*MA

d/dt(MAr)=-k16*BrMAr*MAr-k17*MAr*BrO2-k18*MAr*BrO3+k27*(0.0004-Fe2)
*MA

d/dt(BrMA)=k11*MA*Br2+k12*MA*HOBr-k13*BrMA*HOBr+k14*$(BrMAr)^2$-
k28*(0.0004-Fe2)*BrMA+k29*Fe2*BrMAr

d/dt(BrMAr)=-2*k14*$(BrMAr)^2$-k15*BrMAr*BrO2-k16*BrMAr*MAr-
k20*BrMAr*BrO3 +k28*(0.0004-Fe2)*BrMA-k29*Fe2*BrMAr

d/dt(Fe2)=-k21*Fe2*BrO2-2*Fe2*(k22*BrO3+k23*HBrO2+k24*HOBr+k25*Br2)
+2*(k26+ks26*Br)*(0.0004-Fe2)*Br+k27*(0.0004-Fe2)*MA+k28*(0.0004-Fe2)
*BrMA-k29*Fe2*BrMAr+2*k34*H2Q*(0.0004-Fe2)+2*k42*(0.0004-Fe2)
*CHD+2*k43*(0.0004-Fe2)*BrCHD

d/dt(H2Q)=-k30*H2Q*BrO2-k31*H2Q*Br2-k32*H2Q*BrO3-k33*H2Q*HOBr-k34*H2Q*(0.0004-Fe2) +k38*CHD*HBrO2+k40*CHED+k41*CHD*BrO3 +k42*(0.0004-Fe2)*CHD

d/dt(CHD)=-k35*CHD+k36*CHDE-k38*CHD*HBrO2-k41*CHD*BrO3-k42*(0.0004-Fe2)*CHD

d/dt(CHDE)=k35*CHD-k36*CHDE-k37*CHDE*Br2

d/dt(BrCHD)=k37*CHDE*Br2-k39*BrCHD-k43*(0.0004-Fe2)*BrCHD

d/dt(CHED)=k39*BrCHD-k40*CHED

3. Reaction Rate Equations Corresponding to the Kinetic Mechanism in Table 5.1:

d/dt(Br)=-k1*HOBr*Br+k2*Br2-k3*HBrO2*Br-k4*Br*BrO3+k5*HOBr*HBrO2 +k11*MA*Br2 +k14*BrMA*(0.0008-Ce3) +k15*MAr*BrMA+k19*Brr*MA+ 2*k21*H2Q*Br2+k23*H2Q*HOBr +k27*CHDE*Br2+k29*BrCHD+k33*(0.0008-Ce3)*BrCHD

d/dt(Brr)=k16*MAr*Br2+k17*MAr*HOBr-k19*Brr*MA

d/dt(Br2)=k1*HOBr*Br- k2*Br2-k11*MA*Br2-k16*MAr*Br2-k21*H2Q*Br2-k27*CHDE*Br2

d/dt(HOBr)=-k1*HOBr*Br+k2*Br2+2*k3*HBrO2*Br+k4*Br*BrO3-k5*HOBr*HBrO2+k6*$(HBrO2)^2$ -k12*MA*HOBr-k17*MAr*HOBr- k23*H2Q*HOBr +k28*CHD*HBrO2

d/dt(HBrO2)=-k3*HBrO2*Br+k4*Br*BrO3-k5*HOBr*HBrO2-2*k6*$(HBrO2)^2$-k7*BrO3*HBrO2+k8*$(BrO2)^2$+k9*Ce3*BrO2- k10*HBrO2*(0.0008-Ce3) +2*k20*H2Q*BrO2+k22*H2Q*BrO3-k28*CHD*HBrO2 +k31*CHD*BrO3

d/dt(BrO2)=2*k7*BrO3*HBrO2-2*k8*(BrO2)^2-k9*Ce3*BrO2+k10*HBrO2*(0.0008-Ce3)- 2*k20*H2Q*BrO2

d/dt(BrO3)=-k4*Br*BrO3+k5*HOBr*HBrO2+k6*$(HBrO2)^2$-k7*BrO3*HBrO2+ k8*$(BrO2)^2$ - k22*H2Q*BrO3-k31*CHD*BrO3

d/dt(MA)=-k11*MA*Br2-k12*MA*HOBr-k13*MA*(0.0008-Ce3)+k15*MAr*BrMA +k18*$(MAr)^2$-k19*Brr*MA

d/dt(MAr)=k13*MA*(0.0008-Ce3)-k15*MAr*BrMA-k16*MAr*Br2-k17*MAr*HOBr-2*k18*$(MAr)^2$+k19*Brr*MA

d/dt(BrMA)=$_{k11}$*MA*Br2+k12*MA*HOBr-k14*BrMA*(0.0008-Ce3)-k15*MAr*BrMA +k16*MAr*Br2

d/dt(Ce3)=-k9*Ce3*BrO2+k10*HBrO2*(0.0008-Ce3)+k13*MA*(0.0008-Ce3)+ k14*BrMA*(0.0008-Ce3)+2*k24*H2Q*(0.0008-Ce3)+2*k32*(0.0008- Ce3)*CHD +2*k33*(0.0008-Ce3)*BrCHD

d/dt(H2Q)=-k20*H2Q*BrO2-k21*H2Q*Br2-k22*H2Q*BrO3-k23*H2Q*HOBr -k24*H2Q*(0.0008-Ce3)+k28*CHD*HBrO2+k30*CHED+k31*CHD*BrO3+ k32*(0.0008-Ce3)*CHD

d/dt(CHD)=-k25*CHD+k26*CHDE-k28*CHD*HBrO2-k31*CHD*BrO3-k32*(0.0008-Ce3)*CHD

d/dt(CHDE)=k25*CHD-k26*CHDE-k27*CHDE*Br2

d/dt(BrCHD)=k27*CHDE*Br2-k29*BrCHD-k33*(0.0008-Ce3)*BrCHD

d/dt(CHED)=k29*BrCHD-k30*CHED

References:

(1) Field, R. J; Burger, M. Eds. *Oscillations and Traveling Waves in Chemical Systems*; Wiley-Interscience: New York **1985**.

(2) Scott, S. K. *Chemical Chaos*; Oxford University Press: Oxford, UK, **1991**.

(3) Epstein, I. R.; Pojman, J. A. *An Introduction to Nonlinear Chemical Dynamics*; Oxford University Press: Oxford, UK, **1998**.

(4) Kapral, R.; Showalter, K., Eds. *Chemical Waves and Patterns*; Kluwer Academic Publishers: Netherlands, **1995**.

(5) Epstein, I. R.; Showalter, K. *J. Phys. Chem.***1996**, *100*, 13132.

(6) Belousov, B.P. *Sbornic Referator po Radiatsioni Medizin* (*conference proceedings*), **1958**, P145

(7) Field, R. J.; Koros, E.; Noyes, R. M. *J. Am. Chem. Soc.* **1972**, *94*, 8649

(8) Noszticzius,Z; Gaspar, V; Foersterling, H. D. *J. Am. Chem. Soc.* **1985**, *107*, 2314.

(9) Ruofft, P , *J. Phys. Chem.* **1984,** *88,* 2851

(10) Noszticzius, Z. *J. Am. Chem. Soc.* **1979**, *101,* 3660.

(11) Forsterling, H. D.; Mursinyi, S.; Noszticziusf, Z. *J. Phys. Chem.* **1990**, *94,* 2915

(12) Venkataraman, B.; Sorensen, P. C. *J. Phys. Chem.* **1991**, *95*, 5707.

(13) Keki, S.; Magyar, I.; Beck, M.T.; Gispir, V. *J. Phys. Chem.* **1992,** *96,* 1725

(14) Kalishin, E.Y.; Goncharenko, M. M.; Khavrus, V. A.; Strizhak, P. E.; *Kinetics and Catalysis,* **2002**, *43*, 256.

(15) Orban, M.; Koros, E. *J. Phys. Chem.* **1978**, *82*, 1672.

(16) Szalai, I.; Koros, E. *J. Phys. Chem. A* **1998**, *102,* 6892

(17) Szalai, I.; Csorgei, K.K.; Orban, M. *Phys. Chem. Chem. Phys.*, **2002**, 4, 1271

(18) Szalai, I., Csorgei, K.K.; Epstein, I. R.; Orban, M. *J. Phys. Chem. A* **2003**, *107,* 10074

(19) Huston, J.L. ; Hart, M.; Marinko, D. *J.Chem. Phys.* **1979,** 71, 1601

(20) Wang, J.C.; Sorensen, P. C.; Hynne, F. *J. Phys. Chem.;* **1994**, *98,* 725

(21) Yatsimirskii, K. B.; Strizhak, P. E. *Theor. Eksper. Chem.* **1992**, 28, 382

(22) Strizhak, P. E.; Ivashchenko, T. S.; KawczyAski, A. L. Pol. *J. Phys .Chem.* **1994**, *68,* 2049.

(23) Strizhak, P.E.; Kawczyhski, A.L. *J. Phys. Chem.* ***1995, 99,*** 10830

(24) Rachwalska, M.; Kawczynski, A.L. *J. Phys. Chem. A* **1999**, *103,* 3455

(25) Wang, J.C.; Hynne, F.; Sorensen, P.G.; Nielsen,K. *J. Phys. Chem.* **1996**, *100,* 17593

(26) Petrascu, A.M.; Koch, M.J.; Forsterling, H.D. *J. Phys. Chem. A* **1999**, *103,* 6757

(27) Steinbock, O.; Hamik, C.Y.; Steinbock, B. *J. Phys. Chem. A* **2000**, *104,* 6411

(28) Kalishyn, Y.Y.; Rachwalska, M.; Khavrus, V.O.; Strizhak, P.E. *Phys. Chem. Chem. Phys* , **2005**,7,1680

(29) Strizhak, P.E.; Menzinger, M. *J. Phys. Chem.* **1996,** *100,* 19182

(30) Li, R. S.; Li, J. *Chem. Phys .lett* . **1988**, 96, 144

(31) Sevcik, P.; Adamcikova, I. *Chem. Phys. Lett.* **1988**, 146, 419

(32) Menzinger, M.; Jankowski, P. *J. Phys. Chem.* **1986**, *90,* 1217

(33) Menzinger, M.; Jankowski, P. *J. Phys. Chem.* **1990**, *94,* 4123

(34) Farage, V. J.; Janjic, D. *Chem. Phys. Lett.* **1982**, *88*, 301

(35) Farage, V. J.; Janjic, D. *Chem. Phys. Lett.* **1982**, *93*, 621

(36) Zhao,B.; Wang, J.C. *J. Phys. Chem. A* **2005**, *109,* 3647

(37) Naggy, G.; Koros, E.; Oftedal, N.; Tjelflaat, K.; Ruoff, P. *Chem.Phys. Lett* **1996,** 250, 255

(38)Macro M.; Nadia M.; Vincenzo Z.; Mauro R. *Chem. Phys. Lett* **2001**, 341, 285

(39) Kuhnert, L.; Agladze, K.; Krinsky, V. *Nature* **1990**, *337*, 224.

(40) Hanazaki, I. *J. Phys. Chem.* **1992**, *96*, 5652.

(41) Mori, Y.; Nakamichi, Y.; Sekiguchi, T.; Okazaki, N.; Matsumura, T.; Hanazaki, I. *Chem. Phys. Lett.* **1993**, *211*, 421

(42) Hanazaki, I.; Mori, Y.; Sekiguchi, T.; Rabai, G. *Physica D* **1995**, *84*, 228.

(43) Kaminaga, A.; Hanazaki, I. *J. Phys. Chem. A* **1998**, *102*, 3307

(44) Sekiguchi, T.; Mori, Y.; Okazaki, N.; Hanazaki, I. *Chem. Lett.* **1993**, *211*, 1309

(45) Sorensen, P.G.; Lorenzen, T.; Hynne, F. *J. Phys. Chem.* **1996**, *100,* 19192

(46) Treindl, L; Knudsen, D.; Nakamura, T.; Inoue, T.M.; Jorgensen, K.B; Ruoff, P. *J. Phys. Chem. A* **2000**, *104,* 10783

(47) Huh, D.S.; Kim, H.S.; Wang, J.C; *Chemical Physics Letters* **2003,** 378, 78

(48) Wang, J.C.; Yadav, K.; Zhao, B.; Gao, Q.Y.; Huh, D.S. *J. Chem. Phys.*, **2004,** 121, 10138

(49) Gorner, H. J. *Phys. Chem. A* **2003,** 107, 11587

(50) Heilweil, J.; Henchman, M. J.; Epstein, I. R. *J. Am. Chem. Soc.* **1979**, *101*, 3698.

(51) Rsatogi, R. P.; Misra, G. P.; Das, I.; Sharma, A. *J. Phys. Chem.* **1993**, *97*, 2571.

(52) Rastogi, R.P.; Singh, S.N.; Chand, P. *Chem. Phys. Lett* **2004,** 385 403

(53) Rastogi, R.P.; Srivastava, S. *Chem. Phys. Lett* **1989,** 164, 173

(54) Gray, P.; Scott, S.K.; *Chemical Ocialltions and Instability;* Oxford University Press: Oxford, UK, **1994.**

(55) Epstein, I.R.; Pojman. J.A.; *An Introduction to Nonlinear Chemical Dynamics;* Oxford University Press **1998**

(56) Strogatz, S.H. *Nonlinear dynamics and chaos* Westview Press 2000.

(57) Kruger, F.; Nagy, U. Z.; Muller, S. C. *Physica D* **1995**, *84*, 95.

(58) Maselko, J.; Showalter, K. *Nature* **1989**, *339*, 609.

(59) Vanag, V. K.; Zhabotinsky, A. M.; Epstein, I. R. *J. Phys. Chem. A* **2000**, *104*, 11566

(60) Wang, J.C.; Kadar, S.; Jung, P.; Showalter, K. *Phys. Rev. Lett.* **1999**, *82*, 855

(61) Amemiya, T.; Kettunen, P.; Kadar, S.; Yamaguchi, T.; Showalter, K. *Chaos* **1998**, *8*, 872

(62) Steinbock, O.; Zykov, V. S.; Muller, S. C. *Nature* **1993**, *366*, 322.

(63) Manz, N.; Muller, S. C.; Steinbock, O. *J. Phys. Chem. A* **2000**, *104*, 5895

(64) Kaern, M.; Menzinger, M. *J. Phys. Chem. A* **2002**, *106*, 4897

(65) Ouyang, Q.; Swinney, H. L.; Li, G. *Phys. Rev. Lett.* **2000**, *84*, 1047

(66) Sevcikova, H.; Kosek, J.; Marek, M. *J. Phys. Chem.* **1996**, *100*, 1666.

(67) Manz, N.; Grun, B. T.; Steinbock, O. *J. Phys. Chem. A* **2003**, *107*,11008

(68) Bamforth, J. R.; Toth, R.; Gaspar, V.; Scott, S. K. *Phys. Chem. Chem. Phys.* **2002**, *4*, 1299

(69) Herbine, P.; Field, R. J. *J. Phys. Chem.* **1980**, *84*, 1330.

(70) Gaspar, V.; Showalter, K. *J. Am. Chem. Soc.* **1987**, *109*, 4869.

(71) Simoyi, R. H.; Manyonda, M.; Masere, J.; Mtambo, M.; Ncube, I.; Patel, H.; Epstein, I. R.; Kustin, K. *J. Phys. Chem.* **1991**, *95*, 770.

(72) Rabai G.; Epstein, I. R. *J. Am. Chem. Soc.* **1992**, *114*, 1529

(73) Simoyi, R. H.; Epstein, I. R.; Kustin, K. *J. Phys. Chem.* **1994**, *98*,551

(74) Schreiber, I.; Hung, Y.F.; Ross, J. *J. Phys. Chem.* **1996**, *100*, 8556.

(75) Hauser, M. J. B.; Olsen, L. F.; Bronnikova, T. V.; Schaffer, W. M. *J. Phys. Chem. B* **1997**, *101*, 5075

(76) Masere, J.; Stewart, F.; Meehan, T.; Pojman, J. A. *Chaos* **1999**, *9*,315.

(77) Horvath, A. K.; Nagypal, I.; Epstein, I. R. *J. Am. Chem. Soc.* **2002**,*124*, 10956.

(78) Hudson, J. L.; Hart, M.; Marinko, D. *J. Chem. Phys.* **1979**, *71*, 6104.

(79) Roux, J. C.; DeKepper, P.; Boissonate, J. *Phys. Lett. A* **1983**, 97,168

(80) Ali, F.; Menzinger, M. *J. Phys. Chem.* **1997**, *101*, 2304.

(81) Ruoff, P. *J. Phys. Chem.* **1993**, *97*, 6405.

(82) John, B. R.; Scott, S. K.; Thompson, B. W. *Chaos* **1997**, *7*, 350.

(83) Sevcikova, H.; Schreiber I.; Marek, M. *J. Phys. Chem.* **1996**, *100*,19153

(84) Wittmann, M.; Stirling, P.; Bodiss, J. *Chem. Phys. Lett.* **1987**, *141*,241

(85) Srivastava, P. K.; Mori, Y.; Hanazaki, I. *J. Phys. Chem.* **1991**, *95*,1636.

(86) Li, H.; Huang, X. *Chem. Phys. Lett.* **1996**, *255*, 137

(87) Shin, S. B.; Choe, S. J.; Huh, D. S. *Bull. Korean Chem. Soc.* **2000**, *21*, 215.

(88) Gaspar, V.; Bazsa, G.; Beck, M. T. *Z. Phys. Chem. (Leipzig)* **1983**, *264*, 43

(89) Kurin-Csorgei, K.; Zhabotinsky, A. M.; Orban, M.; Epstein, I. R. *J. Phys. Chem. A* **1997**, *101*, 6827

(90) Dolnik, M.; Gardner, T. S.; Epstein, I. R.; Collins, J. J. *Phys. Rev.Lett.* **1999**, *82*, 1582.

(91) Hohmann, W.; Schinor, N.; Kraus, M.; Schneider, F. W. *J. Phys. Chem. A* **1999**, *103*, 5742.

(92) Votrubova, V.; Hasal, P.; Schreiberova, L.; Marek, M. *J. Phys. Chem.* **1998**, *102*, 1318.

(93) Chen,Y.; Wang, J.C. *J. Phys. Chem. A* **2005,** *109,* 3950

(94) Gyorgyi, L.; Rempe, S.L; Field, R.J; *J. Phys. Chem.;* **1991**; *95*(8); 3159

(95) Wang, J.C.; Zhao, J.P.; Chen, Y.; Gao, Q.Y.; Wang, Y.M. *J. Phys. Chem. A* **2005,** *109,* 1374

Vita Auctoris

Name: Yu Chen

Place of Birth: Shenyang, Liaoning, China

Year of Birth: 1979

Education: Dalian University of Technology, Dalian, China

1998-2002 Honor B. Eng.

University of Windsor, Canada

2003-2005 M. Sc

Publications and Presentations

(2003-2005)

Publications:

1. **Yu Chen,** Jichang Wang "Complex Behavior in Coupled Bromate Oscillators" *J. Phys. Chem. A.* **2005,** *109,* 3950
2. Jinpei Zhao, **Yu Chen,** Jichang Wang "Transient Complex Oscillations in a Closed Chemical System with Coupled Autocatalysis" *J. Chem. Phys* **2005,** 122, 114514
3. Jichang Wang, Jinpei Zhao, **Yu Chen,** Qingyu Gao, and Yumei Wang "Coexistence of Two Bifurcation Regimes in a Closed Ferroin-Catalyzed Belousov-Zhabotinsky Reaction" *J. Phys. Chem. A* **2005,** *109,* 1374
4. **Yu Chen,** Jichang Wang. "Complex Oscillations in the Cerium-BZ-1,4-CHD Oscillator" *J. Phys. Chem. A.* manuscript in preparation

Presentation:

Yu Chen, Jichang Wang. A New Function of a Platinum Electrode in the Study of Chemical Kinetics. *87th* CSC *Conference and Exhibition* May 29-June 1, **2004,** London, Canada